SITE-SPECIFIC IRON-SULFUR CLUSTER CHEMISTRY IN

FERREDOXIN:THIOREDOXIN REDUCTASE

by

ELIZABETH MENGELT WALTERS

(Under the Direction of Michael Kenneth Johnson)

ABSTRACT

Ferredoxin:thioredoxin reductase (FTR) plays a crucial role in light regulation of oxygenic photosynthesis in chloroplasts. FTR catalyzes the reduction of the disulfide in thioredoxin using a [2Fe-2S] ferredoxin as a one-electron donor, and constitutes a unique class of disulfide reductases that utilizes an active site involving a [4Fe-4S] cluster with an adjacent disulfide. The combination of spectroscopic and mutagenesis studies has been used to investigate the catalytic mechanism of FTR. Wild-type, C57S, C87A, H86Y *Synechocystis* FTR, as well as a *N*-ethylmaleimide chemically modified form (NEM-FTR) and a stable heterodisulfide complex formed between FTR and the C40S variant of thioredoxin-*m* (FTR-Trx*m*), have been investigated in all accessible redox states using UV-visible absorption, resonance Raman, electron paramagnetic resonance, variable temperature magnetic circular dichroism, and Mössbauer spectroscopies. The results reveal distinct roles for Cys87 and Cys57 that comprise the active-site disulfide. Cys87 functions as an electron transfer thiol that binds to the cluster in the one-electron reduced form to yield a five-coordinate iron site. Cys57 functions as an interchange thiol that forms a heterodisulfide with the thioredoxin substrate. A role for His86 as a proton donor/acceptor is implicated by dramatic changes in the activity and redox properties of the [4Fe-4S] center in the H86Y variant. Mössbauer spectroscopy has been particularly effective in establishing novel site-specific [4Fe-4S] cluster chemistry in the oxidized, one-electron-reduced and two-electron-reduced forms of FTR. The results are consistent with two distinct mechanistic proposals that differ in terms of whether the heterodisulfide intermediate is formed at the one- or two-electron-reduced level. A novel one-electron reduced intermediate involving a $[4Fe\text{-}4S]^{3+}$ cluster with a five-coordinate iron site is common to both mechanistic proposals and provides a unique method for cleaving biological disulfides in two sequential one-electron steps.

INDEX WORDS: Ferredoxin:thioredoxin reductase, iron-sulfur cluster, catalytic mechanism, disulfide reduction, electron paramagnetic resonance, resonance Raman, magnetic circular dichroism, Mössbauer

SITE-SPECIFIC IRON-SULFUR CLUSTER CHEMISTRY IN FERREDOXIN:THIOREDOXIN REDUCTASE

by

ELIZABETH MENGELT WALTERS

B.S., University of Wisconsin-Madison, 2000

A Dissertation Submitted to the Graduate Faculty of The University of Georgia in Partial Fulfillment of the Requirements for the Degree

DOCTOR OF PHILOSOPHY

ATHENS, GEORGIA

2005

SITE-SPECIFIC IRON-SULFUR CLUSTER CHEMISTRY IN

FERREDOXIN:THIOREDOXIN REDUCTASE

by

ELIZABETH MENGELT WALTERS

Major Professor:	Michael K. Johnson
Committee:	Robert A. Scott Donald M. Kurtz, Jr. Marly K. Eidsness Michael W.W. Adams

Electronic Version Approved:

Maureen Grasso
Dean of the Graduate School
The University of Georgia
May 2005

DEDICATION

In loving memory of my father, Dennis Millman Mengelt.

September 28, 1944 – April 12, 2003

ACKNOWLEDGEMENTS

I wish to truly thank my advisor, Professor Michael K. Johnson, for many years of guidance and support during the course of my graduate career. His understanding during the good and bad times of my stay at The University of Georgia will never be forgotten.

Many thanks are extended to my advisory committee, Dr. Robert A. Scott, Dr. Michael W.W. Adams, Dr. Donald M. Kurtz, and Dr. Marly K. Eidsness, for helpful and thought-provoking discussions.

I thank all my friends in the Johnson lab, both those currently there and those that have graduated before me. Many thanks to both Jeff and Mike for showing me that Midwesterners can do well in the Deep South! I cannot thank Archer and Heather enough for all the support and friendship that they have offered over the past five years. My life is forever changed for the better due to the friendships I have made at UGA.

Finally, I must thank my family. Words can not begin to express my gratitude to my parents, Dennis and Nancy Mengelt, for teaching me the value of hard work and the many years of love and support that were needed to get me here. I thank my mother, my brother Michael, and my sister-in-law Petra, for encouraging me to stick it out during the darkest days when all I wanted to do was bury my head in the sand. I thank all the Walters for welcoming me and making me a part of their family. Lastly and most importantly, I thank my husband Richard for so much, but mostly for giving me unconditional love and support. Thank you so much for our wonderful little son Riches, who was such a good little guy and napped when I needed to work on this the most!

TABLE OF CONTENTS

Page

LIST OF TABLES

Page

LIST OF FIGURES

Page

LIST OF SCHEMES

Page

CHAPTER 1

INTRODUCTION AND LITERATURE REVIEW

Iron-Sulfur Proteins: Background of Structure and Function

Proteins containing iron-sulfur (Fe-S) clusters are ubiquitous throughout nature and are found in almost all organisms from the simplest bacteria to the most complex life forms. Iron-sulfur centers were initially thought to participate solely in electron transport, however research focusing on the structure and function of biological Fe-S proteins over the past 40 years has demonstrated that these unique active-site centers are not limited to this function. In addition to electron transport,[1-3] the roles attributed to Fe-S centers have proliferated to include coupling of electron and proton transfer,[4-7] substrate binding and activation,[8-29] determination of protein structure,[30-33] regulation of gene expression[11;34-39] and enzymatic activity,[40-43] iron, electron, and cluster storage,[44-46] and disulfide reduction.[47-49] Based on the pervasive nature of Fe-S centers in biology and the wide variety of functional roles now attributed to Fe-S centers, it is not surprising that they have been the subject of many books[50] and thorough review articles.[1;2;51-55]

The four basic types of biological Fe-S centers are shown in Figure 1.1. The centers generally have cysteinyl-S ligation and are defined by mononuclear Fe centers, [2Fe-2S], cubane-type [3Fe-4S], and [4Fe-4S] clusters. Many Fe-S cluster containing enzymes function in redox roles and as such, it is critically important to understand the fundamental principles pertaining to the accessible redox states and properties of the five types of biologically relevant Fe-S centers, as summarized in Figure 1.2. Details for

individual cluster types will be discussed in depth below, however, for all cluster types described in Figure 1.2, the stoichiometry of Fe and inorganic-S atoms in the cluster core are indicated within square brackets, while the formal charge for the cluster is noted as a superscript. Furthermore, the number of unpaired electrons in the electronic ground state, as determined experimentally, is indicated by the spin state, *S*. Figure 1.2 also indicates the extent of localization/delocalization as determined by Mössbauer spectroscopy for each type of cluster for each accessible redox state, with formal Fe^{3+} in red, Fe^{2+} in blue, and $Fe^{2.5+}$ in green.

Although technically not a true Fe-S center due to the lack of inorganic-S, mononuclear Fe sites as found in rubredoxin and desulforedoxin are often categorized with complex Fe-S clusters. They comprise mononuclear Fe sites with tetrahedral cysteinyl ligation and function in mediating electron transfer in a variety of different bacterial proteins**.** These sites redox cycle between high-spin Fe(III) ($S = 5/2$) and high-spin Fe(II) ($S = 2$) with redox potentials ranging from +300 mV to –100 mV versus the Normal Hydrogen Electrode (NHE).

Biological [2Fe-2S] clusters are found in two types, the normal-type, which contains tetrahedral Fe atoms with complete cysteinyl ligation, and the Rieske-type, which contain tetrahedral Fe atoms, one with two cysteinyl and the other with two histidyl ligands. [2Fe-2S] clusters function in electron transfer and play critical roles in the photosynthetic and respiratory electron transfer chains. Both normal and Rieske-type [2Fe-2S] clusters redox cycle between the 2+ and 1+ oxidation states, albeit with different midpoint redox potentials, +380 to –460 mV and +380 to –150 mV versus NHE respectively. $[2Fe\text{-}2S]^{2+}$ clusters contain two high-spin Fe(III) ($S = 5/2$)

antiferromagnetically coupled to yield the $S = 0$ ground electronic spin state. $[2Fe\text{-}2S]^{1+}$ clusters contain one high-spin Fe(II) ($S = 2$) and one high-spin Fe(III) ($S = 5/2$) antiferromagnetically coupled to yield the $S = 1/2$ ground electronic spin state. However, examples of valence-delocalized $[2Fe\text{-}2S]^{1+}$ clusters with $S = 9/2$ ground states have been observed in the C56S and C60S variants of *Clostridium pasteurianum* ferredoxin (Fd).[56-58] As discussed below, valence-delocalized $[2Fe\text{-}2S]^{1+}$ fragments are components of many higher nuclearity clusters.

Although biological [3Fe-4S] clusters have been reported in both linear and cubane geometries, only cubane-type [3Fe-4S] clusters with complete cysteinyl ligation appear to be physiologically relevant.[51] Cubane-type [3Fe-4S] clusters have been characterized in the 1+, 0, and 2- oxidation states, however only the 1+/0 redox couple has been observed in biological electron transfer with a midpoint redox potential ranging from +90 mV to –460 mV versus NHE. $[3Fe\text{-}4S]^{1+}$ clusters contain three tetrahedral high-spin Fe(III) ($S = 5/2$) antiferromagnetically coupled to yield the $S = 1/2$ ground electronic spin state. $[3Fe\text{-}4S]^{0}$ clusters comprise a valence-delocalized $[2Fe\text{-}2S]^{1+}$ ($S = 9/2$) fragment antiferromagnetically coupled to a valence-trapped high-spin Fe(III) ($S = 5/2$) to yield the $S = 2$ ground electronic spin state.

The cubane-type biological [4Fe-4S] clusters are most often found in the 3+, 2+, and 1+ core oxidation states and tetrahedral coordination at each Fe site is generally completed by cysteinyl ligation. [4Fe-4S] clusters are the most wide-spread electron transfer centers in biology and undergo one-electron oxidation or reduction processes between either the 2+/1+ redox couple as is found in Fd-type centers or the 3+/2+ redox couple as is found in high-potential iron-proteins (HiPIPs). Fd-type [4Fe-4S] clusters

redox cycle between the 2+ and 1+ oxidation states with midpoint redox potentials ranging from +80 to –715 mV versus NHE, and HiPIP-type [4Fe-4S] clusters redox cycle between the 3+ and 2+ oxidation states with midpoint redox potentials ranging from +500 to +50 mV versus NHE. $[4Fe\text{-}4S]^{1+}$ clusters contain one valence-delocalized ($S = 9/2$) fragment antiferromagnetically coupled to a ferromagnetically coupled diferrous $[2Fe\text{-}2S]^{0}$ ($S = 4$) fragment to yield the observed $S = 1/2$ ground state. $[4Fe\text{-}4S]^{2+}$ clusters contain two valence-delocalized $[2Fe\text{-}2S]^{1+}$ fragments antiferromagnetically coupled to yield an $S = 0$ ground state. $[4Fe\text{-}4S]^{3+}$ clusters contain one ferromagnetically coupled diferric $[2Fe\text{-}2S]^{2+}$ ($S = 5$) fragment antiferromagnetically coupled to a valence-delocalized $[2Fe\text{-}2S]^{1+}$ ($S = 9/2$) fragment to yield the observed $S = 1/2$ ground state.

The range of midpoint potentials recorded for the common redox couples of each cluster type are summarized in Figure 1.3. Based on the wide range of applicable redox potentials that apply to even one type of Fe-S center, it is apparent that the protein environment has a major influence on the redox properties of a specific Fe-S center, often with dramatic implications for the function of the enzyme. One of the most common ways of tuning the properties of biological Fe-S clusters for a particular function is site-specific cluster chemistry. For example, histidine, aspartate, serine, or backbone amide N ligation at a specific Fe site of an electron transfer Fe-S cluster serves to modify redox potential,[59] to gate electron transport,[60] and to facilitate coupling of electron and proton transfer.[4;6;7;59]

Site-specific cluster chemistry also has been employed to functionalize Fe-S centers for substrate binding and activation. Three distinct methods are evident in the literature. The first involves one Fe atom of the cluster having an accessible coordination

site to which substrate directly binds, as found in the [4Fe-4S] clusters of hydratases/dehydratases[11;12] and the radical S-adenosylmethionine family of enzymes.[17;18;61-63] The second method involves the introduction of a heterometal into the cluster as is found in the active site of nitrogenase[8;21] and CO dehydrogenase.[26;27] The third method involves a substrate binding metal coordinated to one Fe of a [4Fe-4S] cluster most often through a bridging cysteinyl residue, as is found in the active sites of acetyl CoA synthase,[24;25;64] Fe-hydrogenase,[24;25] and sulfite and nitrite reductase.[22]

The studies of ferredoxin:thioredoxin reductase (FTR) discussed in this work describe a new way of functionalizing a [4Fe-4S] cluster to achieve site-specific cluster chemistry. This functionalization involves distortion at a unique Fe site to facilitate a five-coordinate ion site. This type of cluster chemistry is emerging as a common feature of disulfide reductases that use a [4Fe-4S] cluster to cleave disulfides in two sequential one-electron steps.

Biological Disulfide Bonds and Disulfide Bond Reduction: Background

Disulfide bonds are important components of the structure and function of many proteins. A biological disulfide bond is a strong covalent bond formed between the functional groups of two cysteine residues contained in the amino acid backbone of a protein. The two-electron reduction of a redox-active disulfide bond (E_m ~ - 220 mV versus NHE) is catalyzed by a disulfide reductase.

There are two known classes of disulfide reductases that affect substrate reduction. Most often, biological disulfide reduction is catalyzed by an enzyme belonging to the very large class of flavoprotein disulfide reductases. By utilizing a two-electron donor and acceptor system, flavoprotein disulfide reductases effect the two-

electron reduction of a substrate disulfide in one concerted two-electron step via a two-electron reduced intermediate. Fe-S disulfide reductases constitute a second, very small family, including only ferredoxin:thioredoxin reductase (FTR) from chloroplasts[47;48;65] and heterodisulfide reductase (HDR) from methanogenic archea.[48;49] Unlike the flavoprotein disulfide reductases, FTR and HDR utilize a one-electron donor and acceptor system to effect disulfide reduction. As such, Fe-S dependent disulfide reductases are proposed to catalyze substrate reduction in two sequential one-electron steps via a one-electron reduced intermediate.

Flavoprotein disulfide reductases

Biological disulfide reduction is generally catalyzed by enzymes belonging to a large family of pyridine nucleotide-disulfide oxidoreductase flavoenymes, which include thioredoxin reductase, glutathione reductase, lipoamide dehydrogenase, trypanothione reductase, mercuric reductase, and NADH peroxidase. This family of enzymes has been well studied both structurally and mechanistically, and has been the subject of many thorough reviews.[66-68] Enzymes in this family mediate the two-electron reduction of substrate disulfide utilizing an active-site comprised of an FAD-cofactor and a nearby disulfide, with enzyme turnover dependent on the presence of an acidic or basic amino acid residue located near the active site.

The generic mechanism by which members of the flavoprotein disulfide reductase family effect substrate disulfide reduction is shown in Scheme 1.1. Scheme 1.1 illustrates a simplified mechanistic scheme for the two-electron reduction of oxidized glutathione disulfide by glutathione reductase.[66] The resting state of the enzyme consists of the active-site in the oxidized form, which contains oxidized FAD (denoted by **F**) adjacent to

an intact asymmetrically disposed disulfide formed between Cys58 and Cys63 (denoted by **S-S**). The initial step involves the two-electron reduction of the FAD-cofactor by NADPH. The reduced FAD immediately donates two electrons to reduce the active-site disulfide, forming a two-electron reduced intermediate. The intermediate is stabilized two-fold, firstly by a charge transfer complex (denoted by a dashed arrow) formed between the thiolate of Cys63 and the FAD-cofactor and secondly by the thiol formed on Cys58 (denoted by **SH**), which is stabilized by a nearby acid-base residue (denoted by **B**). These features stabilize the enzyme to prevent the back reactions of reforming the active-site disulfide and re-reducing the FAD-cofactor. At this point, Cys58 is free to attack the substrate disulfide to form a heterodisulfide intermediate. Finally, Cys63 attacks the heterodisulfide resulting in the reformation of the active-site disulfide and the release of reduced substrate.

Several key features of the enzyme structure are critical to turnover and are typical for most enzymes belonging to this family of disulfide reductases. First, all the available evidence suggests that each cysteine comprising the active-site disulfide plays a distinct role during catalysis and that the loss of either cysteine residue results in partially or completely inactive enzyme.[69;70-80;81-83] The C-terminal cysteine of the active-site disulfide is termed the electron-transfer cysteine and is intimately associated with the FAD-cofactor during turnover, while the N-terminal cysteine of the active-site disulfide is termed the interchange cysteine and is involved in the formation of a heterodisulfide intermediate with substrate. Secondly, an additional amino acid located near the active site has been proposed to act as an acid/base catalyst during turnover.[66;69;82;84-89] This residue has been identified to be critical during catalysis by stabilizing the interchange

cysteine as a thiol upon formation of the two-electron reduced catalytic intermediate. Furthermore, the loss of this residue results in an enzyme with reduced rate of substrate reduction.

By utilizing a two-electron donor and acceptor system, flavoprotein disulfide reductases effect substrate disulfide reduction in one concerted two-electron step. The paradigm of using two-electron chemistry involving NADPH, FAD, and a redox-active disulfide does not always apply however, and an alternative system, the Fe-S disulfide reductase family of enzymes constitutes the other pathway to achieve substrate disulfide reduction.

Iron-Sulfur-dependent disulfide reductases

Over the past decade, ferredoxin:thioredoxin reductase (FTR) and heterodisulfide reductase (HDR) emerged as two types of Fe-S enzymes belonging to a new class of disulfide reductases.[49;65;90] These enzymes differ from the flavoprotein disulfide reductases in that they are proposed to effect substrate disulfide reduction via two sequential one-electron steps. These enzymes utilize one-electron donors and an active-site [4Fe-4S] cluster that will interact directly with either an active-site disulfide in the case of FTR, or the substrate disulfide in the case of HDR. The mechanism and the essential amino acid residues by which two-electron reduction of a disulfide is achieved using the unorthodox one-electron donor and acceptor system of Fe-S-dependent disulfide reductases are of great interest.

Ferredoxin:Thioredoxin Reductase

Ferredoxin:thioredoxin reductase (FTR) is the founding member of the Fe-S disulfide reductase family of enzymes. FTR is the central enzyme of the chloroplast/FTR

system, a redox regulatory system required for the control of the catalytic properties of a wide range of target enzymes involved in oxygenic photosynthesis. FTR transfers a redox signal received by a $[2Fe\text{-}2S]^{2+/1+}$ Fd (E_m = + 420 mV, n = 1) to *f*- and *m*-type thioredoxins (Trxs) (E_m = - 210 mV, n = 2 for both thioredoxins)utilizing a unique active-site consisting of a distorted [4Fe-4S] cluster and a nearby disulfide. The combination of a one-electron donor, reduced ferredoxin, and a one-electron acceptor, FTR, demands that the two-electron reduction of substrate Trx occur in two sequential one-electron steps.

All of the original research probing the structure and function of FTR involved only native enzyme isolated directly from a variety of sources, including spinach leaves, corn, and soybean.[65;90-94] Early spectroscopic characterization of native spinach FTR indicated that the role of the Fe-S center was to facilitate the reduction of substrate disulfide in two one-electron steps through the stabilization of the one-electron reduced catalytic intermediate.[94] The recent construction of overexpression systems for FTR from both spinach[95;96] and the photosynthetic bacterium *Synechocystis* sp. PCC6803,[97;98] and the generation of stable variant forms of FTR,[99] has allowed for a more thorough biochemical and analytical investigation of FTR, however a detailed spectroscopic characterization of the [4Fe-4S] cluster in overexpressed and variant forms of FTR had not been attempted prior to this study. As presented in Chapter 2, the similarities and differences between native and overexpressed enzyme from various sources were spectroscopically analyzed.[48] Native FTR isolated from spinach leaves was found to be spectroscopically indistinguishable from overexpressed spinach and *Synechocystis* enzyme. Furthermore, a comparison of the properties of the Fe-S cluster in FTR to that

in HDR allows a similar mechanism to be invoked for both members of the Fe-S-dependent family of disulfide reductases. Chapter 3 addresses the ligation of the C-terminal cysteine of the active-site disulfide to the [4Fe-4S] cluster in FTR upon formation of a stable analog of the one-electron reduced intermediate.[100] Novel site-specific cluster chemistry is invoked through the covalent attachment of the cysteine residue to a unique Fe site of the cluster, forming a five-coordinate Fe site with two thiolate ligands. Chapter 4 addresses the distinct roles assigned to each of the two cysteines comprising the active-site disulfide during catalysis via spectroscopic analysis of two variant forms of FTR and a stable heterodisulfide complex formed between FTR and a mutant form of Trx.[101] The results clearly indicate that the N-terminal cysteine of the FTR active-site disulfide functions as the interchange cysteine and is associated with the formation of a heterodisulfide intermediate, while the C-terminal cysteine functions as the electron-transfer cysteine and is associated with the [4Fe-4S] cluster upon the formation of the one-electron reduced intermediate. Furthermore, the results reveal site-specific cluster chemistry in all three redox states of FTR (oxidized, one-electron reduced, and two-electron reduced). This raises the possibility of alternative catalytic mechanisms that differ in terms of whether the heterodisulfide intermediate is formed at the one- or two-electron reduced state. The latter mechanism is reminiscent of the mechanism invoked for the flavoprotein disulfide reductase class of enzymes. Chapter 5 addresses the catalytic role of the histidine residue located near the FTR active site. The results suggest that this residue acts as an acid/base residue during catalysis and may be important to the stabilization of thiolate(s)/thiol(s) formed upon reduction of the active-site disulfide.

Bibliography

(1) Johnson, M. K. Iron-Sulfur Proteins; In *Encyclopedia of Inorganic Chemistry*; King, R. B., ed. John Wiley and Sons: Chichester, 1994; pp 1896-1915.

(2) Beinert, H. *J.Biol.Inorg.Chem.* **2000**, *5*, 2-15.

(3) Sticht, H.; Rösch, P. *Prog.Biophys.Mol.Biol.* **1998**, *70*, 95-136.

(4) Peters, J. W.; Stowell, M. H. B.; Soltis, S. M.; Finnegan, M. G.; Johnson, M. K.; Rees, D. C. *Biochemistry* **1997**, *36*, 1181-1187.

(5) Link, T. A. *Adv.Inorg.Chem.* **1999**, *47*, 83-157.

(6) Hunsicker-Wang, L. M.; Heine, A.; Chen, Y.; Luna, E. P.; Todaro, T.; Zhang, Y. M.; Williams, P. A.; McRee, D. E.; Hirst, J.; Stout, C. D.; Fee, J. A. *Biochemistry* **2003**, *42*, 7217.

(7) Lanzilotta, W. N.; Christiansen, J.; Dean, D. R.; Seefeldt, L. C. *Biochemistry* **1998** , *37*, 11376-11384.

(8) Einsle, O.; Tezcan, F. A.; Andrade, S. L. A.; Schmid, B.; Yoshida, M.; Howard, J. B.; Rees, D. C. *Science* **2002**, *297*, 1696-1700.

(9) Nagashima, S.; Nakasako, M.; Dohmae, N.; Tsujimura, M.; Takio, K.; Odaka, M.; Yonda, M.; Kamiya, N.; Endo, I. *Nat.Struct.Biol.* **1998**, *5*, 347-351.

(10) Doan, P. E.; Nelson, M. J.; Jin, H.; Hoffman, B. *J.Am.Chem.Soc.* **1996**, *118*, 7014-7015.

(11) Beinert, H.; Kennedy, M. C.; Stout, C. D. *Chem.Rev.* **1996**, *96*, 2335-2373.

(12) Flint, D. H.; Allen, R. M. *Chem.Rev.* **1996**, *96*, 2315-2334.

(13) Romao, M. J.; Archer, M. Structural Versatility of Proteins Containing Rubredoxin-Type Centers; In *Iron Metabolism*; Ferreira, G. C., Moura, J. J. G., Franco, R., eds. Wiley-VCH Verlag: Weinheim, 1999; pp 341-358.

(14) Jenney, F. A.; Verhagen, M. F. J. M.; Cui, X.; Adams, M. W. W. *Science* **1999**, *286*, 306-309.

(15) Yeh, A. P.; Hu, Y.; Jenney, F. A.; Adams, M. W. W.; Rees, D. C. *Biochemistry* **2000**, *39*, 2499-2508.

(16) Sofia, H. J.; Chen, G.; Hetzler, B. G.; Reyes-Spindola, J. F.; Miller, N. E. *Nucleic Acids Res.* **2001**, *29*, 1097-1106.

(17) Layer.G.; Moser, J.; Heinz, D. W.; Jahn, D.; Schubert, W.-D. *EMBO J.* **2003**, *22*, -6214.

(18) Jarrett, J. T. *Curr.Opin.Chem.Biol.* **200**, *7*, 174-182.

(19) Volbeda, A.; Charon M.-H.; Piras, C.; Hatchikian, E. C.; Frey, M.; Fontecilla-Camps, J. C. *Nature* **1995**, *373*, 580-587.

(20) Volbeda, A.; Garcin, E.; Piras, C.; de Lacey, A. L.; Fernandez, V. M.; Hatchikian, E. C.; Frey, M.; Fontecilla-Camps, J. C. *J.Am.Chem.Soc.* **1996**, *118*, 12989-12996.

(21) Kim, J.; Rees, D. C. *Science* **1992**, *257*, 1677-1682.

(22) Crane, B. R.; Siegel, L. M.; Getzoff, E. D. *Science* **1995**, *270*, 59-67.

(23) Crane, B. R.; Seigel, L. M.; Getzoff, E. D. *Biochemistry* **1997**, *36*, 12120-12137.

(24) Peters, J. W.; Lanzilotta, W. N.; Lemon, B. J.; Seefeldt, L. C. *Science* **1998**, *282*, 1853-1858.

(25) Nicolet, Y.; Cavazza, C.; Fontecilla-Camps, J. C. *J.Inorg.Biochem.* **2002**, *91*, 1-8.

(26) Dobbek, H.; Svetlitchnyi, V.; Gremer, L.; Huber, R.; Meyer, O. *Science* **2001**, *293*, 1281-1285.

(27) Dobbek, H.; Svetlitchnyi, V.; Liss, J.; Meyer, O. *J.Am.Chem.Soc.* **2004**, *126*, 5382-5387.

(28) Doukov, T. I.; Iverson, T. M.; Seravalli, J.; Ragsdale, S. W.; Drennan, C. L. *Science* **2002**, *298*, 567-572.

(29) Darnault, C.; Volbeda, A.; Kim, E. J.; Legrand, P.; Vernèdale, X.; Lindahl, P. A.; Fontecilla-Camps, J. C. *Nat.Struct.Biol.* **2003**, *10*, 271-279.

(30) Cunningham, R. P.; Asahara, H.; Bank, J. F.; Scholes, C. P.; Salerno, J. C.; Surerus, K. K.; Münck, E.; McCracken, J.; Peisach, J.; Emptage, M. H. *Biochemistry* **1989**, *28*, 4450-4455.

(31) Kuo, C.-F.; McRee, D. E.; Fisher, C. L.; O'Handley, S. F.; Cunningham, R. P.; Tainer, J. A. *Science* **1992**, *258*, 434-440.

(32) Porello, S. L.; Cannon, M. J.; David, S. S. *Biochemistry* **1998**, *37*, 6465-6475.

(33) Guan, Y.; Manuel, R. C.; Arvai, A. S.; Parikh, S. S.; Mol, C. D.; Miller, J. H.; Lloyd, R. S.; Tainer, J. A. *Nat.Struct.Biol.* **1998**, *5*, 1058-1063.

(34) Hidalgo, E.; Demple, B. *EMBO J.* **1994**, *13*, 138-146.

(35) Demple, B.; Ding, H.; Jorgensen, M. *Meth.Enzymol.* **2002**, *348*, 355-364.

(36) Kiley, P. J.; Beinert, H. *FEMS Microbiol.Rev.* **1998**, *22*, 341-352.

(37) Popescu, C.; Bates, D. M.; Beinert, H.; Münck, E.; Kiley, P. J. *Proc.Natl.Acad.Sci.USA* **1998**, *95*, 13431-13435.

(38) Kiley, P. J.; Beinert, H. *Curr.Opin.Microbiol.* **2003**, *6*, 181-185.

(39) Schwartz, C. J.; Giel, J. L.; Patschkowski, T.; Luther, C.; Ruzicka, F. J.; Beinert, H.; Kiley, P. J. *Proc.Natl.Acad.Sci.USA* **2001**, *98*, 14895-14900.

(40) Grandoni, J. A.; Switzer, R. L.; Marakoff, C. A.; Zalkin, H. *J.Biol.Chem.* **1989**, *264*, 6058-6064.

(41) Smith, J. L.; Zaluzec, E. J.; Wery, J.-P.; Niu, L.; Switzer, R. L.; Zalkin, H.; Satow, Y. *Science* **1994**, *264*, 1427-1433.

(42) Wu, C.-K.; Dailey, H. A.; Rose, J. P.; Burden, A.; Sellers, V. M.; Wang, B.-C. *Nat.Struct.Biol.* **2001**, *8*, 156-160.

(43) Sellers, V. M.; Johnson, M. K.; Dailey, H. A. *Biochemistry* **1996**, *35*, 2699-2704.

(44) Thauer, R. K.; Schönheit, P. Iron-Sulfur Complexes of Ferredoxin as a Storage Form of Iron in *Clostridium pasteurianum*; In *Iron-Sulfur Proteins*; Spiro, T. G., ed. Wiley: New York, 1982; pp 329-341.

(45) Reeve, J. N.; Beckler, G. S.; Cram, D. S.; Hamilton, P. T.; Brown, J. W.; Krzycki, J. A.; Kolodziej, A. F.; Alex, L. A.; Orme-Johnson, W. H.; Walsh, C. T. *Proc.Natl.Acad.Sci.USA* **1989**, *86*, 3031-3035.

(46) Hedderich, R.; Albracht, S. P. J.; Linder, D.; Koch, J.; Thauer, R. K. *FEBS Lett.* **1992**, *298*, 65-68.

(47) Dai, S.; Schwendtmayer, C.; Johnasson, K.; Ramaswamy, S.; Schürmann, P.; Eklund, H. *Quart. Rev. of Biophy.* **2000**, *33*, 67-108.

(48) Walters, E. M.; Johnson, M. K. *Photosyn.Res.* **2004**, *79*, 249-264.

(49) Duin, E. C.; Madadi-Kahkesh, S.; Hedderich, R.; Clay, M. D.; Johnson, M. K. *FEBS Letters* **2002**, *512*, 263-268.

(50) *Iron-Sulfur Proteins*; Academic Press: San Diego, 1999.

(51) Johnson, M. K.; Smith IV, A. D. Iron-Sulfur Proteins; In *Encyclopedia of Inorganic Chemistry*; King, R. B., ed. John Wiley and Sons: Chichester, 2005; in press.

(52) Beinert, H.; Holm, R. H.; Münck, E. *Science* **1997**, *227*, 653-659.

(53) Rees, D. C. *Annu.Rev.Biochem.* **2002**, *71*, 221-246.

(54) Beinert, H. Iron-Sulfur Proteins: Properties and Functions; In *Cellular Implications of Redox Signaling*; Gitler, C., Danon, A., eds. Imperial College Press: London, 2003; pp 47-72.

(55) Broderick, J. B. Iron-Sulfur Clusters in Enzyme Catalysis; In *Comprehensive Coordination Chemistry II, Vol. 8*; McCleverty, J. A., Meyer, T. J., eds. Elsevier: Oxford, 2004; pp 739-757.

(56) Crouse, B. R.; Meyer, J.; Johnson, M. K. *J.Am.Chem.Soc.* **1995**, *117*, 9612-9613.

(57) Achim, C.; Golinelli, M.-P.; Bominaar, E. L.; Meyer, J.; Münck, E. *J.Am.Chem.Soc.* **1996**, *118*, 8168-8169.

(58) Johnson, M. K.; Duin, E. C.; Crouse, B. R.; Golinelli, M.-P.; Meyer, J. *Valence-Delocalized [2Fe-2S]$^{+}$ Clusters*; In *Spectroscopic Methods in Bioinorganic Chemistry*; Solomon, E. I., Hodgson, K. O., eds. American Chemical Society: Washington, D.C., 1998; pp 286-301.

(59) Link, T. A. *Adv.Inorg.Chem.* **1999**, *47*, 83-157.

(60) Calzolai, L.; Zhou, Z.-H.; Adams, M. W. W.; La Mar, G. N. *J.Am.Chem.Soc.* **1996**, *118*, 2513-2514.

(61) Sofia.H.J.; Chen.G.; Hetzler, B. G.; Reyes-Spindola, J. F.; Miller, N. E. *Nucleic Acids Res.* **2001**, *29*, 1097-1106.

(62) Walsby, C. J.; Hong, W.; Broderick.W.E.; Cheek, J.; Ortillo, D.; Broderick.J.B.; Hoffman, B. M. *J.Am.Chem.Soc.* **2002**, *124*, 3143-3151.

(63) Cheek, J.; Broderick.J.B. *J.Biol.Inorg.Chem.* **2001**, *6*, 209-226.

(64) Svetlitchnyi, V.; Dobbek, H.; Meyer-Klaucke, W.; Meins, T.; Theile, T.; Rõmer, P.; Huber, R.; Meyer, O. *Proc.Natl.Acad.Sci.USA* **2004**, *101*, 446-451.

(65) Staples, C. R.; Gaymard, E.; Stritt-Etter, A.-L.; Telser, J.; Hoffman, B. M.; Schürmann, P.; Knaff, D. B.; Johnson, M. K. *Biochemistry* **1998**, *37*, 4612-4620.

(66) Williams, C. H., Jr. Lipoamide Dehydrogenase, Glutathione Reductase, Thioredoxin Reductase, and Mercuric Ion Reductase-A Family of Flavoenzyme Transhydrogenases; In *Chemistry and Biochemistry of Flavoenzymes*; Müller, F., ed. CRC Press: Boca Raton, FL, 1992; pp 121-211.

(67) Williams, C. H., Jr. *FASEB J.* **1995**, *9*, 1267-1276.

(68) Williams, C. H., Jr.; Arscott, L. D.; Müller, S.; Lennon, B. W.; Ludwig, M. L.; Wang, P.-F.; Veine, D. M.; Becker, K.; Schirmer, R. H. *Eur.J.Biochem.* **2000**, *267*, 6110-6117.

(69) Arscott, L. D.; Thorpe, C.; Williams, C. H., Jr. *Biochemistry* **1981**, *20*, 1513-1520.

(70) Thorpe, C.; Williams, C. H. Jr. *J.Biol.Chem.* **1976**, *251*, 3553-3557.

(71) Thorpe, C.; Williams, C. H. Jr. *J.Biol.Chem.* **1976**, *251*, 7726-7728.

(72) Williams, C. H. Jr.; Thorpe, C.; Arscott, L. D. Functional roles of the two active site cysteine residues generated on reduction of lipoamide dehydrogenase and glutathione reductase; In *Mechanisms of Oxidizing Enzymes*; Singer, T. P., Ondarza, R. N., eds. Elsevier/North-Holland: New York, 1978; pp 3-16.

(73) Schulz, G. E.; Schirmer, R. H.; Sachsenheimer, W.; Pai, E. F. *Nature* **1978**, *273*, 120-124.

(74) Thieme, R.; Pai, E. F.; Schirmer, R. H.; Schulz, G. E. *J.Mol.Biol.* **1981**, *152*, 763-782.

(75) Thorpe, C.; Williams, C. H. Jr. *Biochemistry* **1981**, *20*, 1507-1515.

(76) Fox, B. S.; Walsh, C. T. *Biochemistry* **1983**, *22*, 4082-4086.

(77) Prongay, A. J.; Engelke, D. R.; Williams, C. H. Jr. *J.Biol.Chem.* **1989**, *264*, 2656-2664.

(78) Prongay, A. J.; Williams, C. H. Jr. *J.Biol.Chem.* **1990**, *265*, 18968-18975.

(79) O'Donnell, M. E.; Williams, C. H. Jr. *J.Biol.Chem.* **1984**, *259*, 2243-2251.

(80) Sahlman, L.; Lambeir, A.; Lindskog, S. *Eur.J.Biochem.* **1986**, *156*, 479-488.

(81) Prongay, A. J.; Williams, C. H. Jr. *J.Biol.Chem.* **1992**, *267* , 25181-25188.

(82) Gilberger, T.-W.; Walter, R. D.; Müller, S. *J.Biol.Chem.* **1997**, *272*, 29584-29589.

(83) Veine, D. M.; Mulrooney, S. B.; Wang, P.-F.; Williams, C. H. Jr. *Prot.Sci.* **1998**, *7*, 1441-1450.

(84) Matthews, R. G.; Williams, C. H. Jr. *J.Biol.Chem.* **1976**, *251*, 3956-3964.

(85) Pai, E. F.; Schirmer, R. H.; Schulz, G. E. Structural studies of crystalline glutathione reductase from human erythrocytes; In *Mechanisms of Oxidizing Enzymes*; Singer, T. P., Ondarza, R. N., eds. Elsevier/North-Holland: New York, 1976; pp 17-22.

(86) O'Donnell, M. E.; Williams, C. H. Jr. *J.Biol.Chem.* **1983**, *258*, 13795-13805.

(87) Rietveld, P.; Arscott, L. D.; Berry, A.; Scrutton, N. S.; Deonarain, M. P.; Perham, R. N.; Williams, C. H., Jr. *Biochemistry* **1994**, *33*, 13888-13895.

(88) Mulrooney, S. B.; Williams, C. H., Jr. *Biochemistry* **1994**, *33*, 3148-3154.

(89) Krauth-Siegel, R. L.; Arscott, L. D.; Schönleben-Janas, A.; Schirmer, R. H.; Williams, C. H., Jr. *Biochemistry* **1998**, *37*, 13968-13977.

(90) Staples, C. R.; Ameyibor, E.; Fu, W.; Gardet-Salvi, L.; Stritt-Etter, A.-L.; Schürmann, P.; Knaff, D. B.; Johnson, M. K. *Biochemistry* **1996**, *35*, 11425-11434.

(91) Schürmann, P.; Gardet-Salvi, L. *Chimia* **1993**, *47*, 245-246.

(92) Marc-Martin, S.; Spielmann, A.; Stutz, E.; Schürmann, P. *Biochim. Biophy. Acta* **1993**, *1183*, 207-209.

(93) Tsugita, A.; Yano, K.; Gardet-Salvi, L.; Schürmann, P. *Prot. Seq. Data Anal.* **1991**, *419*.

(94) Chow, L.-P.; Iwadate, H.; Yano, K.; Kamo, M.; Tsugita, A.; Gardet-Salvi, L.; Stritt-Etter, A.-L.; Schürmann, P. *Eur.J.Biochem.* **1995**, *231*, 149-156.

(95) Gaymard, E.; Franchini, L.; Manieri, W.; Stutz, E.; Schürmann, P. *Plant Sci.* **2000**, *158*, 107-113.

(96) Manieri, W.; Franchini, L.; Raeber, L.; Dai, S.; Stritt-Etter, A.-L.; Schürmann, P. *FEBS Lett.* **2003**, *549*, 167-170.

(97) Schwendtmayer, C.; Manieri, W.; Hirasawa, M.; Knaff, D. B.; Schürmann, P. In *Photosynthesis: Mechanisms and Effects*; Garab, G., ed. Kluwer Academic Publishers: Dordrecht, The Netherlands, 1998; pp 1927-1930.

(98) Schürmann, P. *Meth.Enzymol.* **2002**, *347*, 403-411.

(99) Glauser, D. A.; Bourquin, F.; Manieri, W.; Schürmann, P. *J.Biol.Chem.* **2004**, *279*, 16662-16669.

(100) Jameson, G. N. L.; Walters, E. M.; Manieri, W.; Schurmann, P.; Johnson, M. K.; Huynh, B. H. *J.Am.Chem.Soc.* **2003**, *125*, 1146-1147.

(101) Walters, E. M.; Garcia-Serres, R.; Jameson, G. N. L.; Glauser, D. A.; Bourquin, F.; Manieri, W.; Schürmann, P.; Johnson, M. K.; Huynh, B. H. *J.Am.Chem.Soc.* **2005**, *submitted for publication*.

(102) Dauter, Z.; Sieker, L. C.; Wilson, K. S. *Acta Crystallogr.* **1992**, *48*, 42-59.

(103) Jacobson, B. L.; Chae, Y. K.; Markley, J. L.; Rayment, I.; Holden, H. M. *Biochemistry* **1993**, *32*, 6788-6793.

(104) Schipke, C. G.; Goodin, D. B.; McRee, D. E.; Stout, C. D. *Biochemistry* **1999**, *38*, 8228-8239.

(105) Surerus, K. K.; Münck, E.; Moura, I.; Moura, J. J. G.; LeGall, J. *J.Am.Chem.Soc.* **1987**, *109*, 3805-3807.

(106) Breton, J. L.; Duff, J. L. C.; Butt, J. N.; Armstron, F. A.; George, S. J.; Petillot, Y.; Forest, E.; Schafer, G.; Thomson, A. J. *Eur.J.Biochem.* **1995**, *233*, 937-946.

Figure 1.1 The four basic structures for iron-sulfur clusters in biology as determined by x-ray crystallography. Structures are taken from coordinates deposited in the Protein Data Bank: A. Fe Rd, PDB ID# 8RXN, rubredoxin from *Desulfovibrio vulgaris*;[102] B. [2Fe-2S], PDB ID# 1FRD, *Anabaena* pcc7120 Fd;[103] C. [3Fe-4S], PDB ID# 6FDR, *Azotobacter vinelandii* FdI;[104] D. [4Fe-4S], PDB ID# 6FDR, *A. vinelandii* FdI.[104] Color code: purple, Fe; yellow, S. Adapted from reference 51.

A

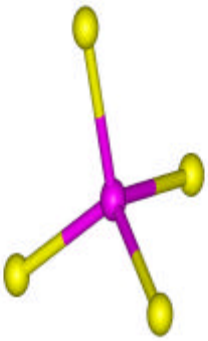

Fe

B

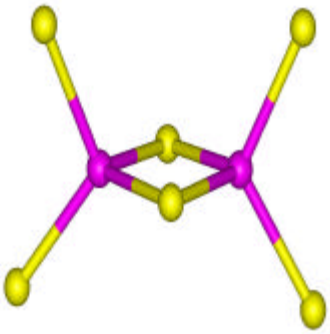

[2Fe-2S]

C

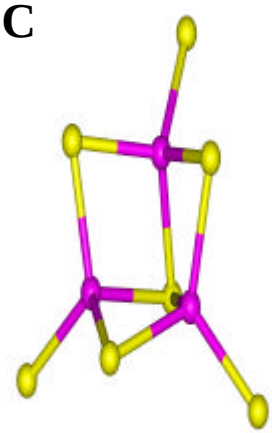

[3Fe-4S]

D

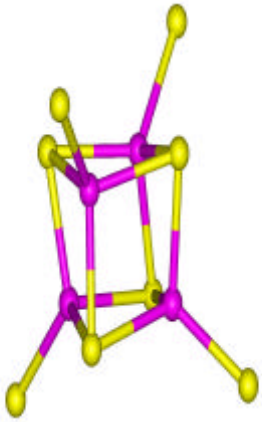

[4Fe-4S]

Figure 1.2 Ground state spin (*S*) and valence-delocalization schemes for the fundamental types of Fe-S centers. Discrete $[3Fe\text{-}4S]^{-}$ clusters are shown in parenthesis since they have not been observed in any protein. These clusters have, however, been identified as fragments of heterometallic cubane clusters.[105] Reduction of the $[3Fe\text{-}4S]^{+}$ clusters by three electrons to yield the $[3Fe\text{-}4S]^{2-}$ cluster occurs with the concomitant addition of three protons.[106] Valence-delocalized $[2Fe\text{-}2S]^{+}$ clusters have only been observed in the C56S and C60S variants of *Clostridium pasteruianum* 2Fe Fd.[56-58] Color code: Fe^{3+}, red; Fe^{2+}, blue; $Fe^{2.5+}$, green; S, yellow; O, white.[51]

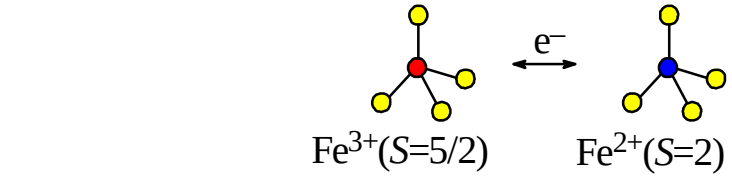

Fe^{3+}(*S*=5/2) Fe^{2+}(*S*=2)

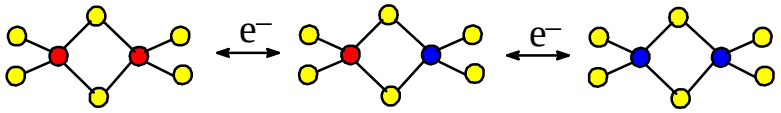

$[2Fe\text{-}2S]^{2+}$(*S*=0) $[2Fe\text{-}2S]^{+}$(*S*=1/2) $[2Fe\text{-}2S]^{0}$ (*S*=0)

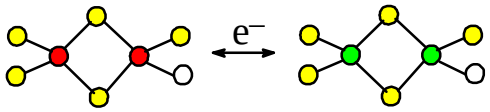

$[2Fe\text{-}2S]^{2+}$(*S*=0) $[2Fe\text{-}2S]^{+}$(*S*=9/2)

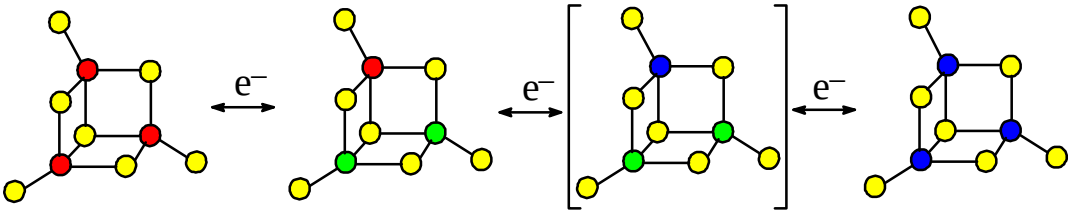

$[3Fe\text{-}4S]^{+}$(*S*=1/2) $[3Fe\text{-}4S]^{0}$(*S*=2) $[3Fe\text{-}4S]^{-}$(*S*=5/2) $[3Fe\text{-}4S]^{2-}$(*S*=?)

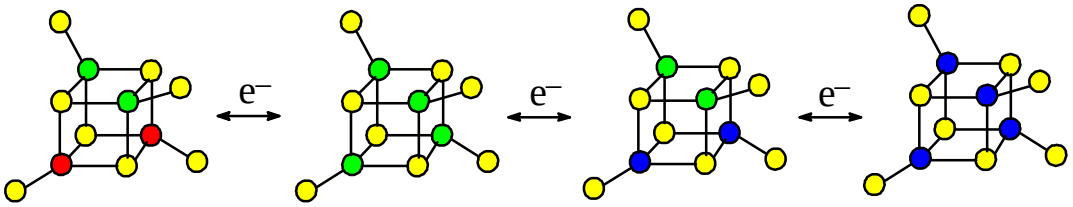

$[4Fe\text{-}4S]^{3+}$(*S*=1/2) $[4Fe\text{-}4S]^{2+}$(*S*=0) $[4Fe\text{-}4S]^{+}$(*S*=1/2 or 3/2) $[4Fe\text{-}4S]^{0}$(*S*=4)

Figure 1.3 Ranges of midpoint potentials (mV versus NHE) for biological Fe-S centers. $[2Fe\text{-}2S]^{2+,+}_{R}$, Rieske-type Fe-S centers.[51]

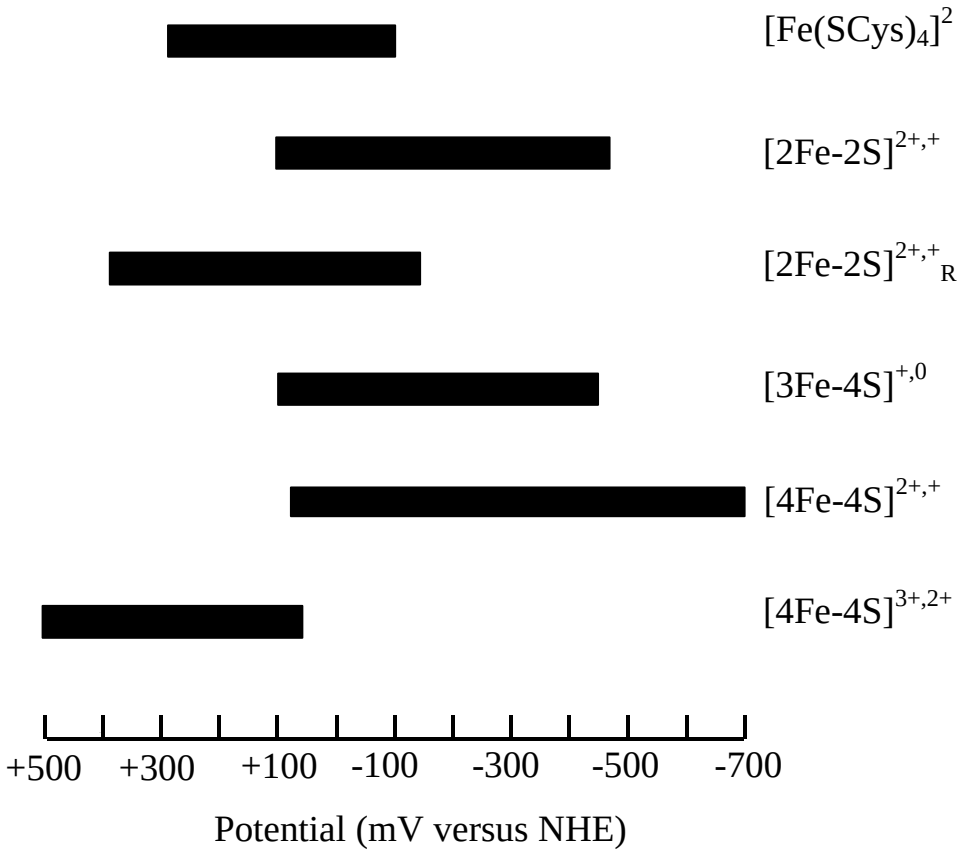
[Fe(SCys)4]2
[2Fe-2S]2+,+
[2Fe-2S]2+,+R
[3Fe-4S]+,0
[4Fe-4S]2+,+
[4Fe-4S]3+,2+
+500
+300
+100
-100
-300
-500
-700
Potential (mV versus NHE)

Scheme 1.1 Simplified mechanistic scheme for the reduction of oxidized glutathione disulfide by glutathione reductase. S^{63}-S^{58}, active-site disulfide between Cys63 and Cys58; F, FAD-cofactor; B, active-site base; GSSG, oxidized glutathione disulfide; GR, glutathione reductase; GSH, reduced glutathione; dashed arrow, charge transfer complex. Adapted from reference 64.

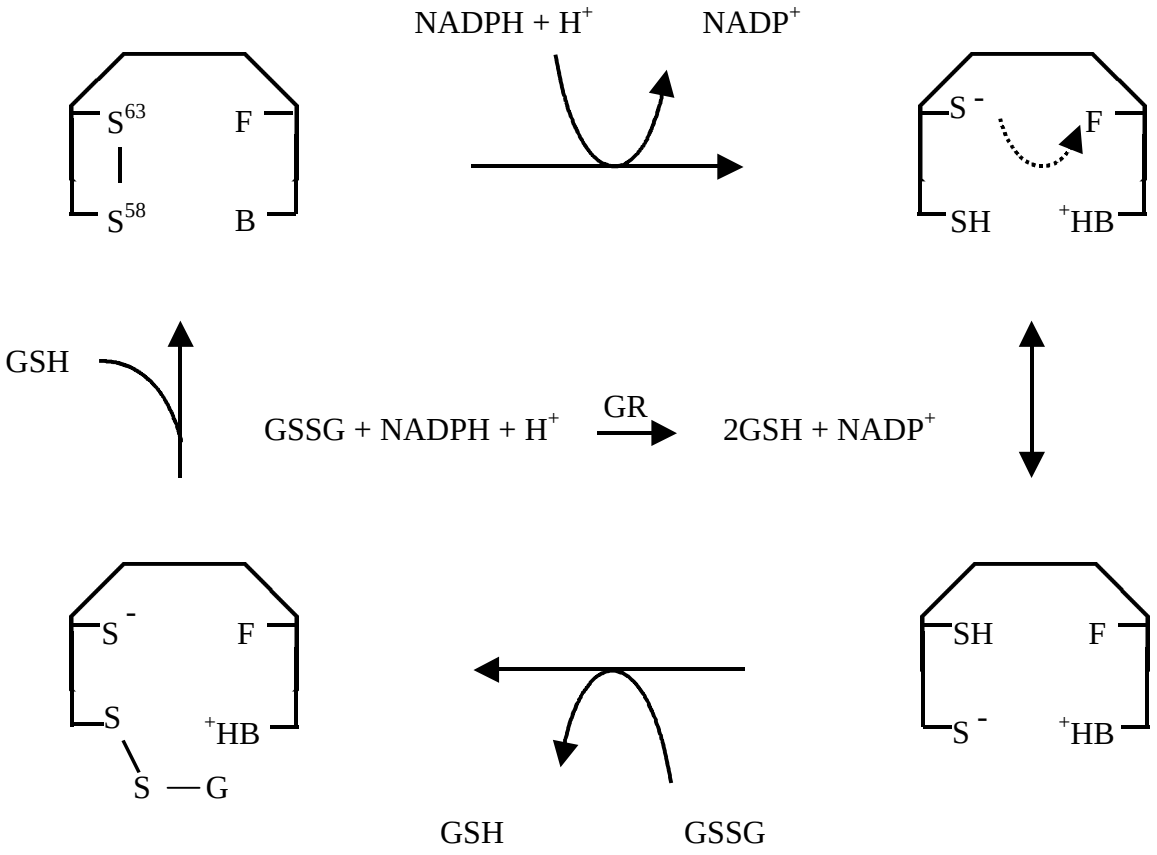
NADPH + H+
NADP+
S63
F
S58
B
S -
F
SH
+HB
GSH
GSSG + NADPH + H+
GR
2GSH + NADP+
S -
F
S
+HB
S — G
SH
F
S -
+HB
GSH
GSSG

CHAPTER 2

FERREDOXIN:THIOREDOXIN REDUCTASE: DISULFIDE REDUCTION CATALYZED VIA NOVEL SITE-SPECIFIC [4Fe–4S] CLUSTER CHEMISTRY[1]

[1] Reproduced in full with kind permission of Springer Science and Business Media from: Walters, E.M. and Johnson, M.K. *Photosynth. Res.* **2004,** *79, 3,* 249-264. Department of Chemistry and the Center for Metalloenzyme Studies, University of Georgia, Athens, GA, 30602, USA.

Key words: Ferredoxin:thioredoxin reductase, heterodisulfide reductase, catalytic mechanism, iron-sulfur cluster, electron paramagnetic resonance, electron-nuclear double resonance, magnetic circular dichroism, resonance Raman, Mössbauer

Abbreviations: FTR – ferredoxin:thioredoxin reductase; HDR – heterodisulfide reductase; Trx – thioredoxin, Fd – ferredoxin, NEM – *N*-ethylmaleimide; HiPIP – high-potential iron-sulfur protein; ENDOR – electron-nuclear double resonance; VTMCD – variable-temperature magnetic circular dichroism; CH_3-S-CoM – methyl coenzyme M; CoM-SH – coenzyme M; CoB-SH – coenzyme B

Abstract

Thioredoxin-mediated light regulation in plant chloroplasts involves a unique class of disulfide reductases that catalyze disulfide reduction in two one-electron steps using a [2Fe–2S] ferredoxin as the electron donor and an active site comprising a [4Fe–4S] cluster and a redox-active disulfide. This review summarizes structural and spectroscopic studies of ferredoxin:thioredoxin reductase (FTR) and a chemically modified form, termed NEM-FTR, which provides a stable analog of the one-electron reduced catalytic intermediate. Detailed spectroscopic characterization of FTR and NEM-FTR using absorption, EPR, electron-nuclear double resonance, variable-temperature magnetic circular dichroism, resonance Raman and Mössbauer spectroscopies indicate that the one-electron reduced catalytic intermediate involves two-electron disulfide reduction coupled with one-electron cluster oxidation of a $[4Fe–4S]^{2+}$ cluster to yield a unique type of $S = 1/2$ $[4Fe–4S]^{3+}$ cluster with two cysteine residues ligated at a specific Fe site. The results provide the basis for a novel mechanism for disulfide cleavage in two one-electron steps involving site-specific [4Fe–4S] cluster chemistry. A similar mechanism is proposed for direct [4Fe–4S]-mediated cleavage of the CoM–S–S–CoB heterodisulfide in methanogenic archaea by heterodisulfide reductases.

Introduction

Biological disulfide reduction is generally catalyzed by a large family of pyridine nucleotide-disulfide oxidoreductase flavoenzymes, including thioredoxin reductase, glutathione reductase, lipoamide dehydrogenase, trypanothione reductase, mercuric reductase, and NADH peroxidase. This family of enzymes use an active-site dithiol-disulfide to transfer reducing equivalents from a nearby FAD to external substrates and have been well characterized both structurally and mechanistically, for reviews see (Williams 1992; Williams 1995; Williams et al. 2000). However, the paradigm of using two-electron redox chemistry involving NADPH, FAD and a redox active disulfide to effect substrate disulfide reduction does not always apply. Over the past decade, ferredoxin:thioredoxin reductase (FTR) in chloroplasts and heterodisulfide reductase (HDR) in methanogenic archaea have emerged as new types of disulfide reductases. These enzymes catalyze disulfide reduction via sequential one-electron redox chemistry using one-electron donors and an active site involving an Fe-S cluster that interacts directly with either an active-site disulfide in the case of FTR or the substrate disulfide in the case of HDR. The objective of this minireview is to summarize the spectroscopic, structural and mechanistic studies that have led to the current understanding of how both FTR and HDR use novel site-specific Fe-S cluster chemistry to effect disulfide reduction in two sequential one-electron steps. A more detailed account of the structural aspects of FTR can be found in the minireview by Eklund and coworkers (Dai et al. 2004).

Ferredoxin:thioredoxin reductase

Ferredoxin:thioredoxin reductase is found in chloroplasts and plays a central role in light regulation of the activity of enzymes involved in oxygenic photosynthesis, for recent review see (Dai et al. 2000a; Schürmann and Buchanan 2001; Schürmann 2003). Upon illumination of thylakoid membranes, the photosynthetic electron transfer chain of photosystem I reduces the chloroplast [2Fe–2S] ferredoxin (Fd). FTR catalyzes the reduction of disulfides on thioredoxin (Trx) *f* and *m* using the reduced [2Fe–2S] Fd as the electron donor:

$$2Fd_{red} + Trx_{ox} + 2H^{+} \rightarrow 2Fd_{ox} + Trx_{red}$$

The reduced thioredoxins activate or inactivate numerous target enzymes involved with oxygenic photosynthesis by reduction of regulatory disulfides (Schürmann and Jacquot 2000; Buchanan et al. 2002; Balmer et al. 2003).

***Structure*:** FTR is a αβ-heterodimer composed of a highly conserved 13 kDa catalytic β-subunit that contains a redox-active disulfide and a [4Fe–4S] cluster, and a variable α-subunit of similar or smaller size with relatively low sequence conservation between species. The structure of FTR from *Synechocystis* sp. PCC6803 has been determined at 1.6 Å resolution and was found to be a concave disk, 40-50 Å in diameter and only 10 Å at the center, where the [4Fe–4S] cluster is located, Fig 2.1 (Dai et al. 2000b). The binding sites for the [2Fe–2S] Fd and Trx were proposed to be on opposite sides of the disk, with the Fd [2Fe–2S] cluster positioned for efficient electron transfer to the FTR [4Fe–4S] cluster and the Trx disulfide in close proximity to the redox-active disulfide on FTR, in accord with likelihood of a heterodisulfide catalytic intermediate.

The crystallographically defined active-site structure of *Synechocystis* FTR comprises an asymmetrically disposed cysteine disulfide in close proximity to an all-cysteinyl ligated [4Fe–4S] cluster, see Fig. 2.2, and is essentially the same as that predicted by cysteine chemical modification (Chow et al. 1995) and spectroscopic studies (Staples et al. 1996) of spinach FTR. In accord with the proposal that one of the cysteines of the active-site disulfide becomes coordinated to the cluster during catalytic cycling (Staples et al. 1996; Staples et al. 1998), the crystal structure shows that the S of Cys87 is positioned 3.1 Å from both a cluster Fe and the S atom of the coordinating cysteine residue and 3.4 Å from the S atom of a μ_3-S^{2-}. The possibility of a weak interaction between the cluster and the active-site disulfide is also suggested by the μ_3-S-Fe-S(Cys55) angle that is 129° compared to the idealized 109.5° expected for a tetrahedrally ligated Fe center. The crystal structure also shows His86 poised to effect protonation of an active-site cysteine following reductive cleavage.

***Spectroscopy*:** Insight into the catalytic mechanism of FTR has largely come from spectroscopic studies of wild-type spinach FTR and a chemically modified inactive form (NEM-FTR) in which Cys54 (equivalent to Cys57 in *Synechocystis* FTR) has been selectively alkylated with *N*-ethylmaleimide (NEM) (Staples et al. 1996; Staples et al. 1998). A summary of the UV-visible absorption, EPR, electron-nuclear double resonance (ENDOR), variable-temperature magnetic circular dichroism (VTMCD), resonance Raman, and Mössbauer results delineated in terms of the as-isolated and NEM-modified forms of FTR is presented below. The majority of the published spectroscopic data was obtained using wild-type spinach FTR (Staples et al. 1996; Staples et al. 1998), and this review provides the opportunity to present data for recombinant spinach FTR and the

structurally characterized recombinant *Synechocystis* FTR. In general, very similar spectroscopic data were observed for all three enzymes. However, both recombinant enzymes were initially purified with varying amounts of FTR in a form that closely resembles NEM-FTR based on EPR studies (up to 20% based on EPR spin quantitations). The EPR silent form of recombinant FTR, termed as-isolated FTR in this review, was generally obtained only after redox cycling the enzyme. Hence, the NEM-FTR-like species in recombinant samples is likely to correspond to an alternative active conformation that is formed as a result of overexpressing FTR that has never undergone catalytic turnover.

As-isolated FTR: The UV-visible absorption spectra of as-isolated forms of native spinach FTR (Staples et al. 1996) and recombinant *Synechocystis* FTR, see Fig. 2.3, consist of a protein band centered at 278 nm, with a poorly resolved shoulder at 330 nm and a broad shoulder centered at 410 nm that are characteristic of multiple overlapping charge transfer transitions of a $[4Fe–4S]^{2+}$ center. The absence of an EPR signal is also consistent with the presence of an $S = 0$ $[4Fe–4S]^{2+}$ cluster, but the most definitive evidence comes from resonance Raman and Mössbauer studies.

The resonance Raman spectrum of recombinant *Synechocystis* FTR in the Fe-S stretching region is shown in Fig. 2.4 and is essentially identical to that reported for wild-type spinach FTR (Staples et al. 1996), except for 2-3 cm^{-1} upshifts in corresponding bands. The spectrum is characteristic of $[4Fe–4S]^{2+}$ clusters with complete cysteinyl ligation and the bands are readily assigned under effective tetrahedral symmetry to symmetric and asymmetric Fe-S stretching modes predominantly involving either bridging (S^b) or terminal (S^t) S atoms (Staples et al. 1996): $\nu(T_2)(Fe\text{-}S^b)$, 253 cm^{-1};

$\nu(T_1)(Fe\text{-}S^b)$, 282 cm^{-1}; $\nu(E)(Fe\text{-}S^b)$, 312 cm^{-1}; $\nu(A_1)(Fe\text{-}S^b)$, 337 cm^{-1}; $\nu(T_2)(Fe\text{-}S^t)$, 360 cm^{-1}; $\nu(T_2)(Fe\text{-}S^b)$, 389 cm^{-1}; $\nu(A_1)(Fe\text{-}S^t)$, 389 cm^{-1}. These assignments are based on the close correspondence with the spectra of synthetic model complexes such as $[[4Fe\text{-}4S](SCH_2Ph)_4]^{2-}$ which have been rigorously assigned based on ^{34}S isotope shifts and normal mode calculations (Czernuszewicz et al. 1987).

Although the distortions from idealized tetrahedral symmetry for the $[Fe_4S^b{}_4S^t{}_4]^{2-}$ center that are apparent in the crystal structure of *Synechocystis* FTR are not manifest in the resonance Raman data, they are evident in Mössbauer data. The Mössbauer spectrum of as-isolated recombinant spinach FTR, purified from cells grown on an ^{57}Fe-enriched medium, shows a quadrupole doublet with a prominent shoulder on the high-energy line, see Fig. 2.5 (Jameson et al. 2003). The ability to deconvolute the spectrum into three components with an intensity ratio of 1:1:2, see Fig. 2.5, coupled with the diamagnetic ground state that is evident in spectra recorded in a strong applied field of 8T, indicate the presence of a site-differentiated $S = 0$ $[4Fe–4S]^{2+}$ cluster. This is anomalous for $[4Fe–4S]^{2+}$ clusters with complete cysteinyl ligation, which generally exhibit Mössbauer spectra composed of two valence-delocalized $Fe^{2.5+}Fe^{2.5+}$ pairs in a 1:1 ratio. While the parameters of the major quadrupole doublet in FTR (δ = 0.44 mm/s, ΔE_Q = 1.23 mm/s) are indicative of a valence-delocalized $Fe^{2.5+}Fe^{2.5+}$ pair, the parameters for the other two Fe sites suggest a more localized valence pair with significant Fe^{2+} (δ = 0.56 mm/s, ΔE_Q = 1.80 mm/s) and partial Fe^{3+} (δ = 0.39 mm/s, ΔE_Q = 1.02 mm/s) character. Since weak interaction with the active-site disulfide would be expected to promote charge build up and hence more ferrous character at a specific Fe site, the site with significant ferrous character is assigned to the unique Fe site that is proximal to the active-site disulfide in

FTR (Jameson et al. 2003), see Fig. 2.2. Hence the unique properties of the $[4Fe–4S]^{2+}$ in the FTR active site are already apparent in the resting state of the enzyme.

Reduction of the $[4Fe–4S]^{2+}$ cluster in FTR does not appear to be possible at physiologically relevant potentials. Dithionite alone is not able to reduce the active-site disulfide (Schürmann et al. 1995) and induces negligible changes in the UV-visible absorption properties of the $[4Fe–4S]^{2+}$ cluster (Staples et al. 1996), see Fig. 2.3. The physiological electron donor, reduced chloroplast [2Fe–2S] Fd, and reduced methyl or benzyl viologen are known to effect reduction of the active-site disulfide in FTR. However, no evidence for $S = 1/2$ or 3/2 $[4Fe–4S]^{+}$ clusters was observed in EPR and VTMCD studies of samples of FTR that were reduced using reduced spinach [2Fe–2S] Fd, reduced methyl or benzyl viologen, or photochemically using deazaflavin (Staples et al. 1996), indicating that the $[4Fe–4S]^{2+,+}$ couple must be < -650 mV in samples of FTR containing a reduced active-site disulfide.

Oxidation of spinach FTR with ferricyanide results in a fast relaxing $S = 1/2$ resonance, $g = 2.092, 2.045, 2.008$, indicative of an $S = 1/2$ $[4Fe–4S]^{3+}$ cluster (Staples et al. 1996), see Fig. 2.6. This EPR signal was first observed in ferralterin (alternative Fe protein) from *Nostoc muscorum* (de la Torre et al. 1982), which was subsequently shown to correspond to FTR by Droux and coworkers (Droux et al. 1987). However, since EPR redox titrations indicate that the midpoint potential of the $[4Fe–4S]^{3+,2+}$ couple in FTR is above +400 mV (de la Torre et al. 1982; Staples et al. 1996), whereas the redox potentials for the $[2Fe–2S]^{2+,+}$ cluster in the [2Fe–2S] Fd and the redox-active disulfide in FTR are –430 mV (n = 1) and –320 mV (n = 2), respectively (Salamon et al. 1995;

Hirasawa et al. 1999), it seems unlikely that the $[4Fe–4S]^{3+,2+}$ couple in FTR is physiologically relevant.

NEM-FTR: Selective NEM alkylation of the one of the active-site cysteine residues (Cys54 in spinach FTR and Cys57 in *Synechocystis* FTR) in reduced FTR results in the formation of NEM-FTR; a stable form of the enzyme with properties completely different to those of as-isolated FTR (Schürmann and Gardet-Salvi 1993; Staples et al. 1996; Staples et al. 1998). NEM-FTR is isolated in a paramagnetic state with a well-defined near-axial $S = 1/2$ EPR signal (g = 2.112, 1.997, 1.984 for spinach NEM-FTR (Staples et al. 1996) and g = 2.108, 1.993, and 1.981 for *Synechocystis* NEM-FTR) accounting for 1.0 spin/FTR, see Fig. 2.6. This EPR signal arises from an oxidized form of the enzyme, since the resonance is lost on dithionite reduction, in a reversible one-electron process with a midpoint potential of –210 mV for spinach NEM-FTR (Staples et al. 1996) and –145 mV for *Synechocystis* NEM-FTR, see Fig. 2.7. The significance of NEM-FTR for understanding the catalytic mechanism of FTR lies in the observation that analogous EPR signals have been observed as transient intermediates during both benzyl viologen reduction and catalytic turnover of wild-type spinach FTR (Staples et al. 1998), see Fig. 2.8. An EPR signal indistinguishable from that observed with NEM-FTR was observed in samples of native FTR that were frozen rapidly following anaerobic reduction with 1 equivalent of reduced benzyl viologen. The resonance maximally accounts for 0.1 spin/molecule and was not observed in samples treated with > 2 equivalents of reduced benzyl viologen. Moreover, the same resonance was observed in samples of FTR that were rapidly frozen during turnover with excess Trx *f*, using reduced benzyl viologen as the electron donor. An additional transient resonance corresponding

either to an isotropic radical centered at 2.01 or an axial $S = 1/2$ resonance with $g_{\|}$ = 2.074 and $g_{\perp}$ = 2.01 was also observed. Detailed freeze-quench EPR studies are currently in progress to clarify the nature and time evolution of the paramagnetic intermediates and the results will be reported elsewhere. Nevertheless, the available EPR data clearly indicate that NEM-FTR provides a stable analog of a one-electron reduced intermediate in the FTR catalytic cycle, and this prompted detailed characterization of the structural, electronic, and magnetic properties using the full range of biophysical spectroscopic approaches.

Since NEM-FTR is paramagnetic in the oxidized state and exhibits an $S = 1/2$ EPR signal with $g_{av} > 2.0$, the most obvious interpretation is that it contains a $[4Fe–4S]^{3+}$ cluster. However, several properties of NEM-FTR are atypical compared to the $[4Fe–4S]^{3+,2+}$ centers in high potential iron-sulfur proteins (HiPIPs) and as-isolated FTR. First, the EPR resonance in oxidized NEM-FTR is slow relaxing and can be observed up to at least 150 K without significant broadening (Staples et al. 1996), whereas conventional $[4Fe–4S]^{3+}$ centers in oxidized HiPIPs (Dunham et al. 1991) and ferricyanide-oxidized FTR (Staples et al. 1996) are fast relaxing and only observable without significant broadening at temperatures below 30 K. Second, the midpoint potential is at least 500 mV more negative than the $[4Fe–4S]^{3+,2+}$ couple in native FTR (+420 mV) and out of the range established for $[4Fe–4S]^{3+,2+}$ couples in HiPIPs (+50 to +450 mV) (Meyer et al. 1983). Third, the equivalent EPR signal is induced in as-isolated FTR under reducing rather than oxidizing conditions. The alternative possibility is that $S = 1/2$ species in NEM-FTR corresponds to a thiyl radical that is stabilized by close proximity to a $[4Fe–4S]^{2+}$ cluster. This hypothesis would account for the anomalous spin

relaxation and redox properties compared to conventional $[4Fe–4S]^{3+}$ clusters and proximity to the cluster could be invoked to explain the large *g*-value anisotropy compared to isolated thiyl radicals.

Although EPR data in isolation cannot discriminate between the $[4Fe–4S]^{3+}$ and cluster-stabilized thiyl radical proposals for NEM-FTR, the combination of UV-visible absorption, resonance Raman, VTMCD, ^{57}Fe- and ^{1}H-ENDOR, and Mössbauer spectroscopies all indicate a novel type of $[4Fe–4S]^{3+}$ cluster. The UV-visible absorption spectrum has pronounced shoulders at 330 and 430 nm, see Fig. 2.3, and is generally similar to that of $[4Fe–4S]^{3+}$ clusters in HiPIPs (Stephens et al. 1978). Furthermore, dithionite reduction results in an absorption spectrum indistinguishable from that of the $[4Fe–4S]^{2+}$ cluster in as-isolated FTR, see Fig. 2.3. Resonance Raman spectroscopy provides a more discriminating probe for structural changes in the cluster than absorption spectroscopy and the spectra of oxidized and reduced spinach (Staples et al. 1996) and *Synechocystis* (Fig. 2.4) NEM-FTR are readily interpreted in terms of presence of $[4Fe–4S]^{3+}$ and $[4Fe–4S]^{2+}$ clusters, respectively. In accord with the anticipated overall strengthening of Fe-S bonds, oxidation of the $[4Fe–4S]^{3+,2+}$ clusters in HiPIPs is generally accompanied by increases of 1-5 cm^{-1} in predominantly Fe-S^b stretching modes and increases of 9-29 cm^{-1} in the predominantly Fe-S^t stretching modes (Moulis et al. 1988; Backes et al. 1991). As shown in Figure 2.4, reduced NEM-FTR exhibits a resonance Raman spectrum essentially identical to that of $[4Fe–4S]^{2+}$ cluster in as-isolated FTR. Moreover, the changes induced by oxidation are completely consistent with the presence of a $[4Fe–4S]^{3+}$ cluster in as-isolated NEM-FTR: 0-3 cm^{-1} upshifts in the predominantly Fe-S^b stretching modes ($\nu(T_2)$(Fe-S^b) at 256 cm^{-1}, $\nu(T_1)$(Fe-S^b) at 282 cm^{-}

[1], $\nu(E)(Fe\text{-}S^b)$ at 313 cm^{-1}, $\nu(A_1)(Fe\text{-}S^b)$ at 340 cm^{-1}, and $\nu(T_2)(Fe\text{-}S^b)$ at 389 cm^{-1} in NEM-FTR) and 9-17 cm^{-1} upshifts in the predominantly $Fe\text{-}S^t$ stretching modes ($\nu(T_2)(Fe\text{-}S^t)$ at 368 cm^{-1} and $\nu(A_1)(Fe\text{-}S^t)$ at 406 cm^{-1} in NEM-FTR).

VTMCD provides a powerful method for investigating the excited-state electronic structure of paramagnetic transition metal centers. Moreover, since the VTMCD intensity of paramagnetic chromophores is critically dependent on spin-orbit coupling which is much larger for metal centers than for organic or sulfur based radicals (Johnson 2000), VTMCD provides a means for discriminating between the paramagnetic cluster and thiyl radical proposals for NEM-FTR. Very similar VTMCD spectra were observed for spinach and *Synechocystis* NEM-FTR, see Fig. 2.9, and magnetization studies at discrete wavelengths confirm that all transitions originate from the $S = 1/2$ ground state that is responsible for the EPR signal (Staples et al. 1996). While differences in the complex pattern of positive and negative bands between NEM-FTR, see Fig. 2.3, and the $[4Fe–4S]^{3+}$ clusters in oxidized HiPIPs (Johnson et al. 1982), reveal differences in the excited state electronic structure, particularly in the low energy region below 21000 cm^{-1}, the intensities are very similar indicating that the unpaired electron is associated with the cluster rather than a nearby thiyl radical. Hence the VTMCD data are consistent with a novel type of $[4Fe–4S]^{3+}$ cluster in oxidized NEM-FTR.

In addition to EPR, both ENDOR and Mössbauer spectroscopy have been used to assess the ground-state electronic properties of the Fe-S cluster in NEM-FTR. ^1H-ENDOR studies revealed non-exchangeable protons with proton hyperfine coupling constants in the range 0-15 MHz (Staples et al. 1998). These coupling constants are in the range reported for the β-CH_2 protons of cysteines ligated to $[4Fe–4S]^{3+}$ clusters (Staples

et al. 1998), but much smaller than the 50-60 MHz proton coupling constants that have been reported for cysteinyl radicals generated via γ-irradiation of cystine (Akasaka et al. 1964). ^{57}Fe-ENDOR studies provided evidence for two distinct Fe sites with ^{57}Fe coupling constants of approximately 34 and 28 MHz (Staples et al. 1998), and comparable values have been reported for the $[4Fe–4S]^{3+}$ clusters in model complexes (Rius and Lamotte 1989) and the oxidized HiPIPs from *Chromatium vinosum* and *Ectothiorhodospira halophila* (Houseman et al. 1992).

The ability of Mössbauer spectroscopy to investigate individual Fe sites within the cluster has led to a detailed assessment of the anisotropy of the ^{57}Fe coupling constants and characterization of the valence delocalization scheme in NEM-FTR (Jameson et al. 2003). In accord with the $S = 1/2$ ground state, the Mössbauer spectrum of NEM-FTR is paramagnetic and the spectrum of recombinant spinach NEM-FTR at 4.2 K in an applied field of 8 T is shown in Fig. 2.10. Three distinct components in a 1:1:2 intensity ratio are observed, with the major component corresponding to a valence-delocalized $Fe^{2.5+}Fe^{2.5+}$ pair with isomer shift and quadrupole splitting ($\delta = 0.44$ mm/s, $\Delta E_Q = 1.2$ mm/s) essentially identical to those in as-isolated FTR. The other two sites correspond to a diferric pair with $\delta = 0.30$ mm/s and $\Delta E_Q = 1.2$ mm/s for ferric site 1 and $\delta = 0.30$ mm/s and $\Delta E_Q = -1.2$ mm/s for ferric site 2. The opposite signs of the magnetic hyperfine coupling tensors, see Fig. 2.10, dictate antiparallel alignment of the spins for the mixed valence and diferric pairs and the magnitudes are similar to those observed for $[4Fe–4S]^{3+}$ clusters in oxidized HiPIPs (Middleton et al. 1980). Hence both the ENDOR and Mössbauer data indicate a $[4Fe–4S]^{3+}$ cluster similar to those found in oxidized

HiPIPs with the $S = 1/2$ ground state arising from antiferromagnetic coupling of the valence-delocalized $Fe^{2.5+}Fe^{2.5+}$ pair and a diferric pair.

The overall picture that emerges from the spectroscopic studies of NEM-FTR is that it contains a $[4Fe–4S]^{3+}$ cluster with vibrational properties as well as valence delocalization and magnetic coupling schemes very similar to those of $[4Fe–4S]^{3+}$ clusters in oxidized HiPIPs. However, the $[4Fe–4S]^{3+,2+}$ center in NEM-FTR is dramatically different from those in conventional HiPIPs and in native FTR in terms of redox potential, anisotropy and relaxation behavior of the $S = 1/2$ ground state, and detailed excited-state electronic structure as revealed by VTMCD. Moreover, because NEM-FTR corresponds to a stable analog of a one-electron reduced intermediate of FTR, structural interpretation of these differences lies at the heart of understanding the catalytic mechanism of FTR and rationalizing the paradox of how one-electron reduction results in one-electron oxidation of the cluster from the $[4Fe–4S]^{2+}$ to $[4Fe–4S]^{3+}$ oxidation states. The latter is best understood by considering the active site as being composed of both the $[4Fe–4S]^{2+}$ and the disulfide, with two-electron cleavage of the disulfide coupled with one-electron oxidation of the cluster resulting in a net one-electron reduction. Hence, the 500-600 mV decrease in the redox potential of the $[4Fe–4S]^{3+,2+}$ couple in the one-electron reduced intermediate compared to as-isolated FTR is required to facilitate cluster oxidation.

The key to understanding the anomalous properties of the $[4Fe–4S]^{3+,2+}$ cluster in NEM-FTR appears to be the availability of an additional cysteine in close proximity to the cluster. Hence the anomalous EPR and MCD properties of the $[4Fe–4S]^{3+}$ cluster in NEM-FTR and the dramatic decrease in midpoint potential of the $[4Fe–4S]^{3+,2+}$ couple

compared to conventional HiPIP-type clusters, were interpreted in terms of redox cycling involving reversible coordination of the $[4Fe–4S]^{3+}$ cluster by a fifth cysteinate ligand (Staples et al. 1996; Staples et al. 1998). However, prior to Mössbauer investigations, the site of attachment was left undefined with the possibilities including Fe, a μ_3-S^{2-}, or even a cysteinyl S (Staples et al. 1998). The key observation in comparing the Mössbauer data for the $[4Fe–4S]^{2+}$ cluster in as-isolated FTR and the $[4Fe–4S]^{3+}$ cluster in NEM-FTR is that the one-electron oxidation of the cluster primarily involves site-specific redox chemistry at the unique Fe site (isomer shift decrease from 0.56 mm/s to 0.30 mm/s) (Jameson et al. 2003). This site-specific redox chemistry implies that the weak interaction with the active-site disulfide that promotes more ferrous character at the unique Fe site in the resting state of FTR, is replaced by cysteinate ligation and hence exclusively ferric character at the unique Fe site in NEM-FTR. Consequently, the Mössbauer data dictate that NEM-FTR and the one-electron reduced intermediate in FTR, involve a $[4Fe–4S]^{3+}$ cluster with a unique five-coordinate Fe site involving two cysteinate ligands. In accord with this proposal, Holm and coworkers have synthesized cubane-type [4Fe–4S] complexes with bidentate thiolate coordination at a unique Fe site and shown that the redox potential for the $[4Fe–4S]^{3+,2+}$ couple is decreased by 600 mV compared to the equivalent complex with monovalent thiolate ligation (Ciurli et al. 1990).

***Mechanism*:** The spectroscopic and structural studies of FTR and NEM-FTR discussed above provide the foundation for the mechanistic proposal shown in Fig. 2.11. The mechanism shows how the cluster facilitates disulfide reduction in two sequential one-electron steps, by stabilizing the one-electron-reduced intermediate, and incorporates the thiol-disulfide interchange mechanism that has been established for the NADPH-

dependent flavin-containing disulfide oxidoreductases (Williams 1992). In common with the flavoprotein disulfide reductases, distinct roles for the cysteines of the active-site disulfide are proposed. The cysteine that forms a covalent adduct with the cluster (Cys87 in *Synechocystis* FTR) is termed the cluster interacting thiol and the cysteine (Cys57 in *Synechocystis* FTR) that attacks the substrate disulfide and forms the heterodisulfide intermediate is termed the interchange thiol.

Central to the mechanism is the formation of a one-electron-reduced intermediate with properties similar to NEM-FTR, following the first electron transfer from reduced [2Fe–2S] Fd. Formation of this intermediate both stabilizes the one-electron disulfide cleavage product, via covalent attachment of the cluster interacting thiol, and frees the interchange thiol to attack the Trx disulfide and form the heterodisulfide intermediate. Subsequent binding and electron transfer from a second molecule of reduced [2Fe–2S] Fd results in reduction of the NEM-FTR-like $[4Fe–4S]^{3+}$ heterodisulfide intermediate, thereby freeing the cluster interacting thiol to attack the heterodisulfide with reformation of the active-site disulfide and release of reduced Trx. Although the specifics of protonation steps are not known at this time, the proximity of His86 suggests an important role for this residue in mediating protonation and possibly deprotonation reactions and mutagenesis experiments are in progress to test this hypothesis. Further support for this mechanism has recently come from spectroscopic characterization of a covalent adduct of FTR and a Trx cysteine-to-alanine variant that provides a model of the heterodisulfide intermediate (Walters, E. M., Garcia-Serres, R., Jameson, G. N. L., Glauser, D.A., Bourquin, F., Manieri, W., Schürmann, P., Johnson, M. K., Huynh, B. H., submitted to *J. Am. Chem. Soc*. 03/24/2005). In addition, distinct roles for the cysteines

of the active-site disulfide have recently been confirmed by spectroscopic investigations of the C87A and C57S variants (Walters, E. M., Garcia-Serres, R., Jameson, G. N. L., Glauser, D.A., Bourquin, F., Manieri, W., Schürmann, P., Johnson, M. K., Huynh, B. H., submitted to *J. Am. Chem. Soc.* 03/24/2005).

The formation of the one-electron reduced intermediate has been shown to involve novel chemistry at a unique Fe site of a [4Fe–4S] cluster. The mechanism of this process is unknown, but is clearly of great interest in understanding the site-specific chemistry of [4Fe–4S] clusters in general and may well be relevant for elucidating the mechanism of the [4Fe–4S] cluster-mediated reductive cleavage of *S*-adenosylmethionine to yield a 5'-deoxyadenosyl radical in the radical-SAM superfamily (Cheek and Broderick 2001; Frey and Magnusson 2003; Jarrett, 2003). Three possible mechanisms are proposed in Fig. 2.12. The first involves a concerted reaction that utilizes the unique properties of the $[4Fe–4S]^{2+}$ cluster in FTR that result from weak interaction with the active-site disulfide (Jameson et al. 2003). This unique interaction induces charge build up on the unique Fe site, making it an electron donor with increased ferrous character, and thereby promoting polarization of the S-S bond such that the interchange thiol becomes an electron acceptor. Hence the active site appears to be tuned to act as one-electron acceptor and to promote disulfide cleavage via the formation of a five-coordinate intermediate. The two alternative mechanisms shown in Figure 2.12 involve conventional nucleophilic thiol chemistry and a radical-based intermediate, following electron transfer to $[4Fe–4S]^{2+}$ cluster to yield a transient $[4Fe–4S]^{+}$ cluster. The former mechanism invokes nucleophilic attack at the S of the cluster interacting thiol by the ligated cysteinyl S to yield a cluster-associated disulfide transient intermediate, which subsequently

accepts two electrons from the cluster to form the $[4Fe–4S]^{3+}$ cluster with two cysteinate ligands at a unique Fe site. The close proximity of the S atoms of Cys87 and Cys55 (3.1 Å, see Fig. 2.2) and the charge polarization of the disulfide may well facilitate the proposed nucleophilic attack. The latter invokes sequential one-electron reductions of the active-site disulfide by the cluster. The first yielding a transient intermediate involving a $[4Fe–4S]^{2+}$ with nearby a thiyl radical (possibly via a cystine anion radical intermediate), and the second resulting in reduction of the thiyl radical to yield a cysteinate that coordinates to the $[4Fe–4S]^{3+}$ cluster. Freeze-quench EPR and Mössbauer experiments are currently in progress in an attempt to discriminate between these three possibilities and to determine the kinetics and overall mechanism of FTR.

Heterodisulfide reductase

In the final step of methanogenesis in methanogenic archaea, methyl coenzyme M reductase catalyzes the reaction of methyl coenzyme M (CH_3–S–CoM) with coenzyme B (CoB–SH) to form methane and the heterodisulfide CoM–S–S–CoB (Thauer 1998). The heterodisulfide functions as the terminal electron acceptor of an energy conserving electron transport chain, in a process called disulfide respiration (Deppenmeier et al. 1999; Hedderich et al. 1998). Heterodisulfide reductase, the terminal enzyme in the disulfide respiratory chain, catalyzes the reversible reduction of the CoM-S-S-CoB heterodisulfide to yield coenzyme M (CoM–SH) and CoB–SH:

$$CoM–S–S–CoB + 2H^+ + 2e^- \rightarrow CoM–SH + CoB–SH$$

The enzyme is highly specific for its CoM–S–S–CoB and CoM–SH plus CoB–SH substrates and does not mediate the oxidation of CoM-SH or CoB-SH to the corresponding homodisulfides (Hedderich et al. 1989).

Two distinct types of HDR have been purified and characterized from *Methanothermobacter marburgensis* (formerly *Methanobacterium thermoautotrophicum* strain Marburg) and *Methanosarcina barkeri*. *M. marburgensis* HDR is an iron-sulfur flavoprotein composed of three subunits, HdrA, HdrB, and HdrC (Hedderich et al. 1990; Hedderich et al. 1994). HdrA contains binding motifs for FAD and four $[4Fe–4S]^{2+,+}$ clusters and HdrC contains binding motifs for two additional $[4Fe–4S]^{2+,+}$ clusters. HdrB has no characteristic Fe-S cluster binding motif, but does have two copies of a $CX_{31–32}CCX_{33–38}CX_2C$ motif that is conserved in the *M. barkeri* HDR and in thiol:fumarate reductase from *M. marburgensis* (Heim et al. 1998). In contrast, *M. barkeri* HDR, and the closely related *Methanosarcina thermophila* HDR (Simianu et al. 1998), are iron-sulfur hemoproteins, composed of a membrane-bound subunit, HdrE, containing two *b*-type cytochromes and a hydrophilic iron-sulfur subunit, HdrD, containing two binding motifs for $[4Fe–4S]^{2+,+}$ clusters in the N-terminus and the conserved cysteine motifs found *M. marburgensis* HdrB in the C-terminus (Künkel et al. 1997). Hence HDRs do not share a common flavin active site. Rather, the *M. barkeri* and *M. thermophila* HdrD subunit appears to be a fusion of *M. marburgensis* HdrC and HdrB subunits and the conserved cysteines that are common to HdrB and HdrD are potential ligands for a common active-site Fe-S cluster that has a role in cleaving the substrate heterodisulfide(Künkel et al. 1997).

***Spectroscopy*:** The number, type and redox properties of Fe-S clusters in *M. marburgensis* HDR has been investigated by EPR and resonance Raman spectroscopies (Madadi-Kahkesh et al. 2001). Oxidized HDR samples exhibited no signals attributable to paramagnetic Fe-S clusters and the resonance Raman spectrum was readily interpreted

exclusively in terms of $S = 0$ $[4Fe–4S]^{2+}$ clusters. In the absence of substrates, dye-mediated EPR redox titrations revealed a high-potential $[4Fe–4S]^{2+,+}$ center (E_m = -153 mV) that gives rise to a $S = 1/2$ $[4Fe–4S]^{+}$ cluster with g = 2.058, 1.938 and 1.863 on reduction, and multiple low-potential $[4Fe–4S]^{2+,+}$ centers (E_m < -300 mV) that give rise to a complex spectrum in dithionite-reduced samples with apparent g values of 2.052, 1.933 and 1.887 and broad wings, indicative of interacting $S = 1/2$ $[4Fe–4S]^{+}$ clusters. Similar results were obtained for redox titrations on HDR from *M. thermophila* (Simianu et al. 1998), with the two $[4Fe–4S]^{2+,+}$ clusters having midpoint potentials of -100 mV and -400 mV.

EPR signals of potential relevance to the catalytic cycle were observed on reaction of duroquinone-oxidized *M. marburgenesis* HDR with either CoM–SH or CoB–SH, the co-substrates for the oxidative reaction (Madadi-Kahkesh et al. 2001). In the presence of CoM–SH, a novel $S = 1/2$ resonance accounting for 1 spin/HDR molecule was observed at temperatures below 50 K, with principal g-values = 2.013, 1.991 and 1.938, see Fig. 2.6. The resonance is lost on reduction (E_m = –185 mV) and on reaction with CoB–SH. Hence, it was attributed to the product of the oxidative half-reaction that occurs in the absence of CoB–SH, in which case it is likely to correspond to a trapped intermediate in the catalytic cycle. A species with similar g-values, g = 2.018, 1.996 and 1.954, and relaxation properties, accounting for ~0.5 spin/HDR molecule, was observed when oxidized HDR was treated with CoB–SH. However, redox titrations revealed a significantly higher midpoint potential (E_m = –30 mV) than the CoM–SH generated species and argue against a role as an intermediate in the HDR catalytic cycle. Both the CoM–SH and CoB–SH induced resonances exhibited ^{57}Fe broadening indicating

assignment to a paramagnetic Fe-S cluster rather than an organic or S-based radical species (Madadi-Kahkesh et al. 2001). Furthermore these resonances are not unique to *M. marburgensis* HDR, since redox titrations of *M. barkeri* HDR in the presence of CoM–SH and CoB–SH revealed similar EPR signals with analogous redox properties (Madadi-Kahkesh et al. 2001).

It was tempting to speculate that the EPR signals of oxidized HDR samples treated with CoM–SH or CoB–SH are related to oxidized NEM-FTR and result from a $[4Fe–4S]^{3+}$ cluster with two thiolate ligands at a unique Fe site (Madadi-Kahkesh et al. 2001). However, initially this assignment was tenuous, in light of the dramatic differences in the g-values (see Fig. 2.6) and relaxation properties of the NEM-FTR and CoM–SH/CoB–SH-treated HDR EPR signals, and the absence of any direct evidence for this type of Fe-S cluster at the active site of HDR. Hence VTMCD was used to assess the type of cluster presence in oxidized HDR treated with CoM–SH by selectively investigating the excited-state electronic transitions associated with paramagnetic Fe-S clusters (Duin et al. 2002), see Fig. 2.9. Variable-field and variable-temperature saturation magnetization studies for individual bands confirmed that all transitions originate for the $S = 1/2$ species observed in the EPR spectrum. Moreover, comparison with the VTMCD spectra of oxidized *Synechocystis* and spinach NEM-FTR revealed a similar pattern of positive and negative MCD bands with each band shifted down in energy by ~2000 cm^{-1} in HDR. Hence the VTMCD spectrum argues strongly in favor of the presence of a novel type of $[4Fe–4S]^{3+}$ in oxidized CoM–SH treated HDR with excited-state electronic properties similar to those of NEM-FTR.

The differences in the ground and excited state properties of the $[4Fe–4S]^{3+}$ clusters in NEM-FTR and CoM–SH treated HDR are most likely related to direct ligation of CoM–S^- at a unique Fe site in HDR, rather than a cysteinate derived from the active-site disulfide as in FTR. Indeed, several lines of evidence argue in favor of a mechanism involving direct interaction of the heterodisulfide substrate with the active-site [4Fe–4S] cluster in HDR rather than the FTR-type mechanism in which cleavage of the substrate disulfide by the [4Fe–4S] cluster is mediated by an active-site disulfide in close proximity to the cluster, see Fig. 2.11. First, the marked differences in the redox and electronic excited state properties of the $[4Fe–4S]^{3+}$ clusters in CoB–SH treated HDR and CoM–SH-treated HDR argues for direct attachment to the cluster. Second, the $[4Fe–4S]^{3+}$ species in HDR are readily formed under oxidizing conditions on addition of exogenous thiols such as CoM–SH, CoB–SH, DTT or β-mercaptoethanol (Madadi-Kahkesh et al. 2001). This does not occur in FTR, since the active-site disulfide that is present in oxidized samples can only be cleaved under reducing conditions using the physiological electron donor, reduced ferredoxin, or mediator dyes such as reduced viologens (Schürmann et al. 1995). The $[4Fe–4S]^{3+}$ species in FTR is only observed as a stable species on oxidation when one of the active-site cysteine residues has been alkylated, and therefore not available to reform the active-site disulfide on oxidation, leaving the free cysteine available to interact with the cluster. Third, *M. marburgensis* HDR is not inhibited by cysteine alkylating reagents at concentrations up to 2 mM (Madadi-Kahkesh et al. 2001), whereas cysteine alkylating reagents are potent inhibitors of FTR as a result of alkylation of the interchange thiol of the active-site disulfide (Schürmann and Gardet-Salvi 1993). Very recently direct evidence for CoM–SH binding

to the $[4Fe–4S]^{3+}$ cluster in *M. marburgensis* and *M. barkeri* HDR has come from broadening of the EPR signals with CoM–^{33}SH as a result of hyperfine interaction with the $I = 3/2$ ^{33}S nucleus and perturbation of the *g*-value anisotropy with CoM–SeH (Duin et al. 2003; Shokes et al. 2005).

Mechanism: Although there are as yet no structural data for any HDR and spectroscopic studies are impeded by the presence of multiple $[4Fe–4S]^{2+,+}$ clusters as well as FAD or heme prosthetic groups, the combination of EPR and VTMCD spectroscopies coupled with the catalytic competence of the oxidized CoM-SH-bound intermediate (Madadi-Kahkesh et al. 2001; Duin et al. 2002; Duin et al. 2003), has provided convincing evidence for a mechanism related to that of FTR, see Fig. 2.13. The major difference is that the substrate disulfide interacts directly with the active-site $[4Fe–4S]^{3+,2+}$ cluster in HDR, rather than with an active-site disulfide in FTR. However both are proposed to involve site-specific [4Fe–4S] cluster redox chemistry and a novel $[4Fe–4S]^{3+}$ cluster intermediate with two thiolate ligands bound at a unique Fe site. The hypothesis that CoM–SH is attached to an Fe rather than a S atom of the $[4Fe–4S]^{3+}$ cluster in HDR, is currently being tested via Se- and Fe-EXAFS studies using oxidized CoM–SeH-treated HDR (Duin et al. 2003: Shokes et al. 2005).

Conclusions and prospects

The studies of FTR and HDR summarized in the review provide an elegant demonstration of the synergy of structural and spectroscopic approaches in establishing a new biological role for [4Fe–4S] clusters. In both enzymes the [4Fe–4S] cluster has been shown to play a key role in mediating disulfide reduction in two one-electron steps via site-specific cluster chemistry involving a $[4Fe–4S]^{3+}$ cluster intermediate with two

thiolate ligands at a unique Fe site. The same overall mechanism appears to be in operation both in the reduction of an active-site disulfide in FTR and the substrate heterodsulfide in HDR. Hence investigations of this new role for Fe-S clusters in FTR and HDR are complementary. FTR is currently more amenable to crystallographic investigations and the presence of a single Fe-S cluster facilitates detailed vibrational and electronic characterization by resonance Raman and Mössbauer spectroscopies. The ability to label the substrate disulfides/dithiols with Se and ^{33}S opens in HDR, however, the potential for detailed investigation of the site and electronic consequences of ligation of an additional thiolate.

Many questions remain concerning the mechanism of formation of the one-electron reduced intermediate, the distinct roles of the cysteines that comprise the active-site disulfide of FTR and the differences in the electronic properties of the $[4Fe\text{-}4S]^{3+}$ cluster intermediates in HDR and FTR. Hence there is clearly a pressing need for detailed freeze-quench EPR and Mössbauer studies to further characterize intermediates and assess the kinetics of the mechanism, for high-resolution structural and spectroscopic studies of wild-type and active-site variants of both FTR and HDR and complexes involving FTR/Fd/Trx, and for calculations to understand the differences in electronic structure and the origin of the site-specific cluster chemistry in both enzymes. The progress thus far suggests that the complementary use of high-resolution structural and spectroscopic approaches will lead to an in-depth understanding of the unique structural and electronic properties of this novel active site and the mechanism of Fe-S cluster-mediated disulfide reduction.

Acknowledgments: Research on FTR and HDR in the Johnson laboratory are funded by the National Institutes of Health (GM62524 to MKJ). This review was prepared in honor of the retirement of Peter Schürmann, our colleague and long-standing collaborator on FTR. His tireless devotion to understanding the biochemistry, enzymology and structure of this fascinating enzyme have been an inspiration to all who study the mechanism of light regulation in photosynthesis. His prolific contributions to our current understanding of FTR are abundantly evident in the references cited in this review.

Bibliography

Akasaka K, Ohnishi S, Suita T and Nitta I (1964) Electron spin resonance of a single crystal of L-cystine dihydrochloride irradiated at low temperature. J Chem Phys 40: 3110-3116

Backes G, Mino Y, Loehr TM, Meyer TE, Cusanovich MA, Sweeney WV, Adman ET and Sanders-Loehr J (1991) The environment of [4Fe-4S] clusters in ferredoxins and high-potential iron proteins. New information from X-ray crystallography and resonance Raman spectroscopy. J Am Chem Soc 113: 2055-2064

Balmer Y, Koller A, del Val G, Manieri W, Schürmann P and Buchanan BB (2003) Proteomics gives insight into the regulatory function of chloroplast thioredoxins. Proc Natl Acad Sci USA 100: 370-375

Buchanan BB, Schürmann P, Wolosiuk RA and Jacquot J-P (2002) The ferredoxin/thioredoxin system: from discovery to molecular structures and beyond. Photosynth Res 73: 215-222

Cheek J and Broderick JB (2001) Adenosylmethionine-dependent iron-sulfur enzymes: versatile clusters in a radical new role. J Biol Inorg Chem 6: 209-226

Chow L-P, Iwadate H, Yano K, Kamo M, Tsugita A, Gardet-Salvi L, Stritt-Etter A-L and Schürmann P (1995) Amino-acid sequence of spinach ferredoxin-thioredoxin reductase catalytic subunit and identification of thiol groups constituting a redox-active disulfide and a [4Fe4S] cluster. Eur J Biochem 231: 149-156

Ciurli S, Carrié M, Weigel JA, Carney MJ, Stack TDP, Papaefthymiou GC and Holm RH (1990) Subsite-differentiated analogues of native [4Fe–4S]$^{2+}$ clusters: Preparation of clusters with five- and six-coordinate subsites and modulation of redox potentials and charge distributions. J Am Chem Soc 112: 2654-2664

Czernuszewicz RS, Macor KA, Johnson MK, Gewirth A and Spiro TG (1987) Vibrational mode structure and symmetry in proteins and analogues containing [4Fe-4S] clusters: Resonance Raman evidence for different degrees of distortion in HiPIP and ferredoxin. J Am Chem Soc 109: 7178-7187

Dai S, Schwendtmayer C, Johansson K, Ramaswamy S, Schürmann P and Eklund H (2000a) How does light regulate chloroplast enzymes? Structure-function studies of the ferredoxin/thioredoxin system. Quart Rev Biophys 33: 67-108

Dai S, Schwendtmayer C, Schürmann P, Ramaswamy S and Eklund H (2000b) Redox signaling in chloroplasts: Cleavage of disulfides by an iron-sulfur cluster. Science 287: 655-658

Dai S, Johansson K, Miginiac-Maslow M, Schürmann P, and Eklund H (2004) Structural basis or redox signaling in photosynthesis: structure and function of ferredoxin:thioredoxin reductase and target enzymes. Photosynth Res 79: 233-248

de la Torre A, Lara C, Yee BC, Malkin R and Buchanan BB (1982) Physiochemical properties of ferralterin, a regulatory iron-sulfur protein functional in oxygenic photosynthesis. Arch Biochem Biophys 213: 545-550

Deppenmeier U, Lienard T and Gottschalk G (1999) Novel reactions involved in energy conservation by methanogenic archaea. FEBS Lett 457: 291-297

Droux M, Jacquot J-P, Miginac-Maslow M, Gadal P, Huet JC, Crawford NA, Yee BC and Buchanan BB (1987) Ferredoxin:thioredoxin reductase, an iron-sulfur enzyme linking light to enzyme regulation in oxygenic photosynthesis: Purification and properties of the enzyme from C_3, C_4, and cyanobacterial species. Arch Biochem Biophys 252: 426-439

Duin EC, Bauer C, Jaun B and Hedderich R (2003) Coenzyme M binds to a [4Fe–4S] cluster in the active site of the heterodisulfide reductase as deduced from EPR studies with the [^{33}S]coenzyme M-treated enzyme. FEBS Lett 538: 81-84

Duin EC, Madadi-Kahkesh S, Hedderich R, Clay MD and Johnson MK (2002) Heterodisulfide reductase from *Methanothermobacter marburgensis* contains an active-site [4Fe–4S] cluster that is directly involved in mediating heterodisulfide reduction. FEBS Lett 512: 263-268

Dunham WR, Hagen WR, Fee JA, Sands RH, Dunbar JB and Humblet C (1991) An investigation of *Chromatium vinosum* high-potential iron-sulfur protein by EPR and Mössbauer spectroscopy: Evidence for a freezing-induced dimerization in NaCl solutions. Biochim Biophys Acta 1079: 253-262

Frey PA and Magnusson OTh (2003) *S*-adenosylmethionine: A wolf in sheep's clothing, or a rich man's adenosylcobalamin. Chem Rev 103: 2129-2148

Hedderich R, Berkessel A and Thauer RK (1989) Catalytic properties of heterodisulfide reductase involved in the final step of methanogenesis. FEBS Lett 255: 67-71

Hedderich R, Berkessel A and Thauer RK (1990) Purification and properties of heterodisulfide reductase from *Methanobacterium thermoautotrophicum* (strain Marburg). Eur J Biochem 193: 255-261

Hedderich R, Klimmek O, Kröger A, Dirmeier R, Keller M and Stetter KO (1998) Anaerobic respiration with elemental sulfur and with disulfides. FEMS Microbiol Rev 22: 353-381

Hedderich R, Koch J, Linder D and Thauer RK (1994) The heterodisulfide reductase from *Methanobacterium thermoautotrophicum* contains sequence motifs characteristic of pyridine-nucleotide-dependent thioredoxin reductases. Eur J Biochem 225: 253-261

Heim S, Kunkel A, Thauer RK and Hedderich R (1998) Thiol:fumarate reductase (Tfr) from *Methanobacterium thermoautotrophicum*. Identification of the catalytic sites for fumarate reduction and thiol oxidation. Eur J Biochem 253: 292-299

Houseman ALP, Oh B-H, Kennedy MC, Fan C, Werst MM, Beinert H, Markley JL and Hoffman BM (1992) ^{14,15}N, ^{13}C, ^{57}Fe, and ^{1,2}H Q-band ENDOR study of Fe-S proteins with clusters that have exogenous sulfur ligands. Biochemistry 31: 2073-2080

Hirasawa M, Schürmann P, Jacquot J-P, Manieri W, Jacquot P, Keryer E, Hartman FC, Knaff DB (1999) Oxidation-reduction properties of chloroplast thioredoxins,

ferredoxin:thioredoxin reductase, and thioredoxin *f*-regulated enzymes. Biochemistry 38: 5200-5205

Jameson GNL, Walters EM, Manieri W, Schürmann P, Johnson MK and Huynh BH (2003) Spectroscopic evidence for site-specific chemistry at a unique iron site of the [4Fe–4S] cluster in ferredoxin:thioredoxin reductase. J Am Chem Soc 125: 1146-1147

Jarrett JT (2003) The generation of 5'-deoxyadenosyl radicals by adenosylmethioine-dependent radical enzymes. Curr Opin Chem Biol 7: 174-182

Johnson MK (2000) CD and MCD Spectroscopy. In: Que L, Jr. (ed) Physical methods in bioinorganic chemistry. Spectroscopy and magnetism, pp 233-286. University Science Books, Sausalito, CA

Johnson MK, Robinson AE and Thomson AJ (1982) Low-temperature magnetic circular dichroism of iron-sulfur proteins. In: Spiro TG (ed) Iron-sulfur proteins, pp 367-406. Wiley-Interscience, New York

Künkel A, Vaupel M, Heim S, Thauer RK and Hedderich R (1997) Heterodisulfide reductase from methanol-grown cells of *Methanosarcina barkeri* is not a flavoenzyme. Eur J Biochem 244: 226-234

Madadi-Kahkesh S, Duin EC, Heim S, Albracht SPJ, Johnson MK and Hedderich R (2001) A paramagnetic species with unique EPR characteristics in the active site of heterodisulfide reductase from methanogenic archaea. Eur J Biochem 268: 2566-2577

Meyer TE, Przysiecki CT, Watkins JA, Bhattacharyya A, Simondson RP, Cusanovich MA and Tollin G (1983) Correlation between rate constants for reduction and redox potential as a basis for systematic investigation of reaction mechanisms of electron transfer proteins. Proc Natl Acad Sci USA 80: 6740-6744

Middleton P, Dickson DPE, Johnson CE and Rush JD (1980) Interpretation of the Mössbauer spectra of the high-potential iron protein from *Chromatium*. Eur J Biochem 104: 289-296

Moulis J-M, Lutz M, Gaillard J and Noodleman L (1988) Characterization of [4Fe-4Se]$^{2+/3+}$ high potential iron-sulfur protein from *Chromatium vinosum*. Biochemistry 27: 8712-8719

Rius G and Lamotte B (1989) Single-crystal ENDOR study of a ^{57}Fe-enriched iron-sulfur $[Fe_3S_4]^{3+}$ cluster. J Am Chem Soc 111: 2464-2469

Salamon Z, Tollin G, Hirasawa M, Gardet-Salvi L, Stritt-Etter A-L, Knaff DB and Schürmann P (1995) The oxidation-reduction properties of spinach thioredoxin *f* and *m* and of ferredoxin:thioredoxin reductase. Biochim Biophys Acta 1230: 114-118

Schürmann P (2003) Redox signaling in the chloroplasts: the ferredoxin/thioredoxin system. Antioxidants & Redox Signaling 5: 69-78

Schürmann P and Buchanan BB (2001) The structure and function of the ferredoxin/thioredoxin system in photosynthesis. Adv Photosynth Respiration 11: 331-361

Schürmann P and Gardet-Salvi L (1993) Chemical modification of the active site of ferredoxin-thioredoxin reductase. Chimia 47: 245-246

Schürmann P and Jacquot J-P (2000) Plant thioredoxin sytems revisited. Annu Rev Plant Physiol Plant Mol Biol 51: 371-400

Schürmann P, Stritt-Etter A-L and Li JS (1995) Reduction of ferredoxin:thioredoxin reductase by artificial electron donors. Photosynth Res 46: 309-312

Shokes JE, Duin EC, Bauer C, Jaun B, Hedderich R, Koch J, and Scott RA (2005) Direct interaction of coenzyme M with the active-site Fe-S cluster of heterodisulfide reductase. FEBS Lett 579: 1741-1744.

Simianu M, Murakami E, Brewer JM and Ragsdale SW (1998) Purification and properties of the heme and iron-sulfur-containing heterodisulfide reductase from *Methanosarcina thermophila*. Biochemistry 37: 10027-10039

Staples CR, Ameyibor E, Fu W, Gaudet-Salvi L, Stritt-Etter A-L, Schürmann P, Knaff DB and Johnson MK (1996) The function and properties of the iron-sulfur center in spinach ferredoxin:thioredoxin reductase: A new biological role for iron-sulfur clusters. Biochemistry 35: 11425-11434

Staples CR, Gaymard E, Stritt-Etter A-L, Telser J, Hoffman BM, Schürmann P, Knaff DB and Johnson MK (1998) Role of the [4Fe-4S] cluster in mediating disulfide reduction in spinach ferredoxin:thioredoxin reductase. Biochemistry 37: 4612-4620

Stephens PJ, Thomson AJ, Dunn JBR, Keiderling TA, Rawlings J, Rao KK, Hall DO (1978) Circular dichroism and magnetic circular dichroism of iron-sulfur proteins. Biochemistry 17: 4770-4778

Thauer RK (1998) Biochemistry of methanogenesis. Microbiology 144: 2377-2406

Williams CH Jr (1992) Flavin-dependent disulfide reductases. In: Müller F (ed) Chemistry and Biochemistry of Flavoenzymes, Vol. III, pp 121-211. CRC Press, Boca Raton, FL

Williams CH Jr (1995) Mechanism and structure of thioredoxin reductase from *Escherichia coli*. FASEB J 9: 1267-1276

Williams CH Jr, Arscott LD, Müller S, Lennon BW, Ludwig ML, Wang P-F, Veine DM, Becker K and Schirmer RH (2000) Thioredoxin reductase. Two modes of catalysis have evolved. Eur J Biochem 267: 6110-6117

Figure 2.1 The FTR heterodimer (Dai et al. 2000a). The catalytic subunit which houses the active-site [4Fe-4S] cluster and redox-active disulfide is shown in blue. The variable subunit is shown in green. (A) Front view of FTR. (B) Side view of FTR.

A

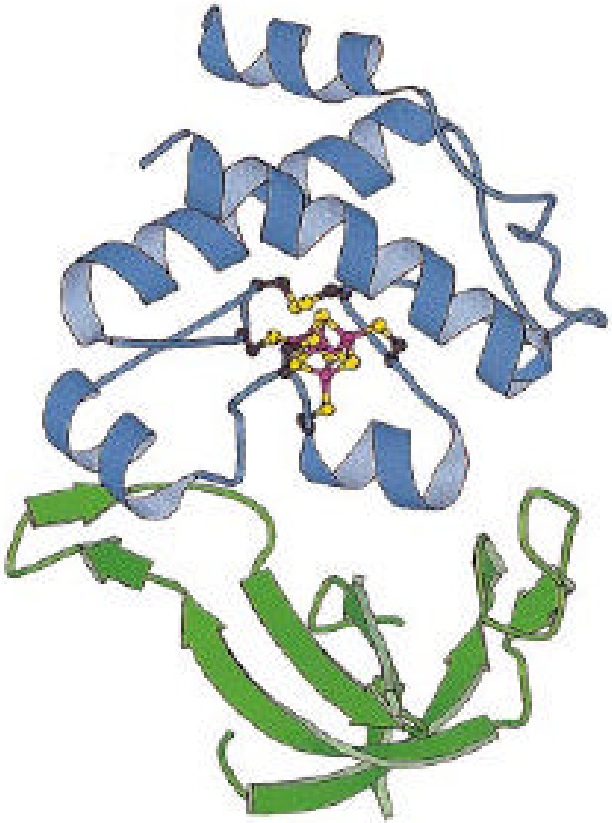

B

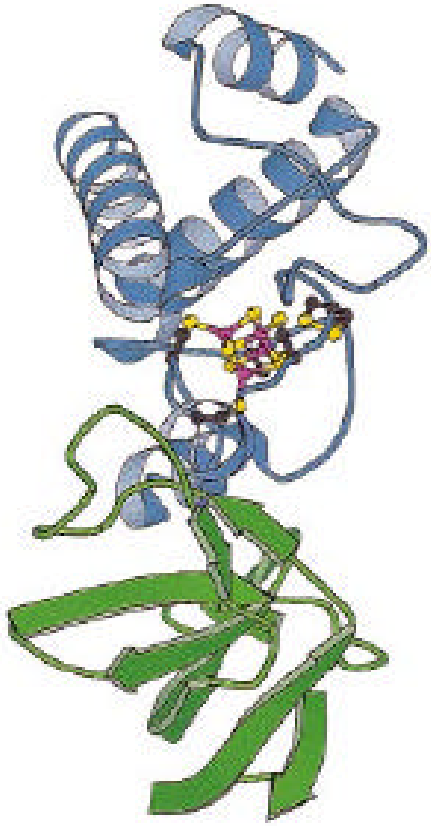

Figure 2.2 Active-site structure of *Synechocystis* FTR (Dai et al. 2000b). Color code: Fe, green; S, yellow; C, gray; N, blue; O, red.

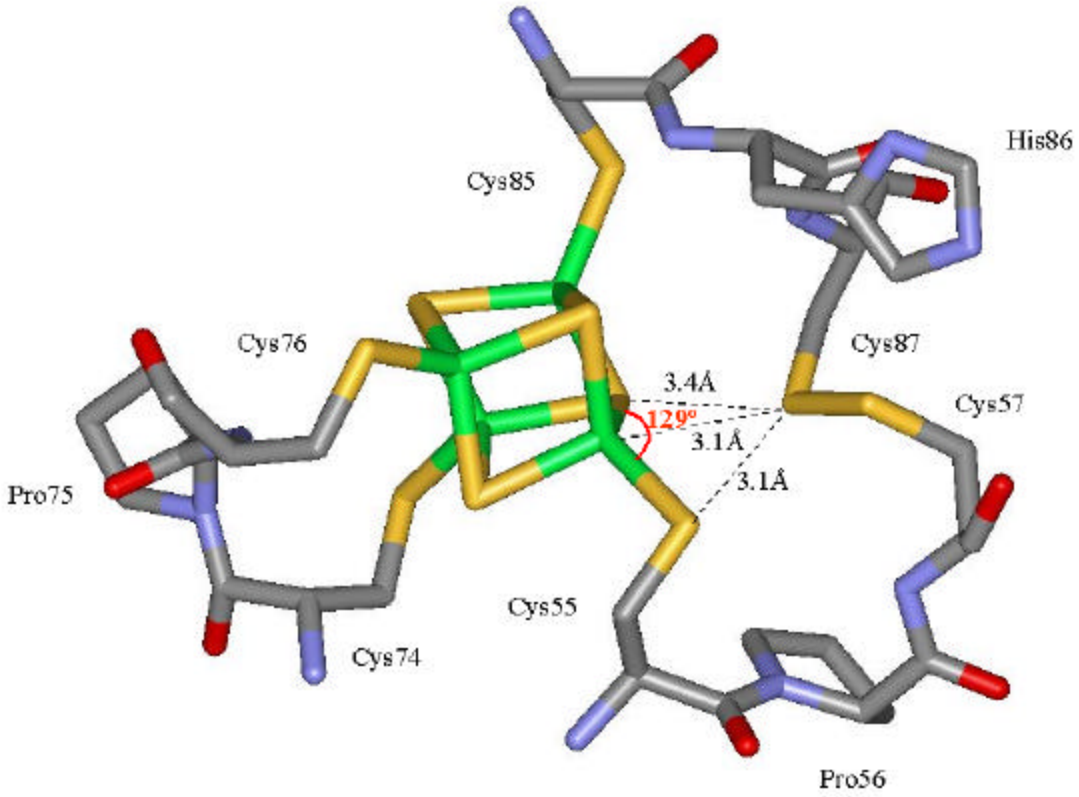
His86
Cys85
Cys76
Cys87
3.4Å
129°
Cys57
3.1Å
3.1Å
Pro75
Cys55
Cys74
Pro56

Figure 2.3 UV-visible absorption spectra of as-isolated (upper panel) and NEM-modified (lower panel) *Synechocystis* FTR. The solid line is the enzyme as prepared and the dashed line is after anaerobic reduction with sodium dithionite. Bands from excess dithionite are indicated by an asterisk.

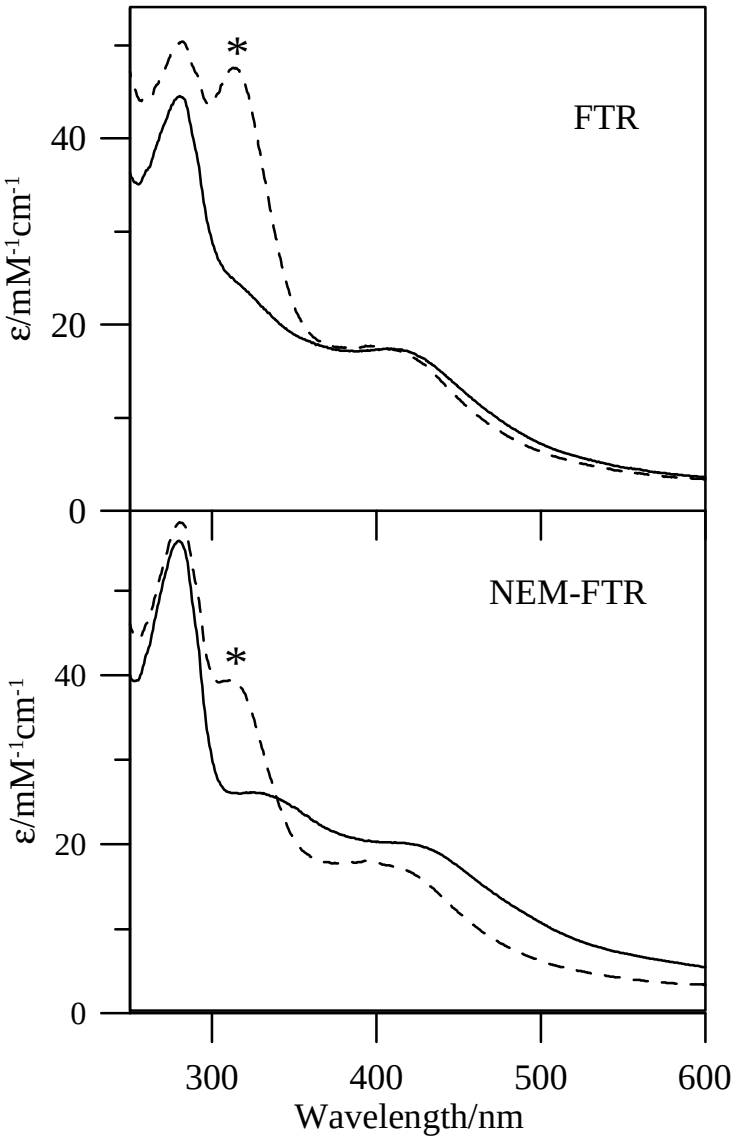
FTR
NEM-FTR
*
*
40
20
0
40
20
0
ε/mM-1cm-1
ε/mM-1cm-1
300
400
500
600
Wavelength/nm

Figure 2.4 Resonance Raman spectra of as-isolated, NEM-modified, and dithionite-reduced NEM-modified *Synechocystis* FTR. Spectra recorded using 2-mM samples frozen at 17 K, using 457.9-nm laser excitation and 7-cm^{-1} spectral bandwidth. The spectra are the sum of at least 30 scans, with each scan involving photon counting for 1 s every 1 cm^{-1}. Vibrational modes originating from lattice modes of ice have been subtracted.

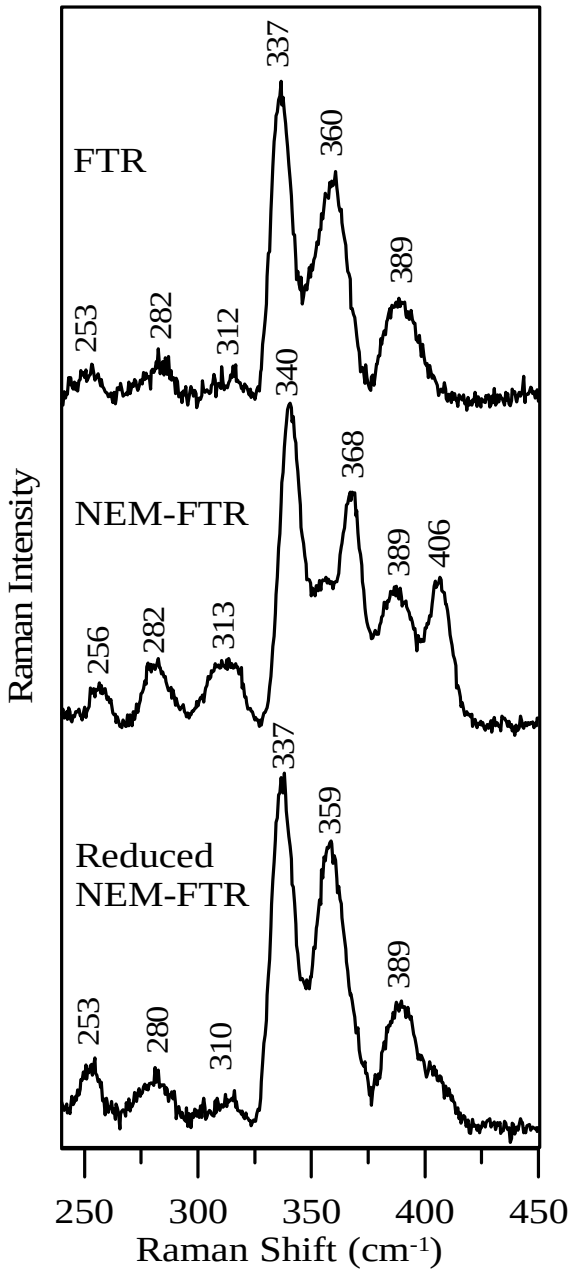
FTR
337
360
389
253
282
312
340
NEM-FTR
368
389
406
256
282
313
Reduced
NEM-FTR
337
359
389
253
280
310
Raman Intensity
250
300
350
400
450
Raman Shift (cm-1)

Figure 2.5 Mössbauer spectrum of ^{57}Fe-enriched spinach FTR as-isolated recorded at 4.2 K in a field of 50 mT applied parallel to the γ beam. The spectrum has been fit (solid line) as the sum of the three components shown above the experimental spectrum: ferric site (δ = 0.39 mm/s, ΔE_Q = 1.02 mm/s, solid line), ferrous site (δ = 0.56 mm/s, ΔE_Q = 1.80 mm/s, solid line) and valence delocalized ($Fe^{2.5+}Fe^{2.5+}$) pair (δ = 0.44 mm/s, ΔE_Q = 1.23 mm/s, dashed line) in a 1:1:2 ratio. Reprinted from Jameson et al. 2003 with permission of the American Chemical Society.

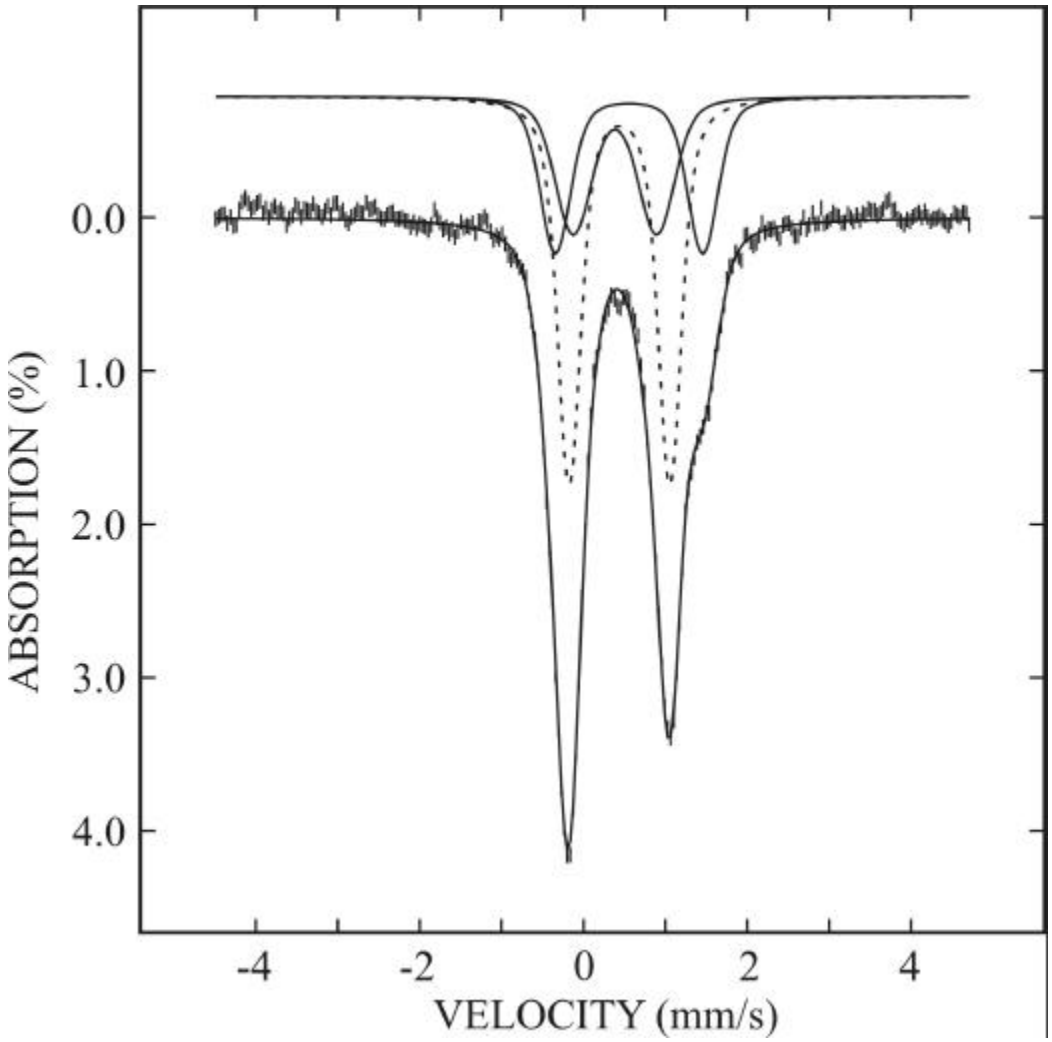
ABSORPTION (%)
0.0
1.0
2.0
3.0
4.0
-4
-2
0
2
4
VELOCITY (mm/s)

Figure 2.6 EPR spectra of oxidized forms of spinach and *Synechocystis* FTR and *M. marburgensis* HDR. (a) Ferricyanide-oxidized spinach FTR (10 K and 10 mW). (b) Spinach NEM-FTR as prepared (50 K, 1 mW). (c) *Synechocystis* NEM-FTR as prepared (35 K, 1 mW). (d) Duroquinone-oxidized HDR incubated with CoM-SH (30 K, 2 mW). All spectra were recorded at a microwave frequency of 9.60 GHz, with a modulation amplitude of 0.6 mT. Principal *g*-values based on spectral simulations are indicated for each spectrum.

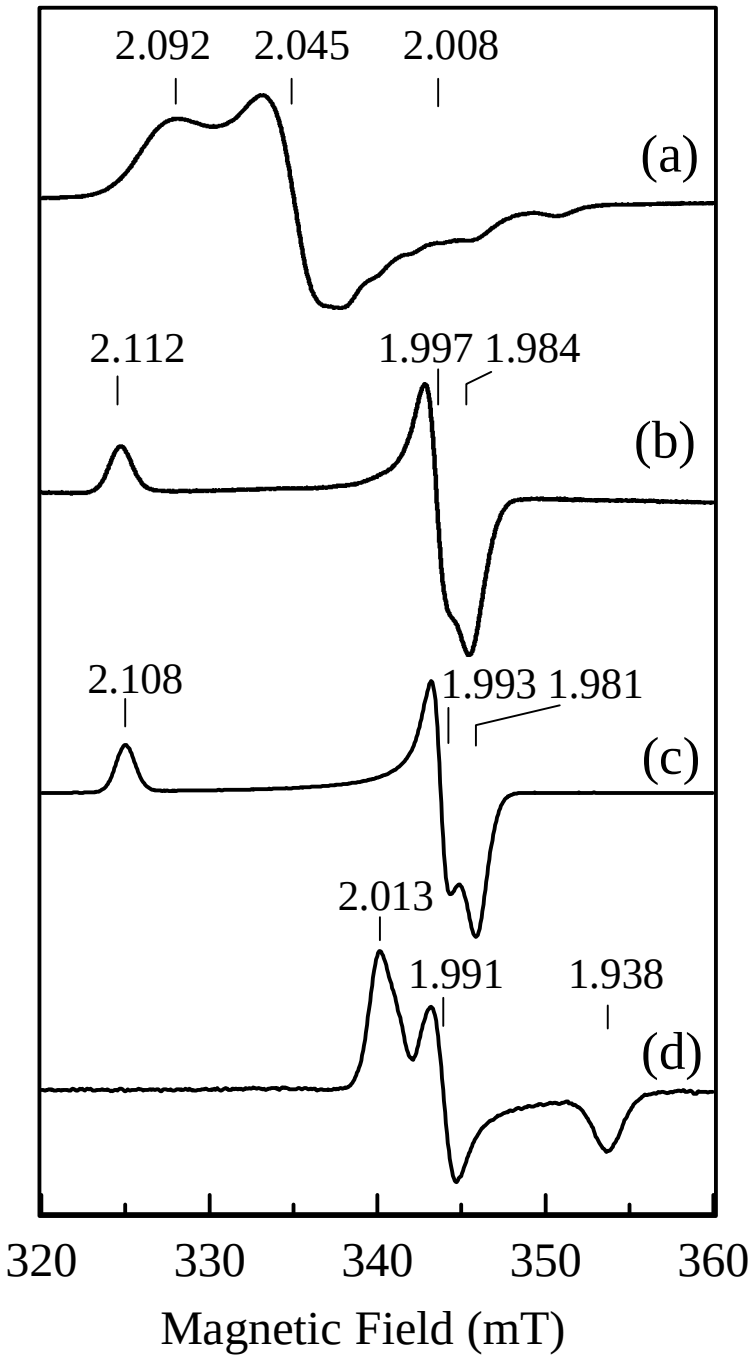
2.092
2.045
2.008
(a)
2.112
1.997
1.984
(b)
2.108
1.993
1.981
(c)
2.013
1.991
1.938
(d)
320
330
340
350
360
Magnetic Field (mT)

Figure 2.7 EPR-monitored, dye-mediated redox titrations for spinach (Δ) and *Synechocystis* (O) NEM-FTR. Solid lines are best fits to one-electron Nernst plots with E_m = -210 mV for spinach NEM-FTR and E_m = -145 mV for *Synechocystis* NEM-FTR.

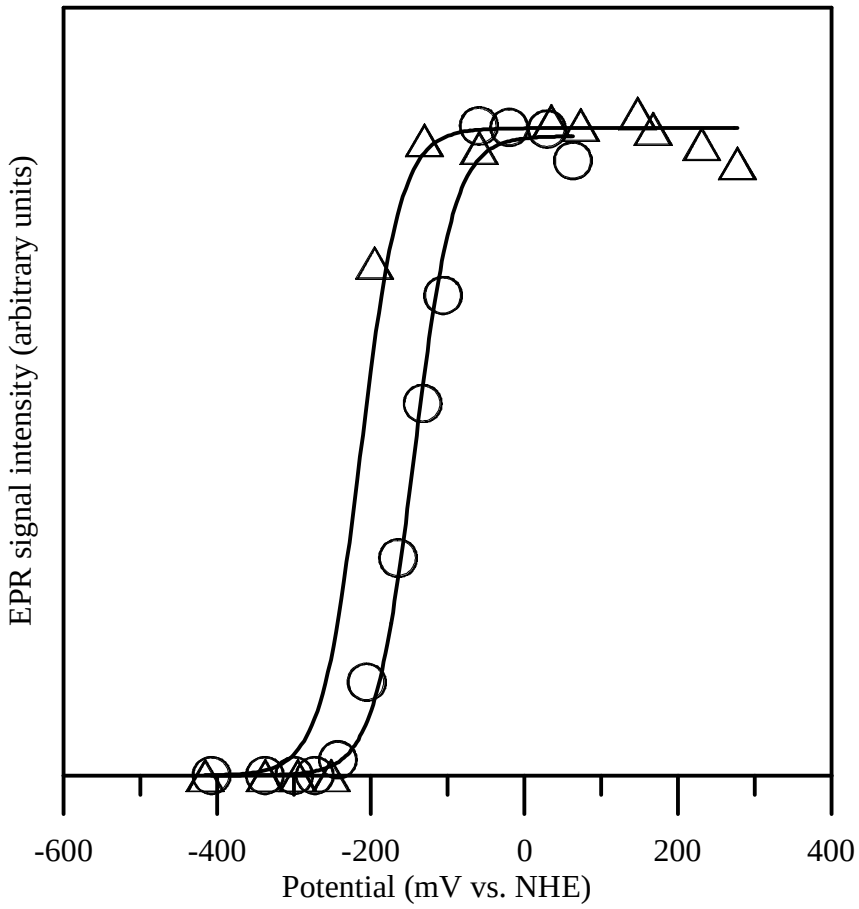
EPR signal intensity (arbitrary units)
-600
-400
-200
0
200
400
Potential (mV vs. NHE)

Figure 2.8 EPR spectra of spinach FTR. (a) NEM-FTR as prepared. (b) Native FTR reduced with one equivalent of reduced benzyl viologen. (c) Native FTR frozen during enzyme turnover using Trx *f* as the substrate and reduced benzyl viologen as the electron donor. EPR conditions: temperature, 35 K; microwave power, 1 mW; modulation amplitude, 0.6 mT; microwave frequency, 9.60 GHz. Modified from Staples et al. 1998 with permission of the American Chemical Society.

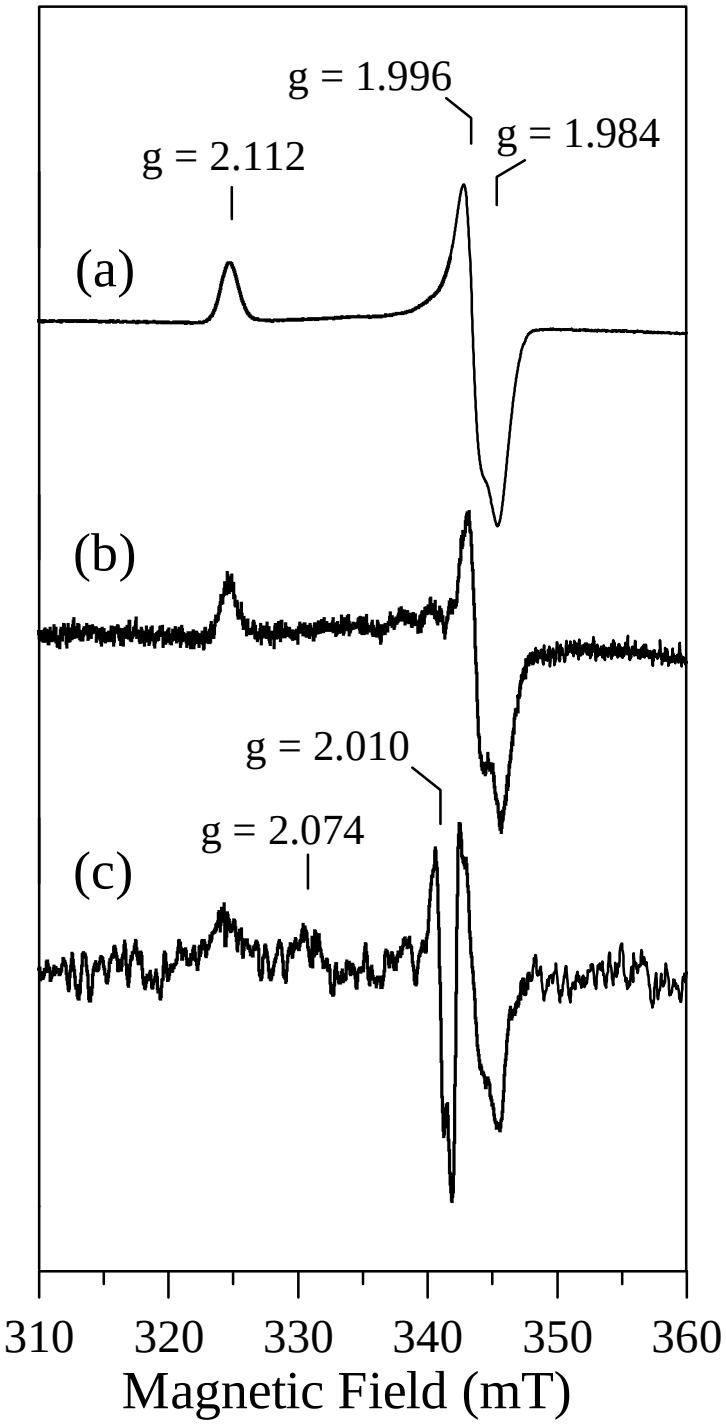
g = 1.996
g = 1.984
g = 2.112
(a)
(b)
g = 2.010
g = 2.074
(c)
310
320
330
340
350
360
Magnetic Field (mT)

Figure 2.9 VTMCD spectra of spinach and *Synechocystis* NEM-FTR as prepared and duroquinone-oxidized *M. marburgensis* HDR incubated with CoM-SH. Spectra recorded at 1.7, 4.2, and 10 K with an applied magnetic field of 6 T. All MCD bands increase in intensity with decreasing temperature.

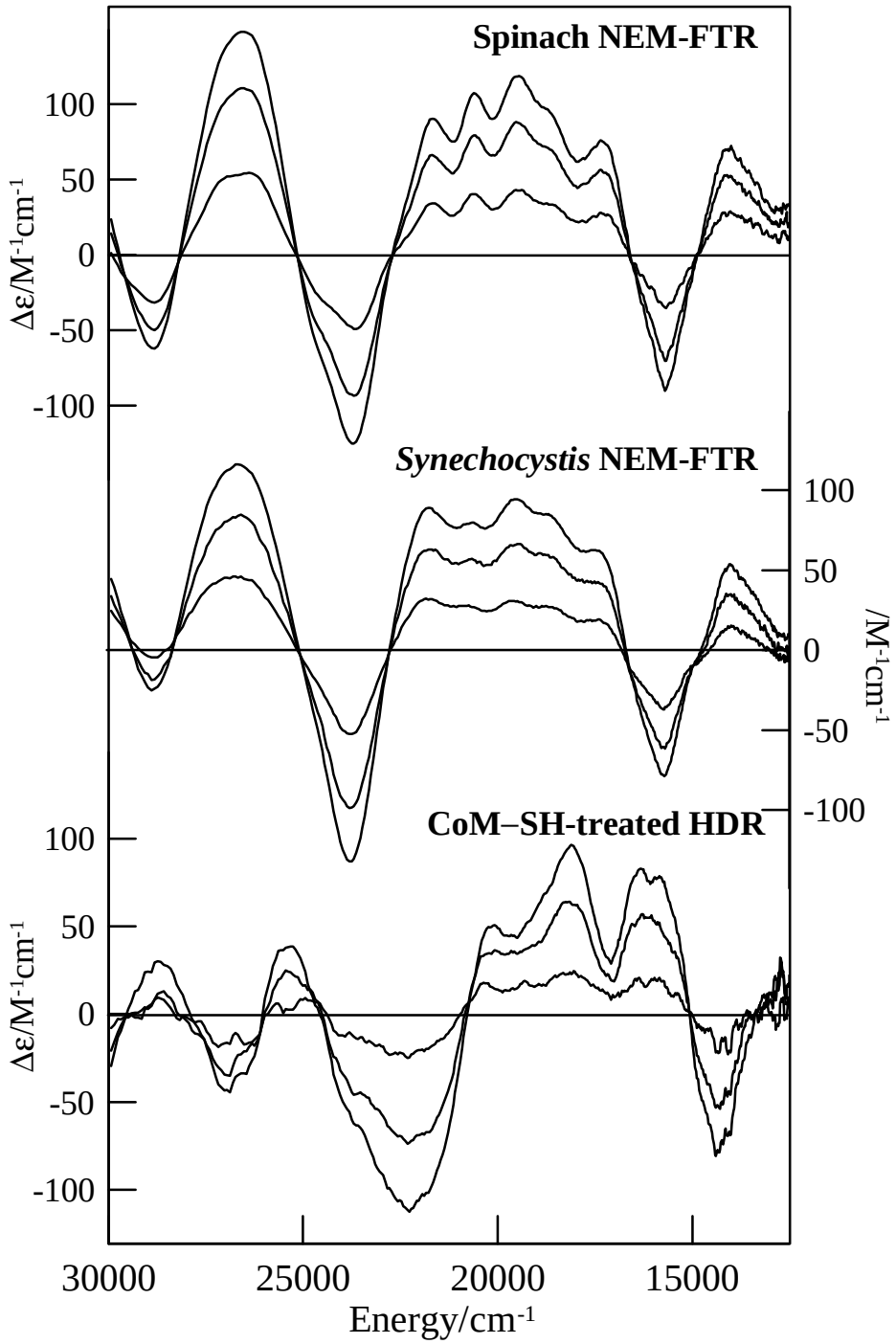
Spinach NEM-FTR
Synechocystis NEM-FTR
CoM–SH-treated HDR
Δε/M-1cm-1
/M-1cm-1
100
50
0
-50
-100
30000
25000
20000
15000
Energy/cm-1

Figure 2.10 Mössbauer spectrum of ^{57}Fe-enriched spinach NEM-FTR recorded at 4.2 K in a field of 8 T applied parallel to the γ beam. The spectrum has been fit (solid line) as the sum of the three components shown above the experimental spectrum: ferric site 1 (δ = 0.30 mm/s, ΔE_Q = 1.2 mm/s, A_x = 22.5 T, A_y = 18.5 T, A_z = 8.0 T, solid line), ferric site 2 (δ = 0.30 mm/s, ΔE_Q = –1.2 mm/s, A_x = 21.5 T, A_y = 19.5 T, A_z = 18.5 T, solid line) and valence delocalized ($Fe^{2.5+}Fe^{2.5+}$) pair (δ = 0.44 mm/s, ΔE_Q = 1.2 mm/s, A_x = –26.5 T, A_y = –29.5 T, A_z = –24.5 T, dashed line) in a 1:1:2 ratio. Reprinted from Jameson et al. 2003 with permission of the American Chemical Society.

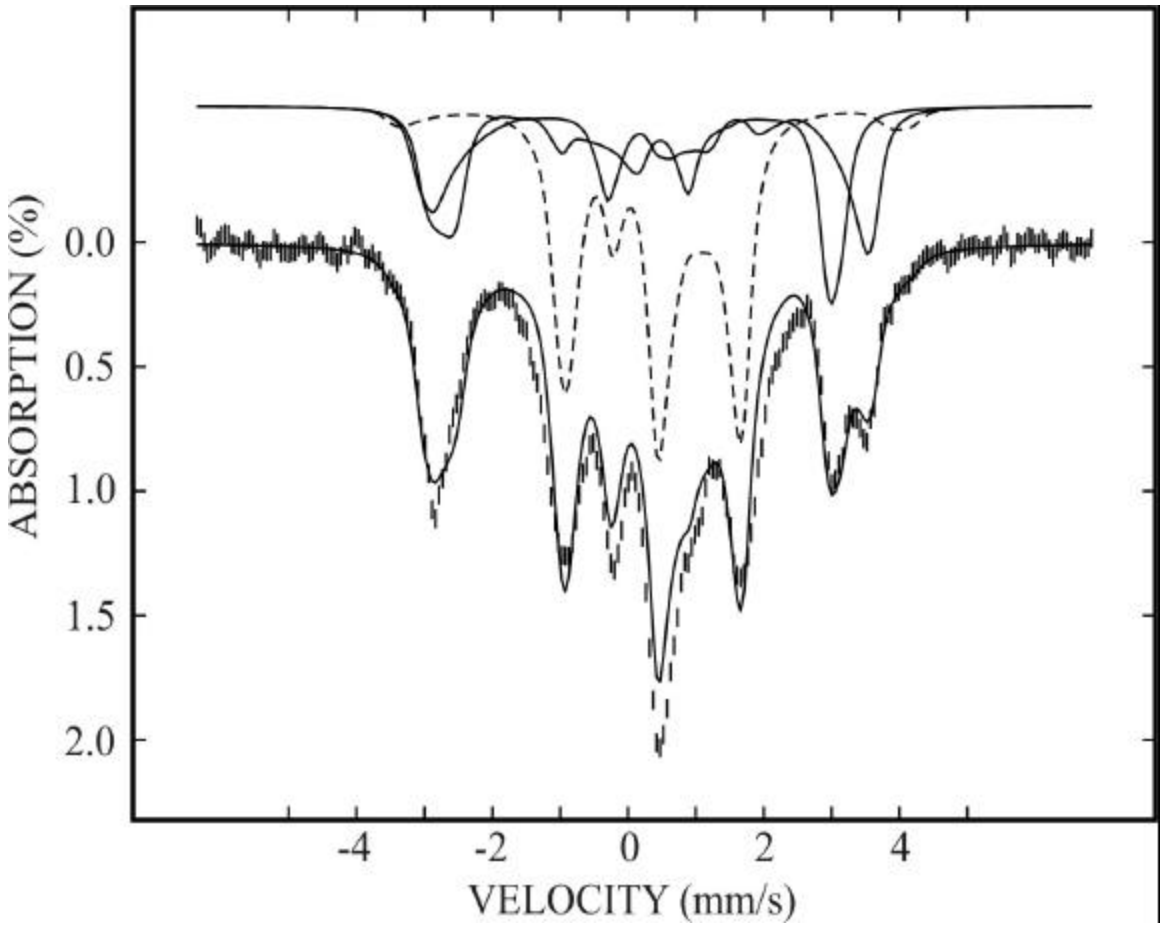
ABSORPTION (%)
0.0
0.5
1.0
1.5
2.0
-4
-2
0
2
4
VELOCITY (mm/s)

Figure 2.11 Proposed catalytic cycle for FTR. Residue numbering is for *Synechocystis* FTR.

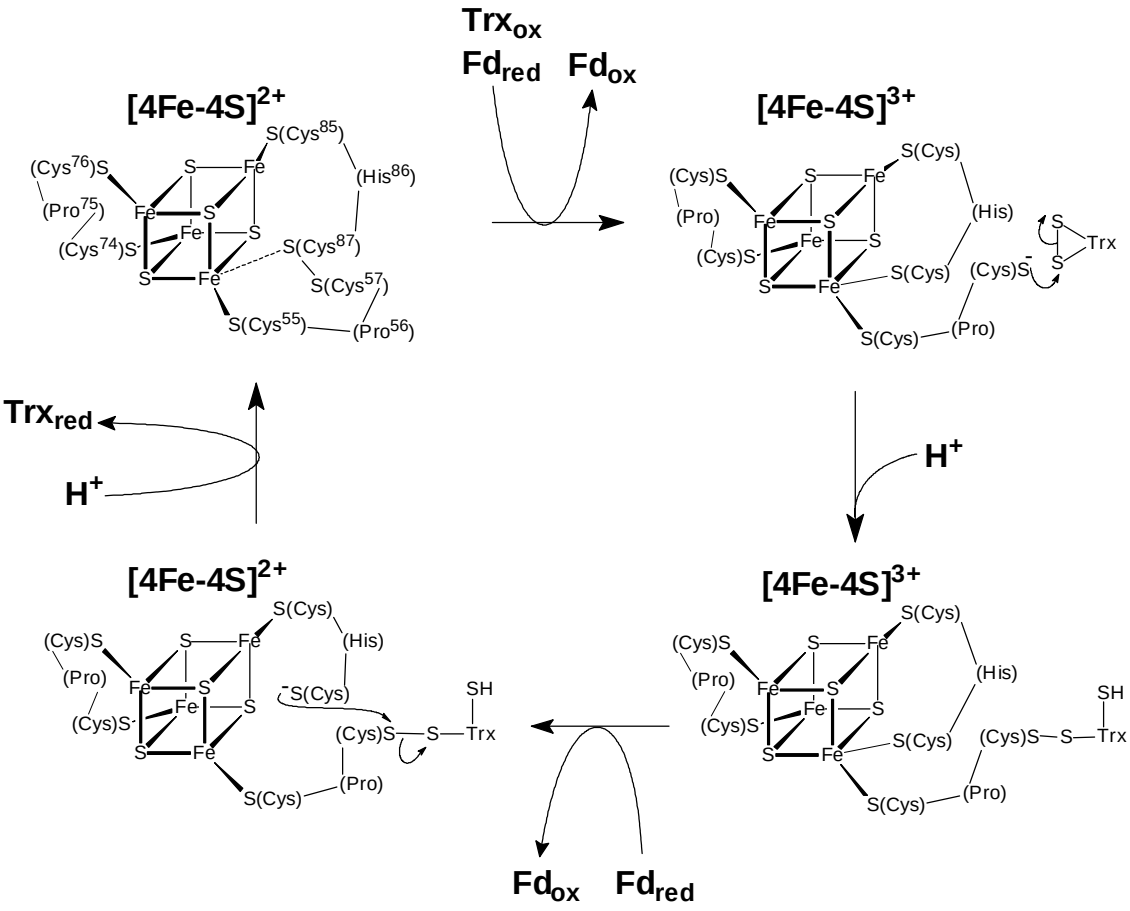
Trx$_{ox}$
Fd$_{red}$
Fd$_{ox}$
[4Fe-4S]$^{2+}$
[4Fe-4S]$^{3+}$
Trx$_{red}$
H^{+}
H^{+}
[4Fe-4S]$^{2+}$
[4Fe-4S]$^{3+}$
Fd$_{ox}$
Fd$_{red}$

Figure 2.12 Possible mechanisms for the formation of the one-electron-reduced intermediate in FTR. Residue numbering is for *Synechocystis* FTR.

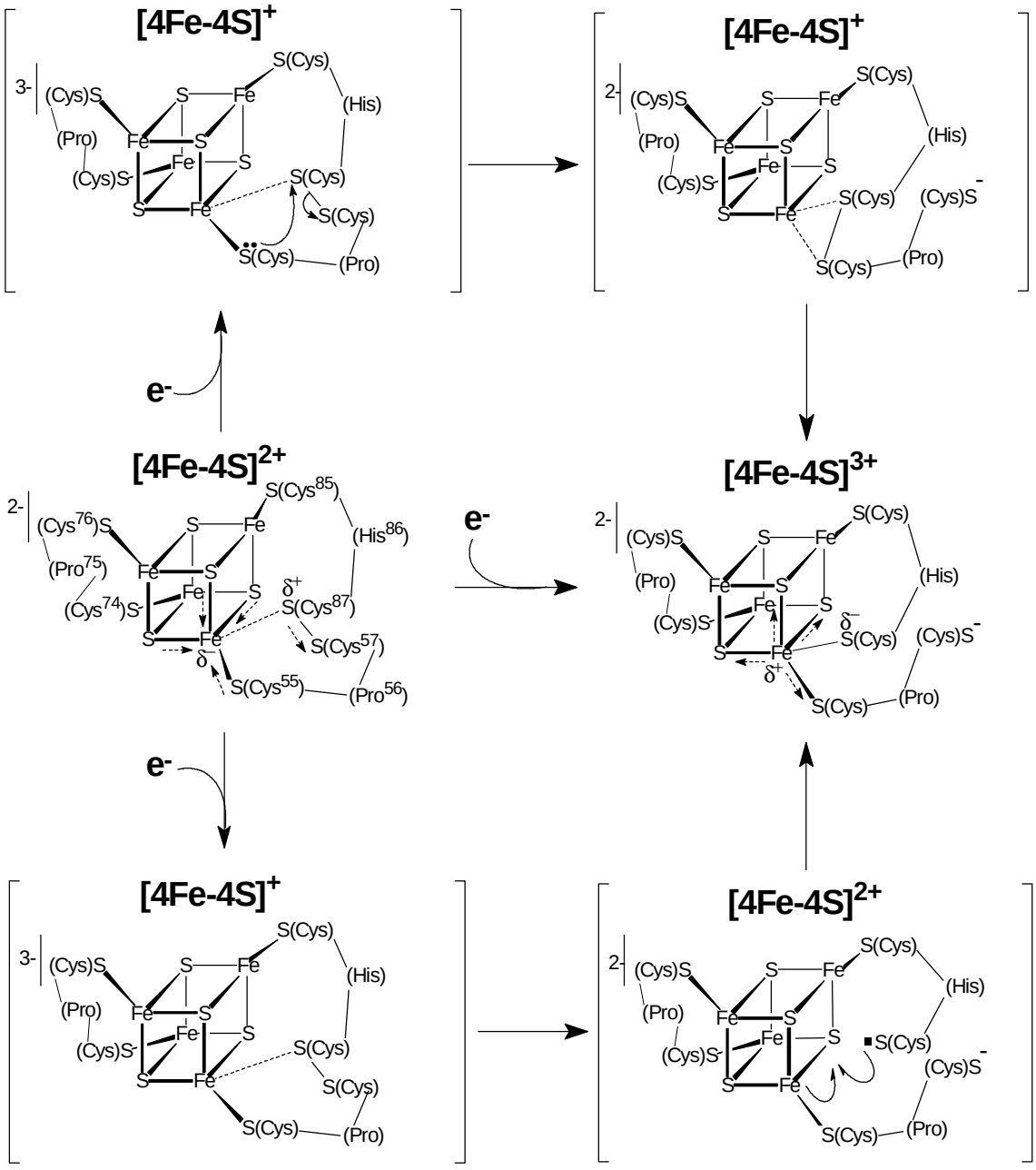
[4Fe-4S]+
[4Fe-4S]+
[4Fe-4S]2+
[4Fe-4S]3+
[4Fe-4S]+
[4Fe-4S]2+
e-
e-
e-

Figure 2.13 Proposed catalytic cycle for HDR.

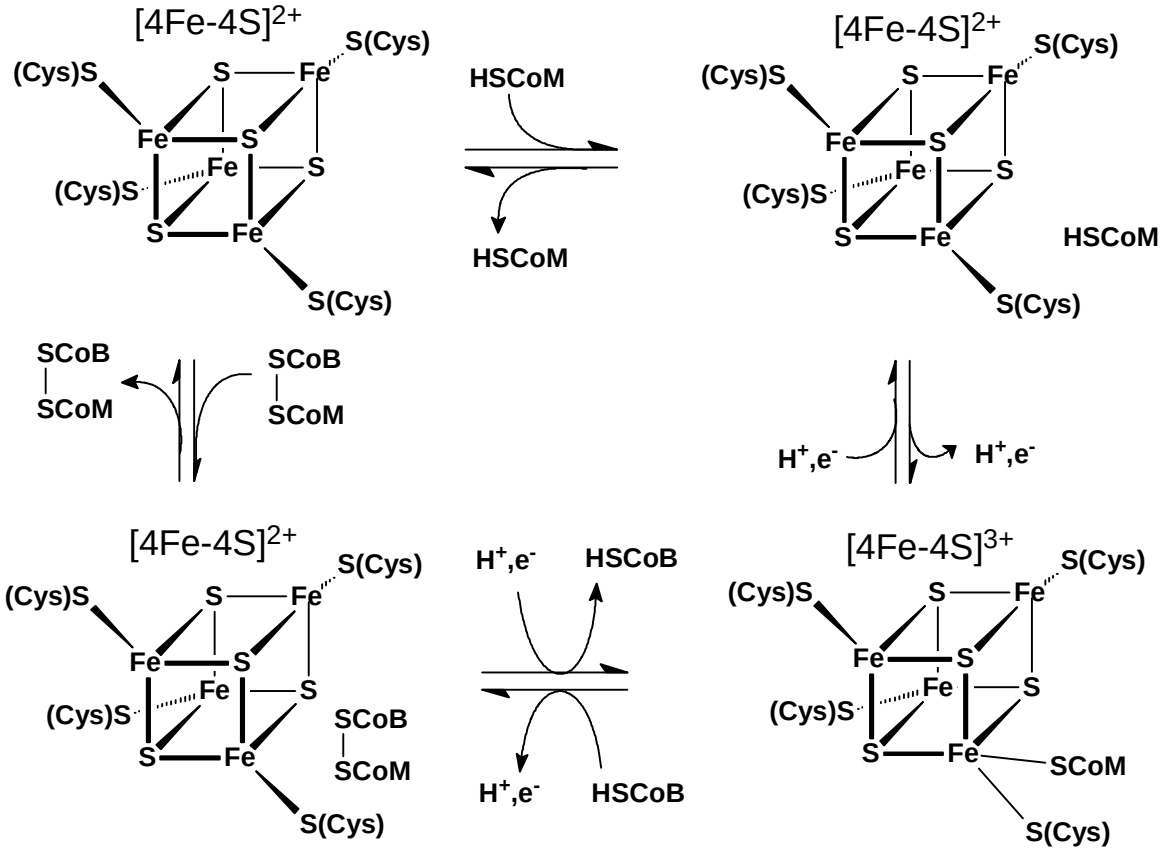
[4Fe-4S]2+
S(Cys)
(Cys)S
S
Fe
HSCoM
HSCoM
[4Fe-4S]2+
S(Cys)
(Cys)S
HSCoM
SCoB
SCoM
SCoB
SCoM
H+,e-
H+,e-
[4Fe-4S]2+
S(Cys)
(Cys)S
SCoB
SCoM
H+,e-
HSCoB
H+,e-
HSCoB
[4Fe-4S]3+
S(Cys)
(Cys)S
SCoM

CHAPTER 3

SPECTROSCOPIC EVIDENCE FOR SITE SPECIFIC CHEMISTRY AT A UNIQUE IRON SITE OF THE [4FE-4S] CLUSTER IN FERREDOXIN:THIOREDOXIN REDUCTASE[1]

[1] Reproduced with permission from Jameson, G.N.L.[§]; Walters, E.M.[†]; Manieri, W.[‡]; Schürmann, P.[‡]; Johnson, M.K.[†]; Huynh, B.H. [§] *J. Am. Chem. Soc.***2003**, *125*, 1146-1147. Copyright 2003 American Chemical Society. [§] Department of Physics, Emory University, Atlanta, GA, 30322, [†] Department of Chemistry and Center for Metalloenzyme Studies, University of Georgia, Athens, GA, 30602, and [‡] Laboratoire de Biochemie Végétale, Université de Neuchâtel, CH-2007 Neuchâtel, Switzerland.

Abstract

Ferredoxin:thioredoxin reductase (FTR) catalyzes the reduction of the disulfide in thioredoxin in two one-electron steps using an active site comprising a [4Fe-4S] in close proximity to a redox active disulfide. Mössbauer spectroscopy has been used to investigate the ligation and electronic properties of the [4Fe-4S] cluster in as-prepared FTR, which has the active-site disulfide intact, and in the *N*-ethylmaleimide (NEM)-modified form, which provides a stable analogue of the one-electron-reduced heterodisulfide intermediate and has one of the cysteines of the active-site disulfide alkylated with NEM. The results reveal novel site-specific cluster chemistry involving weak interaction of the active-site disulfide with a unique Fe site of the $[4Fe\text{-}4S]^{2+}$ cluster in the resting enzyme and cleavage of the active-site disulfide with concomitant coordination of one of the cysteines to yield a $[4Fe\text{-}4S]^{3+}$ cluster with a five-coordinate Fe site ligated by two cysteine residues in the NEM-modified enzyme. The results provide molecular-level insight into the catalytic mechanism of FTR and other Fe-S-cluster-containing disulfide reductases, and suggest a possible mechanism for the reductive cleavage of *S*-adenosylmethionine by the radical SAM family of Fe-S enzymes.

Introduction

Ferredoxin:thioredoxin reductase (FTR) plays an important role in the light-regulated catalytic properties of enzymes involved in the Calvin cycle.[1] The light signal is transmitted in the form of electrons from the chlorophyll-containing thylakoid membranes via a [2Fe-2S] ferredoxin, FTR and thioredoxins to target enzymes, which are activated or deactivated by the reduction of regulatory disulfide bonds. FTR utilizes a unique active site that comprises a $[4Fe\text{-}4S]^{2+}$ cluster with an adjacent disulfide[2-4] to catalyze the two-electron reduction of the thioredoxin disulfide. Previous spectroscopic investigations of the *Spinacea oleracea* FTR[3,5] have shown that alkylation of one cysteine of the active-site disulfide (C_{54}) by N-ethylmaleimide (NEM) affords a stable analog of the one-electron reduced catalytic reaction intermediate. The combined EPR, ENDOR, resonance Raman and MCD data of the NEM-modified FTR suggest a novel type of $[4Fe\text{-}4S]^{3+}$ cluster with five cysteine ligands, but the ligation site of the fifth cysteine ligand was left undetermined.[5] In this study, both the as-purified and NEM-modified forms of FTR from spinach[6] have been investigated by Mössbauer spectroscopy to provide further understanding of the cluster coordination and electronic state. The results demonstrate the presence of a unique iron site in the [4Fe-4S] cluster and suggest that site-specific cluster chemistry, involving the formation of a five-coordinate Fe site with two cysteinate ligands, occurs during catalytic cycling of FTR.

Results and Discussion

The 4.2 K Mössbauer spectrum of the as-purified FTR recorded in a weak magnetic field of 50 mT shows a quadrupole doublet with a prominent shoulder on the side of the high-energy line (Figure 3.1, hatched marks). A spectrum recorded in a strong

magnetic field of 8 T (not presented) indicates that the cluster is diamagnetic, consistent with a $[4Fe\text{-}4S]^{2+}$ assignment. Both spectra can be deconvoluted into three components with an intensity ratio of 1:1:2 (Figure 3.1), corresponding to three distinct Fe sites, *a*, *b* and *c*, respectively (Table 3.1). Typically, the Fe atoms of a $[4Fe\text{-}4S]^{2+}$ cluster can be grouped into two valence-delocalized $Fe^{2.5+}Fe^{2.5+}$ pairs that are antiferromagnetically coupled to form a diamagnetic ground state,[7] and accordingly, the Mössbauer spectrum consists of a symmetric quadrupole doublet that can be deconvoluted into two overlapping equal-intensity doublets with parameters (δ = 0.40-0.45 mm/s, and ΔE_Q = 1.0-1.2 mm/s) that are indicative of $Fe^{2.5+}$ ions with tetrahedral sulfur coordination.[8,9] The observation of three distinct Fe sites for the $[4Fe\text{-}4S]^{2+}$ cluster of the as-purified FTR is therefore unusual, although not unprecedented. The absorption intensity indicates that site *c* represents one of the two $Fe^{2.5+}Fe^{2.5+}$ pairs. Therefore, sites *a* and *b* must represent the other pair. The parameters determined for both sites *b* and *c* are within the ranges observed for typical $[4Fe\text{-}4S]^{2+}$ clusters, indicating that they represent Fe sites of regular coordination. The larger δ and ΔE_Q of site *a*, however, indicate a unique Fe site with atypical coordination environment. This observation is consistent with the x-ray structure of *Synechocystis* FTR[4] which shows that the sulfur atom of one of the cysteine residues forming the active-site disulfide is in Van der Waals contact (3.1 Å) with both the Fe atom ligated by C_{52} (spinach enzyme sequence number) and the sulfur atom of C_{52}, resulting in the Fe site being distorted from tetrahedral coordination with a (C_{52})S-Fe-S angle of 129º that is opened towards the disulfide (Scheme 3.1). The presence of a unique Fe site in $[4Fe\text{-}4S]^{2+}$ clusters has been detected in both model compounds and proteins. In model complex studies, the increases in δ and ΔE_Q are correlated with increases in

coordination number at the unique Fe site.[10] In proteins, unique Fe sites were observed with increased δ upon binding of substrates to the $[4Fe\text{-}4S]^{2+}$ cluster in aconitase,[11] and upon binding of *S*-adenosylmethionine to the clusters in pyruvate formate-lyase activating enzyme,[12] and in biotin synthase.[13] Thus it is tempting to speculate that the larger δ and ΔE_Q of site *a* reflect a weak interaction between the active-site disulfide and the C_{52}-bound Fe in as-purified FTR.

Figure 3.2 shows the 4.2 K spectrum of the NEM-modified FTR recorded in a magnetic field of 8 T (hatched marks). The spectrum is paramagnetic, consistent with the $S = 1/2$ state determined by previous EPR investigation.[3,5] Three distinct components with a 1:1:2 intensity ratio are also observed, indicating that the unique Fe site persists in the NEM-modified FTR. The components corresponding to the two individual Fe sites *a* and *b* can be clearly seen to produce a splitting in the absorption in the region between +3 and +4 mm/s (Figure 3.2). Comparison of the parameters of the NEM-modified form of FTR with those of the as-purified form shows a general reduction in δ for all three Fe sites with the largest reduction of 0.31 mm/s occurring at the unique site *a*. This observation suggests that upon NEM-modification a reducing equivalent is removed from the cluster, mostly from site *a*, and supports previous spectroscopic evidence[3,5] that the cluster is formally in the $[4Fe\text{-}4S]^{3+}$ state. Further, the signs and magnitudes of the magnetic hyperfine coupling tensors compare well to those observed for $[4Fe\text{-}4S]^{3+}$ clusters in high-potential iron-sulfur proteins[14] and reveal the antiferromagnetic coupling between a mixed valence pair (site *c*) and a diferric pair (sites *a* and *b*).

Taken together, the Mössbauer data provide key insights into the FTR mechanism that may be understood in terms of a donor-acceptor approach involving the active-site disulfide and the unique Fe site of the [4Fe-4S] cluster. Partial bonding of the disulfide to the unique iron in the resting state of the cluster promotes charge build up on that iron, making it an electron donor with increased ferrous character, which, in turn, explains the increased isomer shift. Concomitantly, electron density is pushed away from the sulfur of C_{84} onto its sulfur neighbor weakening the S-S bond and making the C_{84} sulfur an electron acceptor (Scheme 3.1). The system is therefore primed and ready to accept an electron from ferredoxin to break the disulfide bond. When this occurs, C_{84} binds to give a five-coordinate Fe site with two cysteinate ligands, thereby freeing C_{54} to attack the disulfide of thioredoxin to form the heterodisulfide intermediate. This one-electron reduced state is modeled by the NEM-modified form (Scheme 3.1). The binding of an additional cysteine to the unique Fe reverses the donor-acceptor properties, and charge is drawn away from the iron. The cluster is then formally in the $[4Fe\text{-}4S]^{3+}$ oxidation state and the unique Fe becomes more ferric, leading to a dramatic decrease in the isomer shift of that iron. This novel site-specific cluster chemistry provides molecular level insight into how the [4Fe-4S] cluster mediates disulfide reduction in two one-electron steps in FTR and the related methanogenic heterodisulfide reductases.[15] In addition it may provide a paradigm for understanding the mechanism of reductive cleavage of *S*-adenosylmethionine to yield methionine and the 5’-deoxy-adenosyl radical in the radical SAM family of Fe-S enzymes.

Acknowledgments

This work was supported by grants from the NIH (GM47295 to B.H.H. and GM62542 to M.K.J.) and the Schweizerischer Nationalfonds (31-56761.99 to P.S.)

Bibliography

(1) Dai, S.; Schwendtmayer, C.; Johansson, K.; Ramaswamy, S.; Schürmann, P.; Eklund, H. *Quart. Rev. Biophys.* **2000**, *33*, 67-108.

(2) Chow, L.-P.; Iwadate, H.; Yano, K.; Kamo, M.; Tsugita, A.; Gardet-Salvi, L.; Stritt-Etter, A.-L.; Schürmann, P. *Eur. J. Biochem.* **1995**, *231*, 149-156.

(3) Staples, C. R.; Ameyibor, E.; Fu, W.; Gardet-Salvi, L.; Stritt-Etter, A.-L.; Schürmann, P.; Knaff, D. B.; Johnson, M. K. *Biochemistry* **1996**, *35*, 11425-11434.

(4) Dai, S.; Schwendtmayer, C.; Schürmann, P.; Ramaswamy, S.; Eklund, H. *Science* **2000**, *287*, 655-658.

(5) Staples, C. R.; Gaymard, E.; Stritt-Etter, A.-L.; Telser, J.; Hoffman, B. M.; Schürmann, P.; Knaff, D. B.; Johnson, M. K. *Biochemistry* **1998**, *37*, 4612-4620.

(6) Overexpression and purification of spinach FTR was performed according to the published procedure (Gaymard, E.; Franchini, L.Manieri, W.; Stutz, E.; Schürmann, P. *Plant Sci.* **2000**, *158*, 107-113). ^{57}Fe incorporation was achieved by addition of ^{57}Fe ferric ammonium citrate to chelex-resin-treated LB media to a final Fe concentration of 5 mg/L. NEM-modified FTR was prepared as previously described,[3] using reduced methyl viologen as the reductant.

(7) Noodleman, L.; Peng, C. Y.; Case, D. A.; Mouesca, J.-M. *Coord. Chem. Rev.* **1995**, *144*, 199-244.

(8) Yoo, S. J.; Angove, H. C.; Burgess, B. K.; Hendrich, M. P.; Münck, E. *J. Am. Chem. Soc.* **1999**, *121*, 2534-2545.

(9) Trautwein, A. X.; Bill, E.; Bominaar, E. L.; Winkler, H. *Struct. Bonding* **1991**, *78*, 1-95.

(10) Ciurli, S.; Carrie, M.; Weigel, J. A.; Carney, M. J.; Stack, T. D. P.; Papaefthymiou, G. C.; Holm, R. H. *J. Am. Chem. Soc.* **1990**, *112*, 2654-2664.

(11) Beinert, H.; Kennedy, M. C.; Stout, C. D. *Chem. Rev.* **1996**, *96*, 2335-2373.

(12) Krebs, C.; Broderick, W. E.; Henshaw, T. F.; Broderick, J. B.; Huynh, B. H. *J. Am. Chem. Soc.* **2002**, *124*, 912-913.

(13) Cosper, M. M.; Jameson, G. N. L.; Eidsness, M. K.; Huynh, B. H.; Johnson, M. K. *J. Am. Chem. Soc*., in press.

(14) Middleton, P.; Dickson, D. P.; Johnson, C. E.; Rush, J. D. *Eur. J. Biochem.* **1980**, *104*, 289-296.

(15) Duin, E. C.; Maladi-Kahkesh, S.; Hedderich, R.; Clay, M. D.; Johnson, M. K. *FEBS Lett.* **2002**, *512*, 263-268.

Figure 3.1 Mössbauer spectrum of as-purified FTR (0.24 mM) recorded at 4.2 K in a field of 50 mT applied parallel to the ã beam (hatched marks). The spectrum can be de-convoluted into three components with an intensity ratio of 1:1:2 representing three Fe sites *a*, *b* and *c* (Table 3.1). The individual components are shown above the spectrum as two solid lines (*a* and *b* sites) and a dotted line (*c*). The solid line overlaid with the experimental spectrum is the sum of the three components.

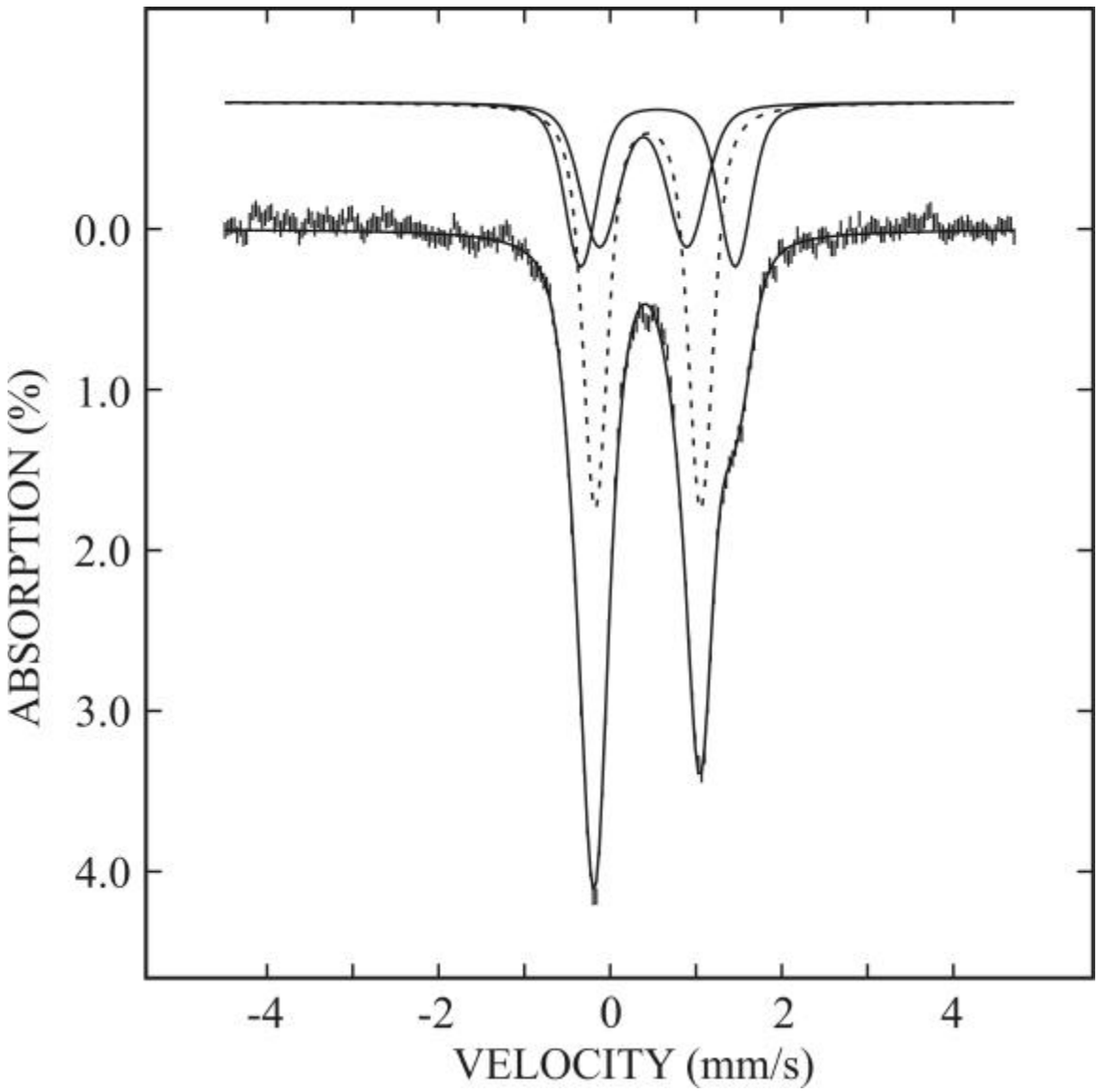
ABSORPTION (%)
0.0
1.0
2.0
3.0
4.0
-4
-2
0
2
4
VELOCITY (mm/s)

Table 3.1 Mössbauer parameters of as-purified and NEM-modified spinach FTR.

protein state	cluster state	Fe site	δ (mm/s)	ΔE_q (mm/s)	η	A_x (T)	A_y (T)	A_z (T)
as purified[a]	$[4Fe\text{-}4S]^{2+}$ $S = 0$	a	0.56	1.80	0.5	-	-	-
		b	0.39	1.02	0.5	-	-	-
		c	0.44	1.23	0.5	-	-	-
NEM modified[b]	$[4Fe\text{-}4S]^{3+}$ $S = 1/2$	a	0.30	1.2	0	22.5	18.5	8.0
		b	0.30	-1.2	0	21.5	19.5	18.5
		c	0.44	1.2	0	- 26.5	- 29.5	- 24.5

[a] The spectrum shown in Figure 3.1 can also be fitted with two quadrupole doublets with an intensity ratio of 1:3. However, the line shape of the high-energy line is better fitted with three components.
[b] To minimize the number of parameters in our analysis, the δ of the two ferric sites and the magnitude of the ΔE_q of all three sites are assumed to be the same. The ΔE_q of site *c* can be determined accurately from the spectrum shown in Figure 3.2.

Figure 3.2 Mössbauer spectrum of NEM-modified FTR (0.23 mM) measured at 4.2 K in a field of 8 T applied parallel to the ã beam (hatched marks). The spectrum has been de-convoluted into three components (shown above the spectrum) with an intensity ratio of 1:1:2 corresponding to two distinct Fe sites of the ferric pair (sites a and b, solid lines) and a delocalized mixed-valence pair (site c, dashed line). The solid line overlaid with the experimental data is the sum of the three components.

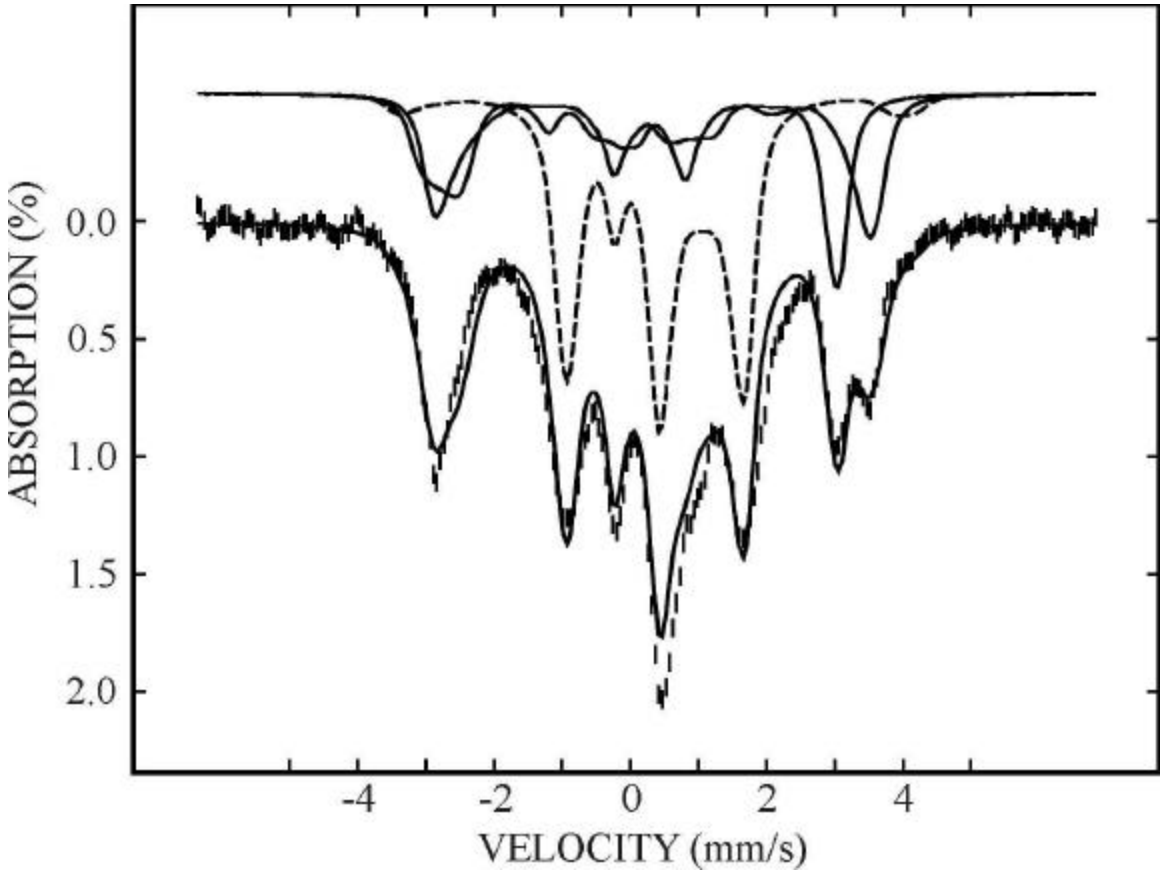
ABSORPTION (%)
0.0
0.5
1.0
1.5
2.0
-4
-2
0
2
4
VELOCITY (mm/s)

Scheme 3.1 Illustration of unique iron site chemistry of the [4Fe-4S] cluster in the as-purified FTR and the one-electron reduced intermediate, as modeled by NEM-modified FTR.

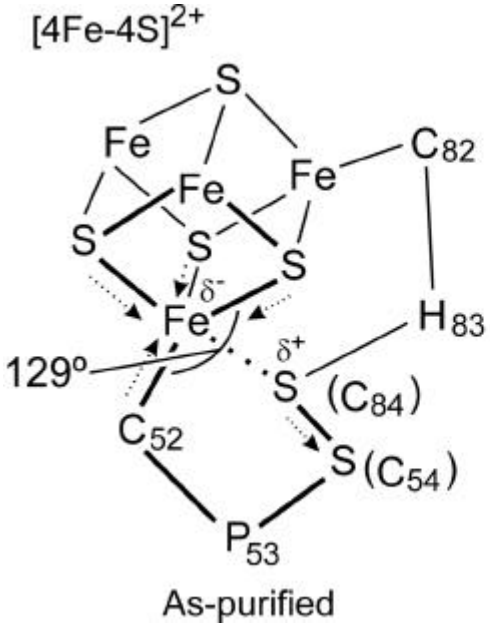

As-purified

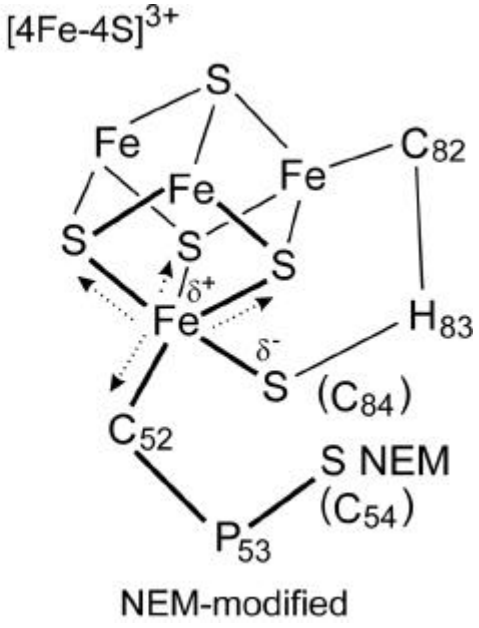

NEM-modified

CHAPTER 4

SPECTROSCOPIC CHARACTERIZATION OF SITE-SPECIFIC [4Fe-4S] CLUSTER CHEMISTRY IN FERREDOXIN:THIOREDOXIN REDUCTASE: IMPLICATIONS FOR THE CATALYTIC MECHANISM[1]

[1] Walters, E.M.[§]; Garcia-Serres, R.[†]; Jameson, G.N.L.[†]; Glauser, D.A.[‡]; Bourquin, F.[‡]; Manieri, W.[‡]; Schürmann, P.[‡]; Johnson, M.K.[§]; Huynh, B.H.[†] Submitted to *J. Am. Chem. Soc.*, 03/24/2005 [§] Department of Chemistry and Center for Metalloenzyme Studies, University of Georgia, Athens, GA, 30602, [†] Department of Physics, Emory University, Atlanta, GA, 30322, and [‡] Laboratoire de Biochemie Végétale, Université de Neuchâtel, CH-2007 Neuchâtel, Switzerland.

Abstract

Light regulation in oxygenic photosynthesis is mediated by ferredoxin:thioredoxin reductase (FTR), a novel class of disulfide reductase with an active-site comprising a $[4Fe\text{-}4S]^{2+}$ cluster and an adjacent disulfide, that catalyzes reduction of the thioredoxin disulfide in two sequential one-electron steps using a $[2Fe\text{-}2S]^{2+/+}$ ferredoxin as the electron donor. In this work we report on spectroscopic (EPR, VTMCD, resonance Raman and Mössbauer) and redox characterization of the active site of FTR in a variety of different forms: wild-type, variants involving point mutations of each of the cysteines of the active-site disulfide (C57S and C87A), and chemically modified forms in which Cys57 is alkylated with *N*-ethylmaleimide (NEM-FTR) or covalent attached via a heterodisulfide to the active-site cysteine of C40S thioredoxin *m* (FTR/Trx *m* heterodisulfide complex). The results reveal distinct and non-interchangeable roles for the active-site cysteines, with Cys87 interacting with the cluster to facilitate one-electron reductive cleavage of the active site disulfide and Cys57 facilitating nucleophilic attack and cleavage of the substrate disulfide, and demonstrate the viability of the FTR/Trx heterodisulfide complex as a one-electron-reduced catalytic intermediate with spectroscopic and redox properties similar to those of oxidized NEM-FTR. In addition, Mössbauer studies reveal novel site-specific [4Fe-4S] cluster chemistry in all three redox states of FTR. In the oxidized (resting) state, mutagenesis results confirm a weak interaction between a unique Fe site and the disulfide that results in partial valance localization of one of the two valence-delocalized $Fe^{2+}Fe^{3+}$ pairs of the $[4Fe\text{-}4S]^{2+}$ cluster and primes the active site for one-electron reduction with concomitant cleavage of the active-site disulfide . Oxidized NEM-FTR and the FTR/Trx heterodisulfide complex are

potential analogs of a one-electron-reduced intermediate and comprise $[4Fe\text{-}4S]^{3+}$ clusters with two cysteinate ligands at the unique Fe site. The most intriguing result is that two-electron-reduced FTR, in which the disulfide is reduced to a dithiol, contains an unprecedented electron-rich $[4Fe\text{-}4S]^{2+}$ cluster comprising both valence-delocalized and valence-localized $Fe^{2+}Fe^{3+}$ pairs. This result is interpreted in terms of stabilization of a Fe^{2+} site via strong H-bonding interaction between the thiol form of Cys87 and the coordinated S atom of Cys55. Consequently, Cys87 is likely to be anchored by interaction with the cluster in both the one-electron-reduced and two-electron-reduced forms of FTR, leaving Cys57 free to attack the substrate disulfide. Two possible catalytic mechanisms are therefore proposed that differ in terms of whether interaction with thioredoxin to form a heterodisulfide intermediate occurs at the one-electron or two-electron-reduced levels.

Introduction

Ferredoxin:thioredoxin reductase (FTR) is a novel type of disulfide reductase that plays a central role in light regulation of oxygenic photosynthesis in chloroplasts.[1] FTR functions as a signal transducer, catalyzing the conversion of the light-induced electronic signal in the form of reduced [2Fe-2S] ferredoxin (Fd) to a chemical signal in the form of the reduced dithiol form of thioredoxins (Trx) *m* and *f*:[2]

$$2Fd_{red} + Trx_{ox} + 2H^{+} \rightarrow 2Fd_{ox} + Trx_{red}$$

The reduced Trxs subsequently activate or inactivate a range of target enzymes via dithiol/disulfide exchange in order to optimize light-dependent metabolism.[1,3] The majority of disulfide reductases in biology are flavoenzymes that function by concerted two-electron steps, using NAD(P)H as the electron donor to reduce an active-site flavin which in turn reduces an adjacent disulfide.[4-6] In contrast, FTR is unique in using a one-electron donor in the form of reduced [2Fe-2S] Fd and an active site comprising a [4Fe-4S] cluster in close proximity to an active-site disulfide.[7-9] Understanding the molecular role of the active-site Fe-S cluster in mediating disulfide reduction in two sequential one-electron steps and facilitating substrate reduction promises to reveal new site-specific functionality for biological [4Fe-4S] clusters.

FTR is a heterodimer comprising a highly conserved 13-kDa catalytic subunit, which houses the [4Fe-4S] cluster and the adjacent disulfide, and a variable subunit of similar or smaller size, which shows little sequence conservation between species.[7,8] *Synechocystis* sp. PCC6803 FTR has been structurally characterized in the oxidized state by x-ray crystallography at 1.6 Å resolution and found to be a concave disk, 40–50 Å in diameter and 10 Å across at the center.[9] The cluster and disulfide are positioned near the

center of the disk with putative binding sites for the [2Fe-2S] Fd on the [4Fe-4S] cluster side and for Trx on the disulfide side.[9] Crystallography confirmed the active-site structure deduced from spectroscopic and chemical modification studies of spinach FTR,[7,8,10] comprising a [4Fe-4S] cluster ligated by four cysteinyl ligands (Cys55, Cys74, Cys76, and Cys85 for *Synechocystis*) adjacent to an asymmetrically disposed disulfide (Cys57 and Cys87 for *Synechocystis*). As shown in Figure 4.1, the active-site disulfide is very close to the cluster with the S atom of Cys87 3.1 Å from both a cluster Fe and the S atom of the coordinating Cys residue (Cys55) and 3.4 Å from a μ_3-S^{2-}.[9] Moreover, the possibility of a weak interaction between the disulfide and the unique Fe site is suggested by the μ_3–S–Fe–S(Cys55) angle that is opened to 129° and Mössbauer studies.[11,12]

Spectroscopic studies of wild-type spinach FTR and a chemically modified inactive form, termed NEM-FTR, in which Cys54 (corresponding to Cys57 in *Synechocystis* FTR) is selectively alkylated with N-ethylmaleimide (NEM), have provided insight into the catalytic mechanism and the nature of the one-electron-reduced intermediate.[8,10,11] While both the oxidized (disulfide) and two-electron-reduced (dithiol) forms of FTR contain $S = 0$ $[4Fe\text{-}4S]^{2+}$ clusters, a transient $S = 1/2$ species corresponding to a one-electron-reduced intermediate was observed via freeze-quench EPR studies on reduction with stoichiometric reduced methyl viologen and during catalytic turnover in the presence of Trx, and found to have EPR properties identical to oxidized NEM-FTR.[10] Hence NEM-FTR provides a stable analog of the one-electron-reduced intermediate, thereby facilitating detailed spectroscopic characterization. The combination of UV-visible absorption, EPR, ^{57}Fe and ^{1}H electron nuclear double resonance (ENDOR), variable-temperature magnetic circular dichroism (VTMCD), resonance Raman, and

Mössbauer spectroscopies have shown that NEM-FTR contains a novel type of S =1/2 $[4Fe\text{-}4S]^{3+}$ cluster with an anomalously low redox potential for the $[4Fe\text{-}4S]^{3+/2+}$ couple (E_m = –210 mV at pH 7).[8,10,11] The structural and redox properties, coupled with the Mössbauer characterization of oxidized wild-type spinach FTR and oxidized spinach NEM-FTR, which indicate that one-electron reduction is accompanied by site-specific oxidation at a unique Fe site of the [4Fe-4S] cluster,[11] have lead to the proposal that oxidized NEM-FTR and, by analogy, the one-electron-reduced intermediate, comprise a $[4Fe\text{-}4S]^{3+}$ cluster with two cysteinate ligands at the unique Fe site (Cys55 and Cys87 in *Synechocystis* FTR; Cys52 and Cys84 in spinach FTR).[11,12] Hence one-electron-reduction can be formally viewed as two-electron-reduction of the disulfide with concurrent one-electron-oxidation of the cluster due to coordination of an additional cysteinate ligand. This provides a means of anchoring one of the active-site thiol ligands via cluster coordination (the cluster-interacting or electron-transfer thiol), while freeing the other thiol (interchange thiol) for nucleophilic attack of the Trx disulfide to form an FTR/Trx heterodisulfide intermediate. Further one-electron reduction reduces the cluster to the $[4Fe\text{-}4S]^{2+}$ state and releases the electron-transfer thiol to reform the active-site disulfide, with concomitant cleavage of the heterodisulfide and formation of the reduced dithiol form of Trx. The proposed mechanistic scheme is depicted in Figure 4.2.[12]

The mechanistic scheme shown in Figure 4.2 predicts specific and non-interchangeable roles for each of the two active-site cysteines and the existence of an FTR/Trx heterodisulfide intermediate analogous to oxidized NEM-FTR. The primary objective of this study was therefore to test these predictions by characterizing the spectroscopic and redox properties of the [4Fe-4S] clusters in variants involving site-

specific mutations of each of the active-site cysteine residues and in a stable heterodisulfide complex involving FTR and an active-site cysteine variant of Trx.[13] To this end we report EPR, VTMCD, resonance Raman, Mössbauer and redox studies of wild-type, NEM-modified, C57S, and C87A *Synechocystis* FTR as well as the *Synechocystis* FTR/Trx *m* heterodisulfide complex. The results confirm the proposal of distinct and non-interchangeable roles for the active-site cysteines and the formation of an FTR/Trx heterodisulfide complex that is a potential analog of a one-electron-reduced catalytic intermediate, with spectroscopic and redox properties similar to those of oxidized NEM-FTR. In addition, the Mössbauer studies reveal novel site-specific [4Fe-4S] cluster chemistry in all three redox states of FTR (oxidized, one-electron-reduced and two-electron-reduced) and raise the possibility of an alternative mechanism in which FTR is reduced by two electrons prior to interaction with Trx.

Experimental Methods

Protein Expression and Purification. The construction of the overexpression strains as well as the procedures used for overexpression and purification of wild-type, C87A and C57S *Synechocystis* FTR, wild-type spinach FTR, and the C40S variant of spinach Trx *m* have been described elsewhere.[13,14] Incorporation of ^{57}Fe for Mössbauer analysis was effected by addition of ^{57}Fe ferric ammonium citrate to chelex-resin-treated LB media to a final Fe concentration of 5 mg/L.[11]

Sample Preparation and Handling. Recombinant wild-type spinach and *Synechocystis* FTR was initially purified with varying amounts of the enzyme in a form that closely resembles NEM-FTR based on EPR studies (up to 20% based on EPR spin quantitations). The EPR-silent oxidized form of recombinant FTR was generally

obtained only after redox cycling the enzyme by dithionite reduction followed by O_2 oxidation. This redox-cycled form of oxidized wild-type FTR was used as the starting material for the formation of methyl viologen reduced FTR, NEM-FTR and the heterodisulfide complex between FTR and C40S Trx *m*. The formation of the heterodisulfide complex was performed as described elsewhere.[13] Both C87A and C57S FTR were used in the as-purified form and spectroscopic studies gave no indication of heterogeneity in the vicinity of the $[4Fe\text{-}4S]^{2+}$ cluster. Unless otherwise indicated, all forms of FTR were in 20 mM triethanolamine-HCl buffer, pH 7.3, and were handled under anaerobic conditions in a Vacuum Atmospheres glove box under an Ar atmosphere (<1 ppm O_2).

Selective NEM modification of Cys57 of WT FTR to form NEM-FTR was carried out by reducing FTR under anaerobic conditions with a 3-fold excess of reduced methyl viologen, incubating for 30 minutes to ensure complete reduction of the active-site disulfide, followed by cooling on ice for 10 mins and treating with a 5-fold excess of NEM for two minutes prior to quenching the reaction by exposure to air. Excess reagents were removed by gel-filtration and the sample was concentrated by Amicon ultrafiltration using a YM10 membrane. Sample concentrations were based upon $\varepsilon_{410} = 17400\ M^{-1}\ cm^{-1}$ for WT and C87A FTR, and $\varepsilon_{410} = 19500\ M^{-1}\ cm^{-1}$ for NEM-FTR, C57S FTR, and the FTR/C40S Trx *m* heterodisulfide complex.[13,16]

Dye-mediated redox titrations were performed on NEM-FTR and the FTR/C40S Trx *m* heterodisulfide complex at ambient temperature (25-27 ºC) in a Vacuum Atmospheres glove box under argon (<1 ppm O_2). The pH dependence of the midpoint redox potential was determined using enzyme in a buffer cocktail containing 200 mM

MES, MOPS, and TAPS buffers which allows for easy variation of the pH in the desired range (6.0-8.5). Mediator dyes were added, each to a final concentration of 50 μM, in order to cover the desired range of redox potentials, i.e., methyl viologen, benzyl viologen, neutral red, safranin, phenosafranin, anthroquinone-1,5-disulfonate, indigodisulfonate, methylene blue, 1,2-napthoquinone, duroquinone, and 1,2-napthoquinone-4-sulfonate. The starting point of the titrations was the oxidized as prepared sample and the potential was poised by reductive titration using 10 mM dithionite in the redox titration buffer at the same pH as the protein titration mixture. Upon completion of the reductive titration, 10 mM potassium ferricyanide in the same redox titration buffer was added to return the potential to a value approximately that of the starting material in order to test whether the reduction was reversible and to access the extent of reoxidation. For all data points, a 0.25-mL aliquot was transferred to an EPR tube after equilibration at the desired potential and the sample was immediately frozen in liquid nitrogen. Potentials were measured with a platinum working electrode and a saturated calomel reference electrode and are reported relative to NHE. All redox titration data have been normalized for dilution effects that occur throughout the reduction titration. To assess if cleavage of the FTR/C40S Trx *m* heterodisulfide occurs concomitant with the EPR-monitored reduction of the complex, samples poised at selected potentials were removed and loaded onto a 5-mL High-Performance Q-Sepharose column under strictly anaerobic conditions inside the glove box. A linear gradient from 0.0 to 0.5 M NaCl in 20 mM triethanolamine-HCl, pH 7.3 buffer was used to elute the components and separate the FTR/Trx *m* complex from free C40S Trx *m* and wild-type FTR. The components in the elution profile were identified by parallel studies

of the elution profiles of the oxidized FTR/Trx *m* complex, C40S Trx *m* and wild-type FTR.

Spectroscopic Measurements. X-band (~9.6 GHz) EPR spectra were recorded on a Bruker ESP300E spectrometer equipped with an ER-4116 dual mode cavity and an Oxford Instruments ESR-9 flow cryostat. Raman spectra were recorded with an Instruments SA U1000 spectrometer fitted with a cooled RCA 31034 photomultiplier tube, using 457-nm excitation from Coherent Innova 10-W Ar^+ laser. Scattering was collected at 90º from the surface of a frozen 15 μL droplet of protein in a specially constructed anaerobic cell mounted on the coldfinger of an Air Products Displex model CSA-202E closed cycle refrigerator.[17] The spectrum of the frozen buffer solution, normalized to the intensity of the ice-band at 230 cm^{-1}, has been subtracted from all the spectra shown in this work. Variable-temperature magnetic circular dichroism (VTMCD) measurements were carried out with an Oxford Instruments Spectromag 4000 split-coil superconducting magnet mated to a Jasco J715 spectropolarimeter using the published protocols.[18,19] Mössbauer spectra were recorded using the previously described spectrometers.[20] The zero velocity refers to the centroid of the room temperature spectra of metallic iron foil. Analysis of the Mössbauer data was performed with the program WMOSS (WEB Research).

Results

Previous spectroscopic investigations on FTR have been concentrated on the oxidized and NEM-modified forms of the native and recombinant forms of the spinach enzyme.[8,10,11] In this manuscript, the emphasis is on spectroscopic characterization of crystallographically defined recombinant FTR from *Synechocystis* and selected site-

specific variants, in each of their accessible redox states. Spectroscopic data of oxidized and NEM-modified *Synechocystis* FTR will also be presented for the purposes of establishing the commonality between the spinach and *Synechocystis* enzymes, and for providing references for comparison studies with those of the other forms of FTR that are characterized in this work.

Oxidized FTR. Figure 4.3 shows the 4.2-K Mössbauer spectra of oxidized recombinant *Synechocystis* FTR recorded in a weak magnetic field of 50 mT (A) and a strong field of 6 T (B) applied parallel to the γ beam. The presence of a unique Fe site in the [4Fe-4S] cluster is readily observable as a prominent shoulder on the side of the high energy line of both spectra. Similar to oxidized recombinant spinach FTR,[11] these spectra can be interpreted as superpositions of three spectral components with an intensity ratio of 1:1:2, corresponding to three distinct Fe sites, *a*, *b* and *c* (Table 4.1), arising from the diamagnetic $S = 0$ ground state of a $[4Fe\text{-}4S]^{2+}$ cluster. Within experimental errors, the parameters obtained for *Synechocystis* FTR (Table 4.1) are identical to those reported for spinach FTR.[11] Sites *b* and *c* exhibit parameters within the ranges observed for typical $[4Fe\text{-}4S]^{2+}$ clusters, and thus represent Fe sites of regular coordination (i.e., tetrahedral S coordination) and oxidation state ($Fe^{2.5+}$) that are expected for a $[4Fe\text{-}4S]^{2+}$ cluster.[21-24] The doubled absorption intensity determined for site *c* indicates further that it represents a valence-delocalized $Fe^{2+}Fe^{3+}$ pair within the cluster. Site *a*, however, with its larger ΔE_Q, represents a unique Fe site with atypical coordination environment. Based on the x-ray crystallographic structure determined for *Synechocystis* FTR,[9] site *a* is assigned to the Fe atom coordinated to residue C55 (C52 for spinach FTR). This Fe atom and the coordinated cysteinyl-S atom are in Van der Waals contact (3.1 Å) with one of the S

atoms that form the active-site disulfide (C57 and C87), see Figure 4.1, resulting in an iron site having a distorted tetrahedral coordination,[9,11,12] and thus increased DE_Q. We have suggested that this interaction between the unique Fe and the active-site disulfide is of mechanistic importance:[11] It promotes charge buildup at the unique Fe site (and therefore the increased δ value), making it an electron donor, and polarizes the disulfide bond, making the interacting S of C87 an electron acceptor. The resting enzyme is therefore primed to accept an electron for the breaking of the disulfide bond.

The resonance Raman spectrum of the oxidized recombinant *Synechocystis* FTR (Figure 4.4A) is very similar to that reported and assigned for the native spinach enzyme as purified,[8] and the frequencies and relative intensities of the bands are characteristic of $[4Fe\text{-}4S]^{2+}$ clusters with complete cysteinyl-S coordination.[25] Weak interaction between the unique Fe site and the disulfide is not readily apparent in the resonance Raman spectrum. However, as discussed below, interaction with the disulfide is suggested by changes in the resonance Raman spectra of the $[4Fe\text{-}4S]^{2+}$ center in oxidized FTR compared to the spectra of the $[4Fe\text{-}4S]^{2+}$ centers in as purified C87A variant and dithionite-reduced C57S variant, see Figure 4.4.

Oxidized NEM-FTR. One of the cysteine residues forming the active-site disulfide (Cys54 in spinach FTR and Cys57 in *Synechocystis* FTR) becomes solvent exposed on reduction and hence can be selectively alkylated by NEM in methyl viologen-reduced FTR, resulting in the formation of NEM-FTR. In contrast to oxidized wild-type FTR which is EPR silent, NEM-FTR shows an intense near-axial $S = 1/2$ EPR signal in the oxidized (as purified) form.[8,10] Figure 4.5A shows the 35-K EPR spectrum of oxidized *Synechocystis* NEM-FTR, which comprises a near-axial resonance with $g =$

2.11, 1.99 and 1.98. Very similar EPR signals have been reported for the oxidized NEM-modified form of native spinach FTR,[8,10] and in both the resonances account for approximately 1 spin/FTR and can be observed up to 150 K without significant broadening.

The observations that oxidized NEM-FTR exhibits an EPR signal with an average *g* value larger than 2.0 and that one-electron reduction converts the *S* = 1/2 EPR-active NEM-FTR into an EPR-silent form with a *S* = 0 $[4Fe\text{-}4S]^{2+}$ cluster [8] are consistent with NEM-FTR containing a $[4Fe\text{-}4S]^{3+,2+}$ cluster. Moreover, optical absorption, resonance Raman, ENDOR, VTMCD and Mössbauer spectroscopies [8,10,11] have been used to characterize oxidized spinach NEM-FTR and the results unambiguously confirmed the presence of a $[4Fe\text{-}4S]^{3+}$ cluster. The VTMCD spectra of oxidized *Synechocystis* NEM-FTR (Figure 4.6A) are very similar to those observed for the spinach enzyme,[8] and show saturation magnetization behavior consistent with transitions originating from a *S* = 1/2 ground state, indicating that both the EPR and VTMCD transitions are arising from the same paramagnetic ground state. The complex and intense pattern of VTMCD bands observed for oxidized NEM-FTR can only be interpreted in terms of the unpaired spin being associated with a $[4Fe\text{-}4S]^{3+}$ cluster. However, the VTMCD spectra are quite distinct from those observed for $[4Fe\text{-}4S]^{3+}$ clusters in high-potential iron-sulfur proteins (HiPIPs),[26] suggesting some unique excited-state electronic properties for this type of $[4Fe\text{-}4S]^{3+}$ center. The resonance Raman spectrum of oxidized *Synechocystis* NEM-FTR (Figure 4.7A) is also very similar to that reported and assigned for oxidized spinach NEM-FTR.[8] Furthermore, the changes in the resonance Raman spectrum of oxidized *Synechocystis* NEM-FTR compared to that of the $[4Fe\text{-}4S]^{2+}$ center in oxidized

Synechocystis FTR (cf. Figures 4.7A and 4.4A), i.e. small upshifts (≤ 3 cm^{-1}) in most of the predominantly bridging Fe–S stretching modes and large upshifts (≤ 17 cm^{-1}) in all of the predominantly terminal Fe–S(Cys) stretching modes, are consistent with the presence of a $[4Fe\text{-}4S]^{3+}$ cluster in oxidized NEM-FTR. Nevertheless, the resonance Raman spectrum of NEM-FTR shows significant differences, compared to those reported for $[4Fe\text{-}4S]^{3+}$ centers in HiPIPs,[27,28] suggesting some unique structural properties for this type of $[4Fe\text{-}4S]^{3+}$ center. In addition, there are intriguing differences in the redox and ground-state electronic properties for the $[4Fe\text{-}4S]^{3+}$ cluster in oxidized NEM-FTR compared to those in HiPIPs.[8,10] In particular, the midpoint potential for the $[4Fe\text{-}4S]^{3+,2+}$ couple is at least 500mV lower and ground-state spin relaxation rate for the $S = 1/2$ $[4Fe\text{-}4S]^{3+}$ center is much slower. The difference in spin relaxation is manifest by the ability to observe the EPR signal at 150 K without broadening for oxidized NEM-FTR samples, whereas the oxidized HiPIP EPR signals can only be observed at a temperature below 30 K.[29] These differences suggest a new-type of $[4Fe\text{-}4S]^{3+}$ cluster in NEM-FTR.

In oxidized NEM-FTR the active-site disulfide bond has been cleaved by a two-electron reduction and, as indicated by the above mentioned spectroscopic data, the [4Fe-4S] cluster is in the 3+ state. Consequently, oxidized NEM-FTR is one-electron more reduced than the resting enzyme. Previous investigations have shown that $S = 1/2$ EPR signals analogous to that of oxidized NEM-FTR were observed as transient species in spinach FTR during catalytic turnover and during reduction with sub-stoichiometric amounts of reducing agent.[10] On the basis of these observations, it has been suggested that NEM-FTR provides a stable analog of a one-electron reduced catalytic intermediate in the enzymatic cycle.[10] Furthermore, the difference in solvent accessibility of the two

thiols of the active-site disulfide, has lead to the proposal that the more exposed thiol (Cys57 in *Synechocystis*), termed the interchange thiol, is responsible for attacking the substrate disulfide, while the less exposed thiol (Cys87 in *Synechocystis*), termed the cluster-interacting thiol, interacts with the nearby [4Fe-4S] cluster, resulting in a novel cluster with five cysteine ligands. The observed anomalous structural, electronic and redox properties for the $[4Fe\text{-}4S]^{3+}$ center in oxidized NEM-FTR were thus attributed to coordination of the cluster-interacting cysteine, Cys87, to the [4Fe-4S] cluster.[10] The binding site for the fifth cysteine ligand, however, was not identified. More recently, our initial Mössbauer characterization of the spinach FTR has confirmed the binding of a fifth cysteine ligand to the $[4Fe\text{-}4S]^{3+}$ cluster in oxidized NEM-FTR.[11] Furthermore, due to the ability of Mössbauer spectroscopy to differentiate and detect individual Fe sites within a cluster, the fifth cysteine coordination site was revealed to be the unique Fe site *a*. Here, a more detailed Mössbauer study of the *Synechocystis* NEM-FTR is presented.

At 4.2-K, oxidized *Synechocystis* NEM-FTR exhibits magnetic field-dependent Mössbauer spectra (Figure 4.8) that are consistent with a paramagnetic $S = 1/2$ electronic ground state. These spectra are very similar to those observed for oxidized spinach NEM-FTR,[11] and, as reported for the spectra of the spinach enzyme, can also be decomposed into three components with an intensity ratio of 1:1:2. This intensity ratio, together with the parameters (Table 4.1) determined for the components, indicate a cluster composed of two ferric sites (sites *a* and *b*) and a valence-delocalized $Fe^{2+}Fe^{3+}$ pair (site *c*), consistent with the $[4Fe\text{-}4S]^{3+}$ assignment. The magnitudes and signs of the magnetic-hyperfine *A* tensors compare well with those of the $[4Fe\text{-}4S]^{3+}$ cluster in HiPIP.[30,31] The opposite signs of the *A* tensors reflect the antiparallel orientations between the spin of the mixed-

valence pair and the spins of the two ferric sites. A major difference observed between the $[4Fe\text{-}4S]^{3+}$ clusters in HiPIP and in NEM-FTR is that the two ferric ions are indistinguishable in HiPIP, but they are distinct in NEM-FTR. This distinction between the two ferric sites is most obvious in the 8-T spectrum (Figure 4.8C) in which the corresponding spectral components, *a* and *b*, are clearly resolved in the region between +3 mm/s and +4 mm/s. Moreover, our detailed analysis of these field-dependent spectra yielded different ***d*** values for the two ferric sites (Table 4.1). While the smaller ***d*** value, 0.29 mm/s, determined for site *b* is consistent with ferric sites with tetrahedral sulfur coordination,[32,33] the larger ***d*** value, 0.32 mm/s, determined for site *a* suggests a ferric site with a higher coordination number, consistent with binding of a fifth ligand at this site. A comparison of the parameters of NEM-FTR with those of the as-purified FTR shows that while there are practically no changes observed for the DE_Q and ***d*** values for site *c*, significant reductions in the ***d*** values are observed for sites *a* and *b*, indicating that oxidation of the cluster occurs at these two Fe sites. The larger reduction of ***d*** observed for site *a* (0.54 mm/s to 0.32 mm/s) further indicates that most of the reducing equivalent is removed from this unique Fe site *a*. Consequently, the Mössbauer data not only confirms the 3+ oxidation state of the [4Fe-4S] cluster in NEM-FTR, the data also reveal detailed electronic and structural changes at the [4Fe-4S] cluster upon NEM-modification. That is, the unique Fe site, identified in the as-purified FTR, retains its distinctiveness in the NEM-FTR complex, in which alkylation of Cys57 results in coordination of Cys87 to the unique Fe site and oxidation of the cluster. Moreover, the unique Fe site provides most of the reducing equivalent removed from the cluster.

Wild-type FTR/C40S Trx *m* heterodisulfide complex. Recently, a detailed investigation on the interactions of wild-type and site-specific variants of *Synechocystis* FTR with spinach Trx *m* and *f* has shown that stable FTR/Trx heterodisulfide complexes can be formed using active-site modified Trxs.[13] These complexes are analogs of a potential catalytic intermediate (see Figure 4.2), and have been shown to exhibit optical spectra indicative of an oxidized $[4Fe\text{-}4S]^{3+}$ cluster in the oxidized (as purified) form. To further investigate the structural and electronic properties of the [4Fe-4S] cluster in FTR/Trx heterodisulfide complexes, we report here a detailed spectroscopic characterization of the FTR/Trx heterodisulfide complex formed with wild-type *Synechocystis* FTR and spinach C40S Trx *m*.

Figure 4.5B shows the 35-K EPR spectrum of the FTR/C40S Trx *m* heterodisulfide complex. The spectrum is very similar to that of NEM-FTR shown in Figure 4.5A and exhibits a near-axial $S = 1/2$ EPR signal with $g = 2.11$, 1.99 and 1.98. This signal accounts for approximately 1 spin per molecule of the complex. As mentioned above, the $[4Fe\text{-}4S]^{3+}$ cluster in NEM-FTR displays atypical electronic relaxation behavior that allows its EPR signal to be observed up to 150 K. Similarly, the EPR signal of the FTR/Trx *m* complex can also be observed up to 150 K without significant broadening. The VTMCD spectrum of the heterodisulfide complex (Figure 4.6B) displays a complex pattern of temperature-dependent bands that is very similar to that of oxidized NEM-FTR (Figure 4.6A) and exhibits similar temperature and magnetic-field dependence. Not surprisingly, the resonance Raman spectrum of the FTR/Trx heterodisulfide complex (Figure 4.7B) also shows Raman bands that are very similar to those detected for NEM-FTR (Figure 4.7A), in both intensities and frequencies. To

further establish the similarities between the clusters in oxidized NEM-FTR and in FTR/C40S Trx *m* heterodisulfide complex, Mössbauer spectra of the heterodisulfide complex were recorded over a wide range of magnetic fields (50 mT to 8 T) for a detailed characterization of the distinguishable Fe sites present in the cluster of the heterodisulfide complex. Within experimental uncertainties, the field-dependent Mössbauer spectra of the heterodisulfide complex were found to be identical to those of NEM-FTR. Since the spectra of the three distinct Fe sites (*a*, *b* and *c*) are best resolved in an applied field of 8 T, we present, in Figure 4.9, the 4.2-K 8-T Mössbauer spectrum of the heterodisulfide complex (Figure 4.9B) in comparison with the corresponding spectrum of NEM-FTR (Figure 4.9A). Clearly, it can be seen that the two spectra are identical. Thus, the overwhelming spectroscopic evidence presented here has firmly established that the electronic structures of the [4Fe-4S] cluster in oxidized NEM-FTR and in the FTR/C40S Trx *m* heterodisulfide complex are identical, strongly supporting the suggestion that NEM-FTR represents a stable analog of the one-electron reduced FTR/Trx heterodisulfide complex in the proposed mechanistic pathway (Figure 4.2).

C57S and C87A variants of *Synechocystis* FTR. To obtain further information on the specific roles played by the two cysteine residues of the active-site disulfide, site-specific *Synechocystis* FTR variants of these two residues (Cys57 and Cys87) have been expressed in *E. coli*, purified, and characterized by a variety of biochemical methods and UV-vis absorption spectroscopy.[13] Substitutions at either Cys57 or Cys87 result in inactive enzymes, establishing that both residues are essential for FTR function.[13] In accord with distinct roles for each of the two active-site cysteines, the oxidized (as purified) forms of the C87A and C57S variants were found to exhibit UV-vis absorption

spectra typical of $[4Fe\text{-}4S]^{2+}$ and $[4Fe\text{-}4S]^{3+}$ centers, respectively.[13] Here, we present the resonance Raman spectrum, the 35-K EPR spectrum, the VTMCD spectra, and the 4.2-K 8-T Mössbauer spectrum of oxidized *Synechocystis* C57S FTR, respectively, in Figures 4.5C, 4.6C, 4.7C, and 4.9C for comparison with the corresponding spectra of the oxidized *Synechocystis* NEM-FTR and the wild-type *Synechocystis* FTR/C40S Trx *m* heterodisulfide complex. It is plainly apparent that the spectroscopic data of these three forms of FTR are almost indistinguishable, indicating strongly that the electronic structures of the [4Fe-4S] clusters in all three proteins are identical. In other words, oxidized C57S FTR also contains a novel five-cysteine coordinated $[4Fe\text{-}4S]^{3+}$ cluster with a unique five-coordinate Fe site. Thus, the spectroscopic data demonstrate that substitution of the interchange thiol, Cys57, frees the cluster-interacting thiol, Cys87, to react with the [4Fe-4S] cluster and results in coordination of Cys87 to the unique Fe site *a* in the oxidized state. These data provide strong support for the detailed mechanism proposed for the interaction between Cys87 and the [4Fe-4S] cluster.[11]

In accord with the UV-vis absorption spectroscopy,[13] the resonance Raman spectrum of *Synechocystis* C87A FTR as purified (Figure 4.4B) shows vibrational bands indicative of $[4Fe\text{-}4S]^{2+}$ cluster. The spectrum is very similar to that of oxidized *Synechocystis* FTR (Figure 4.4A), and the only significant difference lies in a 5-cm^{-1} upshift in the highest frequency Fe–S stretching band which is centered at 393 cm^{-1} in the C87A variant. This band is broad due to the overlap of two Fe-S stretching modes, an asymmetric stretching mode of the [4Fe-4S] core and the symmetric Fe–S(Cys) stretching mode,[8] and the change in frequency is likely to reflect greater resonance enhancement of the higher energy symmetric Fe–S(Cys) stretching mode. This would be

consistent with more symmetrical cluster ligation in the C87A variant due to loss of the interaction with active-site disulfide. However, the identical frequencies for the Fe–S stretching modes of the $[4Fe\text{-}4S]^{2+}$ core in wild-type and C87A FTR (asymmetric modes at 252 and 283 cm^{-1} and symmmetic (breathing) mode at 337 cm^{-1}) indicate that loss of the active-site disulfide has no significant effect on the structure of the [4Fe-4S] core. The Mössbauer spectrum of C87A FTR recorded at 4.2 K in a weak magnetic field of 50 mT (Figure 4.10) shows a nearly symmetric quadrupole doublet with apparent parameters (DE_Q = 1.33 mm/s and d = 0.45 mm/s) that are characteristic of $[4Fe\text{-}4S]^{2+}$ clusters.[22,23,31,34] Interestingly, in comparison with the corresponding spectrum of wild-type *Synechocystis* FTR (Figure 4.3A), the prominent shoulder observed in the high-energy line of the wild-type spectrum is almost invisible in the spectrum of the C87A FTR. In order to obtain a quantitative comparison with the wild-type FTR, the spectrum of the variant is analyzed also by assuming that it is a superposition of three quadrupole doublets with an intensity ratio of 1:1:2 corresponding to the three Fe sites, *a*, *b*, and *c*. (However, it should be noted that such a decomposition of the variant spectrum is not unique. The lack of resolution of the variant spectrum prohibits a unique decomposition of the spectrum.) The resulting parameters are listed in Table 4.1, and the corresponding theoretical simulations are shown in Figure 4.10. In comparison with the parameters of the wild-type FTR, the parameters obtained for sites *c* are comparable. A decrease in the *d* value of site *a* and an increase in the *d* value of site *b* are observed. The difference between the *d* values of sites *a* and *b* has reduced from 0.15 mm/s in the as-purified wild-type FTR to 0.08 mm/s in the C87A variant. Thus, on the basis of such an analysis, it is concluded that the C87A substitution has the effect of equalizing the charge distribution

between sites *a* and *b*, resulting in a reduction of the ferrous character of the unique Fe site *a* making it more ferric-like. This conclusion is consistent with the proposal that interaction between the cluster and the active-site disulfide (via Cys87) promotes the observed charge buildup at the unique Fe site in the resting enzyme.

C57S FTR can be reduced by dithionite, and the reduced protein shows optical spectra characteristic of a $[4Fe\text{-}4S]^{2+}$ cluster.[13] Thus, the reduced C57S FTR provides an ideal system for studying the interaction between the $[4Fe\text{-}4S]^{2+}$ cluster and the Cys87 residue free of restrictions caused by the disulfide bonding. The resonance Raman spectrum of reduced C57S FTR, shown in Figure 4.4C, confirms the presence of a $[4Fe\text{-}4S]^{2+}$ cluster. Moreover, the marked changes in the frequencies and relative intensities of Raman bands, compared to the $[4Fe\text{-}4S]^{2+}$ centers in oxidized FTR which has the disulfide intact (see Figure 4.4A) and C87A FTR which lacks both the disulfide and the cluster-interacting Cys87 (see Figure 4.4B), suggest that significant changes in cluster ligation and core structure are associated with having Cys87 as a free thiol in close proximity to the cluster. For example, the symmetric (breathing) mode of the [4Fe-4S] core is no longer the most intense resonance Raman band in reduced C57S FTR and is shifted to 335 cm^{-1}, compared to 337 cm^{-1} in oxidized wild-type and C87A FTR, while the asymmetric Fe–S(Cys) stretching mode becomes the most intense band and is shifted to 356 cm^{-1}, compare to 360 cm^{-1} in wild-type and C87A FTR, see Figure 4.4. In addition, pronounced frequency and intensity changes are apparent in the weak low-frequency asymmetric stretching modes of the [4Fe-4S] core in the 260-320 cm^{-1} region for the $[4Fe\text{-}4S]^{2+}$ center in reduced C57S FTR.

Mössbauer studies of reduced C57S FTR revealed that the presence of Cys87 as a free thiol in close proximity to the $[4Fe\text{-}4S]^{2+}$ center has a dramatic effect on the electronic properties of the cluster. Figure 4.11 shows the 4.2-K Mössbauer spectra of a dithionite-reduced C57S FTR sample recorded in a magnetic field of 50 mT (A) and 8 T (B) applied parallel to the γ-radiation. In addition to an intense central quadrupole doublet, which is similar to those of $[4Fe\text{-}4S]^{2+}$ clusters, the weak-field spectrum (Figure 4.11A) shows a resolved outer quadrupole doublet that accounts for approximately 25% of the total Fe absorption. This outer doublet exhibits parameters (DE_Q = 2.52 mm/s and d = 0.67 mm/s) that are indicative of a tetrahedral sulfur-coordinated high-spin (S = 2) ferrous center. The 8-T spectrum (Figure 4.11B) shows that both doublets originate from a diamagnetic S = 0 ground state, indicating unambiguously that the high-spin ferrous ion is an integral part of a diamagnetic Fe cluster. The percent absorption of this ferrous site further suggests that it represents one single Fe site of a $[4Fe\text{-}4S]^{2+}$ cluster. Taken together, the data establish that the reduced C57S FTR contains a novel $[4Fe\text{-}4S]^{2+}$ cluster with a valence-localized high-spin ferrous site. In line with assumptions used for analyzing the spectra of other S = 0 $[4Fe\text{-}4S]^{2+}$ clusters in FTR, the spectra of reduced C57S FTR are also least-squares fitted with three quadrupole doublets of an intensity ratio of 1:1:2 corresponding to sites *a*, *b* and *c*. The high-spin ferrous site is assigned to site *a*. The results are listed in Table 4.1. By comparing these parameters obtained for reduced C57S FTR with those of the as-purified wild type FTR and C87A FTR, the effect of Cys87 on the charge distribution of the $[4Fe\text{-}4S]^{2+}$ cluster in FTR can be clearly seen. The d value of the unique Fe site *a* is observed to increase progressively from a minimum value of 0.51 mm/s in C87A FTR, in which Cys87 has been substituted by alanine, to a

medium value of 0.54 mm/s in the as-purified FTR, in which Cys87 forms a disulfide with Cys57, and to a maximum value of 0.67 mm/s in reduced C57S FTR, in which Cys87 is free of disulfide bonding. Concomitantly, a gradual decrease in the *d* value of site *b* is observed (from 0.43 mm/s in C87A FTR, to 0.39 mm/s in as-purified FTR, to 0.35 mm/s in reduced C57S FTR). These data establish clearly that an interaction between the Cys87 residue and the $[4Fe\text{-}4S]^{2+}$ cluster is indeed present in FTR and that the effect of this interaction is to polarize the charge distribution between the two Fe ions (sites *a* and *b*) of one of the two $Fe^{2+}Fe^{3+}$ mixed-valence pairs. In reduced C57S FTR, the residue Cys87 is free of disulfide bonding and thus the interaction is observed to generate a maximum effect, resulting in a novel $[4Fe\text{-}4S]^{2+}$ cluster with a valence-localized $Fe^{2+}Fe^{3+}$ pair. In the as-purified enzyme, this interaction is weakened by bonding of Cys87 to Cys57, resulting in only a partial localization of the valence electron and ending with a charge buildup at the unique Fe site *a*. In C87A FTR, replacing Cys87 with a nonpolar alanine further diminishes the strength of the interaction between residue 87 and the cluster, resulting in an additional reduction of the charge difference between sites *a* and *b*. Interestingly, the valence-delocalized $Fe^{2+}Fe^{3+}$ pair (site *c*) in reduced C57S FTR also shows a significant increase in the *d* value (0.49 mm/s). Thus, the overall *d* value of the cluster in reduced C57S FTR (0.50 mm/s) is considerably higher and outside of the range of *d* values (0.42-0.45 mm/s)[22] generally observed for a regular $[4Fe\text{-}4S]^{2+}$ cluster. This observation indicates that the reduced C57S FTR contains a $[4Fe\text{-}4S]^{2+}$ cluster that is more electronegative than regular $[4Fe\text{-}4S]^{2+}$ clusters and suggests a possible additional function for residue Cys87 of promoting an overall charge buildup at the $[4Fe\text{-}4S]^{2+}$ cluster.

Methyl viologen-reduced spinach FTR. In the above section, dithionite-reduced C57S FTR has been shown to contain an unprecedented electron-rich $[4Fe\text{-}4S]^{2+}$ cluster composed of a valence-localized and a valence-delocalized $Fe^{2+}Fe^{3+}$ mixed-valence pair. Since our spectroscopic data have also established that the as-purified C57S FTR represents a stable analog of a one-electron reduced FTR intermediate (see above), the dithionite-reduced C57S FTR must represent an analog of two-electron reduced FTR. In wild-type FTR, the active-site disulfide can be reduced by methyl viologen, but not by dithionite.[35] Moreover, reduced methyl viologen can function as the electron donor for catalytic turnover of FTR,[35] and the methyl viologen-reduced enzyme exhibits an optical spectrum indicative of a $[4Fe\text{-}4S]^{2+}$ cluster and can form heterodisulfide complexes with Trx substrates. Thus, the methyl viologen-reduced FTR represents a functionally active two-electron reduced form of FTR. To investigate whether the novel state of the $[4Fe\text{-}4S]^{2+}$ cluster detected in reduced C57S FTR has any functional relevance, Mössbauer spectroscopy has been used to characterize methyl viologen-reduced spinach FTR. Figure 4.12A shows the Mössbauer spectrum (hatched marks) of the methyl viologen-reduced FTR sample recorded at 4.2 K in a 50 mT applied field. Detailed analysis of the spectrum shows that the sample contains approximately 14% as-purified FTR (i.e., enzyme that has not been reduced by methyl viologen). Removal of the contribution of the as-purified FTR (solid line in Figure 4.12A) from the raw data results in a spectrum representing the methyl viologen-reduced enzyme (Figure 4.12B). This spectrum is very similar to that observed for the reduced C57S FTR (Figure 4.11A). Most importantly, a resolved outer quadrupole doublet, typical of tetrahedral sulfur-coordinate high-spin ferrous ions and accounting for ~25% of the Fe absorption, is clearly observable. This spectrum can also

be least squares fitted with three quadrupole doublets with an intensity ratio of 1:1:2. The resulting parameters are listed in Table 4.1. Within experimental uncertainties, these parameters are identical to those obtained for the reduced C57S FTR, establishing firmly that the two-electron reduced FTR also contains a novel electron-rich $[4Fe\text{-}4S]^{2+}$ cluster composed of valence-localized and valence-delocalized $Fe^{2+}Fe^{3+}$ pairs. The biological implications of this unique and unexpected type of $[4Fe\text{-}4S]^{2+}$ cluster in two-electron-reduced FTR are discussed below.

Redox properties of NEM-FTR, C57S FTR, and wild-type FTR/Trx *m* heterodisulfide complex. Oxidized NEM-FTR can be reduced by dithionite or reduced benzyl viologen, and reduced NEM-FTR is EPR silent. Hence dye-mediated EPR redox titrations provide a means of assessing redox potential and the number of electrons and protons involved in reducing NEM-FTR. Figure 4.13A shows redox titrations of *Synechocystis* NEM-FTR performed at pH 7.0 and pH 8.0 monitored by the intensity of the g = 2.11 EPR signal. The reduction-oxidation process at these pH values was found to be fully reversible. The solid lines shown in Figure 4.13A are least-squares fits to the data using a one-electron Nernst equation with midpoint reduction potentials of E_m = –145 ±10 mV and –200 ±10 mV at pH 7.0 and pH 8.0, respectively. This observed negative shift of the redox potential by approximately 60mV/pH unit with increasing pH indicates that the one-electron reduction of NEM-FTR is coupled with the uptake of one proton. The protonation site is likely to be Cys87, since one-electron reduction of the $[4Fe\text{-}4S]^{3+}$ cluster in NEM-FTR is proposed to result in cleavage of the Fe-S(Cys87) bond, see Figure 4.2. EPR redox titrations of *Synechocystis* C57S FTR showed the same redox properties as *Synechocystis* NEM-FTR, i.e. one-electron redox process with E_m = –145

±10 mV at pH 7.0 and –200 ±10 mV at pH 8.0 (data not shown). An earlier EPR redox titration study of the spinach NEM-FTR reported a more negative redox potential of –210 ±10 mV at pH 7.[8]

Analogous dye-mediated EPR-monitored redox titrations were also performed with the wild-type *Synechocystis* FTR/C40S Trx *m* heterodisulfide complex at pH 7.0 and 8.0, see Figure 4.13B. At both pH values the titrations were fully reversible and the data were fit using a one-electron Nernst equation with midpoint reduction potentials of E_m = –60 ±10 mV (pH 7.0) and –110 ±10 mV (pH 8.0). While the potentials are ~90 mV higher than for *Synechocystis* NEM-FTR, the pH-dependence again indicates that one-electron reduction is coupled with the uptake of one proton. The mechanistic scheme shown in Figure 4.2 proposes that one-electron reduction of the $[4Fe\text{-}4S]^{3+}$ cluster-containing heterodisulfide intermediate results in cleavage of the Fe-S(Cys87) bond and concomitant reformation of the FTR disulfide coupled with cleavage of the heterodisulfide. Hence the status of the heterodisulfide during a parallel dye-mediated redox titration at pH 7.3 was assessed by anaerobic chromatographic separation of FTR, C40S Trx *m*, and the FTR/C40S Trx *m* heterodisulfide complex for samples poised at selected potentials using a high-performance Q-Sepharose column. Samples were loaded onto the column at low salt and protein fractions were eluted with a 0.0-0.5 M NaCl gradient. Elution profiles for samples poised at +100 mV, –85 mV (estimated midpoint potential of the complex at pH 7.3), and –400 mV are shown in Figure 4.14 and protein bands were identified by parallel chromatographic studies with oxidized forms of FTR, C40S Trx *m*, and the FTR/C40S Trx *m* heterodisulfide complex. The data unambiguously demonstrate that one-electron reduction of the complex with a midpoint potential of –60

±10 mV (pH 7.0) and −110 ±10 mV (pH 8.0) results in the reversible cleavage of the heterodisulfide resulting in the ability to chromatographically separate FTR and Trx *m*. Hence the protonation site is likely to be the thiolate that is generated on C40S Trx *m* on cleavage of the heterodisulfide.

Discussion

The primary objective of the spectroscopic studies of FTR reported herein was to evaluate the underlying assumptions of the mechanistic hypothesis shown in Figure 4.2 for [4Fe-4S]-cluster-mediated disulfide reduction in two sequential one-electron steps. This scheme proposes distinct, non-interchangeable roles for cysteines of the active-site disulfide, site-specific cluster chemistry in the oxidized and one-electron-reduced intermediate, and the existence of a stable one-electron-reduced FTR/Trx heterodisulfide intermediate that undergoes further one-electron reduction leading to the reformation of the active-site disulfide and release of reduced Trx. These proposals have been comprehensively assessed via EPR, VTMCD, resonance Raman, Mössbauer and redox studies of wild-type and NEM-modified forms of FTR, site-specific variants of each of the active-site cysteines, and of a heterodisulfide complex involving FTR and the C40S variant of Trx *m*.

The properties the C57S and C87A FTR variants compared with those of wild-type and NEM-modified FTR clearly demonstrate distinct roles for the cysteine residues of the active-site disulfide. Both the C57S and C87A variants are inactive, indicating that both cysteines of the active-site disulfide are essential for catalytic activity.[13] However, the C87A and C57S variants have entirely different spectroscopic and redox properties. C87A FTR contains a redox-inactive $[4Fe\text{-}4S]^{2+}$ cluster, whereas C57S FTR contains a

redox-active $[4Fe\text{-}4S]^{3+/2+}$ center with spectroscopic and redox properties almost indistinguishable from those of the $[4Fe\text{-}4S]^{3+/2+}$ center in NEM-FTR. Moreover, in accord with our preliminary Mössbauer analysis,[11] the unique spectroscopic properties of the $[4Fe\text{-}4S]^{3+}$ cluster in NEM-FTR can only be rationalized in terms of selective oxidation at a unique Fe site resulting from coordination of Cys87 to yield a five-coordinate Fe site. In accord with the mechanism depicted in Figure 4.2, the mutagenesis results, therefore, identify Cys87 as the cluster-interacting thiol and demonstrate that Cys57 cannot assume this role in the C87A variant. In addition, the ability of C87A, but not C57S FTR, to form a heterodisulfide complex with active-site variants of Trxs,[13] identifies Cys57 as the interchange thiol responsible for attacking the Trx disulfide.

The spectroscopic properties of C87A variant also support the proposal for a weak interaction between the active-site disulfide and the unique Fe site of the $[4Fe\text{-}4S]^{2+}$ cluster in the oxidized resting state of FTR. Mössbauer studies of spinach[11] and *Synechocystis* FTR in the oxidized resting state suggest that the asymmetrically disposed disulfide is responsible for promoting charge buildup on the unique Fe site, resulting in a $[4Fe\text{-}4S]^{2+}$ cluster comprising one fully valence-delocalized $Fe^{2+}Fe^{3+}$ pair and one partially valence-delocalized $Fe^{2+}Fe^{3+}$ pair. This conclusion is substantiated by the observation that the loss of the disulfide in the C87A variant results in a $[4Fe\text{-}4S]^{2+}$ cluster that more closely approximates a conventional Fd-type $[4Fe\text{-}4S]^{2+}$ cluster with two valence-delocalized $Fe^{2+}Fe^{3+}$ pairs. Any residual charge asymmetry in one of the valence-delocalized pairs in the C87A variant, see Table 4.1, is likely to be a consequence of the anomalous coordination geometry at the unique Fe site (see Figure 4.1). Hence the interaction between the cluster and the active-site disulfide (via Cys87)

promotes the observed charge buildup at the unique Fe site in the resting enzyme and primes the active-site for one-electron reduction leading to cleavage of the disulfide and attachment of Cys87 at the unique Fe site.[11]

Characterization of the oxidized form of the wild-type FTR/C40S Trx *m* heterodisulfide complex reveals a form of FTR that is spectroscopically indistinguishable from oxidized NEM-FTR. This observation is entirely consistent with the proposal for a one-electron-reduced heterodisulfide intermediate containing a $[4Fe\text{-}4S]^{3+}$ cluster in which Cys87 is ligated to yield a five-coordinate Fe site and Cys57 is part of the heterodisulfide, see Figure 4.2. Moreover, the viability of this species as a stable analog of the one-electron-reduced catalytic intermediate is confirmed by redox studies which reveal that one-electron-reduction of the FTR/C40S Trx *m* heterodisulfide complex (E_m = –60 ±10 mV at pH 7.0 and –110 ±10 mV at pH 8.0) results in cleavage of the heterodisulfide coupled with protonation of free thiolate on C40S Trx *m*. Parallel redox studies of NEM-FTR show a similar one-electron-reduction, albeit at lower potentials (E_m = –145 ±10 mV at pH 7.0 and –200 ±10 mV at pH 8.0) due to increased solvent exposure at the active site in the absence of Trx, and in this case the pH dependence is attributed to release and protonation of Cys87 on reduction. Taken together, these redox results suggest that cleavage of the heterodisulfide occurs via reductive release of Cys87 and subsequent nucleophilic attack of the heterodisulfide by Cys87, resulting in cleavage of the heterodisulfide and reformation of the active-site disulfide, as shown in Figure 4.2.

Interestingly, a much lower redox potential (E_m = –280 mV at pH 7.0) was determined for cleavage of the heterodisulfide in the *Synechocystis* wild-type FTR/C40S Trx *m* heterodisulfide complex using dithiothreitol (DTT), a two-electron reductant that is

particularly effective in cleaving disulfides.[13] These redox titrations involved poising samples of the heterodisulfide complex at specific potentials using mixtures of oxidized and reduced DTT and assessing cleavage of the heterodisulfide using native gel electrophoresis to separate FTR, Trx and the FTR/Trx heterodisulfide complex. The difference in potentials presumably reflects the efficacy of cleaving the heterodisulfide with a one-electron donor via reduction of the $[4Fe\text{-}4S]^{3+}$ cluster compared to direct two-electron cleavage of the heterodisulfide using dithiol/disulfide chemistry. This rationalization of the redox properties has since been verified by subsequent experiments in which the cleavage reaction of the heterodisulfide using a 2500-excess of reduced DTT showed a long lag phase of about 50 min before a separation of the proteins, accompanied by a change in absorption properties of the $[4Fe\text{-}4S]^{3+}$ cluster, is observed (unpublished observations). The high potential for the one-electron reduction and cleavage of the heterodisulfide in the oxidized FTR/C40S Trx *m* complex (E_m = –110 ±10 mV at pH 8.0, the physiological pH of light-adapted chloroplasts), suggests that the second reducing equivalent used by FTR need not be derived from reduced Fd and may not require a specific electron donor. This is in accord with the observation that ferredoxin is not obligatory for cleaving the heterodisulfide and that other potential physiological electron donors such as a NADPH and ferredoxin:$NADP^+$ reductase can act as effective reductants *in vitro*.[13]

The most interesting and unexpected result to emerge from these spectroscopic studies of FTR concerns the properties of the $[4Fe\text{-}4S]^{2+}$ cluster in the two-electron reduced form of FTR. Reduced methyl viologen is known to reduce the active-site disulfide and is a catalytically competent reductant for FTR.[35] Mössbauer studies confirm

the presence of a $S = 0$ $[2Fe\text{-}2S]^{2+}$ cluster in methyl viologen-reduced FTR, but reveal an unprecedented type of electron-rich $[4Fe\text{-}4S]^{2+}$ cluster composed of both valence-localized and valence-delocalized $Fe^{2+}Fe^{3+}$ pairs. An analogous species is also observed in the dithionite-reduced C57S FTR, which can be regarded as a two-electron-reduced analog that is lacking Cys57, and resonance Raman studies confirm significant structural changes in the ligation and core structure of the cluster compared to the $[4Fe\text{-}4S]^{2+}$ clusters in oxidized forms of FTR. Moreover the pH-dependence of the redox potentials of NEM-FTR and C57S FTR strongly suggest that Cys87 dissociates and becomes protonated on one-electron reduction. Hence the unique properties of the $[4Fe\text{-}4S]^{2+}$ cluster in two-electron-reduced forms of FTR are likely to result, at least in part, from the presence of a free thiol (Cys87) in close proximity to the cluster. Our interpretation of the anomalous properties of the $[4Fe\text{-}4S]^{2+}$ cluster in two-electron-reduced FTR is that they originate in large part from a strong H-bonding interaction between the thiol form of Cys87 and the coordinated S atom of Cys55. A substantial increase in H-bonding interactions involving the coordinated cysteinyl-S would be expected to promote charge build up at the unique Fe site, thereby creating a valence-localized $Fe^{2+}Fe^{3+}$ pair and an electron rich $[4Fe\text{-}4S]^{2+}$ cluster.

The discovery of site-specific cluster chemistry in the two-electron-reduced form of FTR raises an alternative possibility for the catalytic mechanism in which FTR is reduced by two electrons prior to interaction with Trx, see Figure 4.15. This mechanism invokes a transient one-electron-reduced intermediate with properties analogous to oxidized NEM-FTR and C57S FTR, as observed in freeze-quench studies under turnover conditions and during reduction with stoichiometric reduced methyl viologen,[10] but this

intermediate is reduced to yield the two-electron-reduced species prior to interaction with Trx. The strong H-bonding interaction anchors the cluster-interacting thiol Cys87, in the two-electron-reduced form thereby freeing the interchange thiol Cys57 for nucleophilic attack of Trx. Hence the substrate disulfide is cleaved via conventional dithiol/disulfide chemistry, with the cluster playing a role in facilitating disulfide reduction in two sequential one-electron steps and in anchoring the cluster-interacting thiol in order to facilitate the initial nucleophilic attack by the interchange thiol. In many respects this mechanism is very similar to that found in the more extensively studied nucleotide-dependent disulfide reductases,[4-6] with the $[4Fe\text{-}4S]^{2+}$ cluster performing the role of the flavin in anchoring one of the active-site thiols in order to free the other for attacking the substrate disulfide. The major difference resides in the use of a $[4Fe\text{-}4S]^{2+}$ cluster to facilitate active-site disulfide reduction using a one electron donor.

The primary rationale for invoking formation of the heterodisulfide intermediate at the one-electron-reduced level in the mechanistic scheme proposed in Figure 4.2, was that attachment of the cluster interacting thiol, Cys87, frees the interchange thiol for nucleophilic attack and cleavage of the Trx disulfide. Clearly a strong H-bonding interaction involving the cluster interacting thiol can perform the same function in the two-electron reduced form. The alternative mechanism is also clearly viable since reductants such as reduced methyl viologen that rapidly cleave the active-site disulfide, have been shown to be catalytically competent electron donors.[35] Moreover, this mechanism obviates the need for Fd/FTR/Trx triple complex as part of the catalytic mechanism and enables the light-mediated generation of a pool of two-electron-reduced FTR that is always available for Trx reduction. Nevertheless, as demonstrated in this

work, there is now good evidence for a catalytically competent one-electron-reduced heterodisulfide intermediate and it is not possible to discriminate between the mechanistic proposals shown in Figs. 4.2 and 4.15 on the basis of the currently available evidence. Future studies are planned to address this question and characterize the role of the conserved His86 in the active-site acid-base chemistry.

Acknowledgments

This work was supported by grants from the National Institutes of Health (GM62542 to M.K.J., GM47295 to B.H.H.) and from the Swiss National Science Foundation (grants no 31-56761.99 and 3100-067934 to P.S.)

Bibliography

(1) Buchanan, B. B.; Schürmann, P.; Wolosiuk, R. A.; Jacquot, J.-P. *Photosynth. Res.* **2002,** *73*, 215-222.

(2) Schürmann, P. *Antioxid. Redox Signal.* **2003,** *5*, 69-78.

(3) Balmer, Y.; Koller, A.; del Val, G.; Manieri, W.; Schürmann, P.; Buchanan, B. B. *Proc. Natl. Acad. Sci. U.S.A.* **2003,** *100*, 370-375.

(4) Williams, C. H., Jr. In *Chemistry and Biochemistry of Flavoenzymes, Vol. III*, Müller, F., Ed.; CRC Press: Boca Raton, FL, 1992; pp 121-211.

(5) Williams, C. H., Jr. *FASEB J.* **1995,** *9*, 1267-1276.

(6) Williams, C. H., Jr.; Arscott, L. D.; Müller, S.; Lennon, B. W.; Ludwig, M. L.; Wang, P.-F.; Veine, D. M.; Becker, K.; Schirmer, R. H. *Eur. J. Biochem.* **2000,** *267*, 6110-6117.

(7) Chow, L.-P.; Iwadate, H.; Yano, K.; Kamo, M.; Tsugita, A.; Gardet-Salvi, L.; Stritt-Etter, A.-L.; Schürmann, P. *Eur. J. Biochem.* **1995,** *231*, 149-156.

(8) Staples, C. R.; Ameyibor, E.; Fu, W.; Gaudet-Salvi, L.; Stritt-Etter, A.-L.; Schürmann, P.; Knaff, D. B.; Johnson, M. K. *Biochemistry* **1996,** *35*, 11425-11434.

(9) Dai, S.; Schwendtmayer, C.; Schürmann, P.; Ramaswamy, S.; Eklund, H. *Science* **2000,** *287*, 655-658.

(10) Staples, C. R.; Gaymard, E.; Stritt-Etter, A.-L.; Telser, J.; Hoffman, B. M.; Schürmann, P.; Knaff, D. B.; Johnson, M. K. *Biochemistry* **1998,** *37*, 4612-4620.

(11) Jameson, G. N. L.; Walters, E. M.; Manieri, W.; Schürmann, P.; Johnson, M. K.; Huynh, B. H. *J. Am. Chem. Soc.* **2003,** *125*, 1146-1147.

(12) Walters, E. M.; Johnson, M. K. *Photosynth. Res.* **2004,** *79*, 249-264.

(13) Glauser, D. A.; Bourquin, F.; Manieri, W.; Schürmann, P. *J. Biol. Chem.* **2004,** *279*, 16662-16669.

(14) Gaymard, E.; Franchini, L.; Manieri, W.; Stutz, E.; Schürmann, P. *Plant Sci.* **2000,** *158*, 107-113.

(15) Droux, M.; Jacquot, J.-P.; Miginac-Maslow, M.; Gadal, P.; Huet, J. C.; Crawford, N. A.; Yee, B. C.; Buchanan, B. B. *Arch. Biochem. Biophys.* **1987,** *252*, 426-439.

(16) Schürmann, P.; Gardet-Salvi, L. *Chimia* **1993,** *47* (6), 245-246.

(17) Drozdzewski, P. M.; Johnson, M. K. *Appl. Spectrosc.* **1988,** *42*, 1575-1577.

(18) Johnson, M. K. In *Metal clusters in proteins*, Que, L., Jr., Ed.; American Chemical Society: Washington,D.C., 1988; pp 326-342.

(19) Thomson, A. J.; Cheesman, M. R.; George, S. J. *Meth. Enzymol.* **1993,** *226*, 199-232.

(20) Ravi, N.; Bollinger, J. M.; Huynh, B. H.; Edmondson, D. E.; Stubbe, J. *J. Am. Chem. Soc.* **1994,** *116*, 8007-8014.

(21) Middleton, P.; Dickson, D. P. E.; Johnson, C. E.; Rush, J. D. *Eur. J. Biochem.* **1978,** *88*, 135-141.

(22) Tong, W.-H.; Jameson, G. N. L.; Huynh, B. H.; Rouault, T. A. *Proc. Natl. Acad. Sci. U.S.A.* **2003,** *100*, 9762-9767.

(23) Trautwein, A. X.; Bill, E.; Bominaar, E. L.; Winkler, H. *Struct. Bonding* **1991,** *78*, 1-95.

(24) Yoo, S. J.; Angove, H. C.; Burgess, B. K.; Hendrich, M. P.; Münck, E. *J. Am. Chem. Soc.* **1999,** *121*, 2534-2545.

(25) Conover, R. C.; Kowal, A. T.; Fu, W.; Park, J.-B.; Aono, S.; Adams, M. W. W.; Johnson, M. K. *J. Biol. Chem.* **1990,** *265*, 8533-8541.

(26) Johnson, M. K.; Robinson, A. E.; Thomson, A. J. In *Iron-sulfur proteins*, Ist ed.; Spiro, T. G., Ed.; Wiley-Interscience: New York, 1982; pp 367-406.

(27) Czernuszewicz, R. S.; Macor, K. A.; Johnson, M. K.; Gewirth, A.; Spiro, T. G. *J. Am. Chem. Soc.* **1987,** *109*, 7178-7187.

(28) Backes, G.; Mino, Y.; Loehr, T. M.; Meyer, T. E.; Cusanovich, M. A.; Sweeney, W. V.; Adman, E. T.; Sanders-Loehr, J. *J. Am. Chem. Soc.* **1991,** *113*, 2055-2064.

(29) Dunham, W. R.; Hagen, W. R.; Fee, J. A.; Sands, R. H.; Dunbar, J. B.; Humblet, C. *Biochim. Biophys. Acta* **1991,** *1079*, 253-262.

(30) Bertini, I.; Campos, A. P.; Luchinat, C.; Teixeira, M. *J. Inorg. Biochem.* **1993,** *52*, 227-234.

(31) Middleton, P.; Dickson, D. P. E.; Johnson, C. E.; Rush, J. D. *Eur. J. Biochem.* **1980,** *104*, 289-296.

(32) Moura, I.; Huynh, B. H.; Hausinger, R. P.; LeGall, J.; Xavier, A. V.; Münck, E. *J. Biol. Chem.* **1980,** *255*, 2493-2498.

(33) Yoo, S. J.; Meyer, J.; Achim, C.; Peterson, J.; Hendrich, M. P.; Münck, E. *J. Biol. Inorg. Chem.* **2000,** *5*, 475-487.

(34) Middleton, P.; Dickson, D. P. E.; Johnson, C. E.; Rush, J. D. *Eur. J. Biochem.* **1978,** *88,* 135-141.

(35) Schürmann, P.; Stritt-Etter, A.-L.; Li, J. S. *Photosynth. Res.* **1995,** *46*, 309-312.

Table 4.1: Mössbauer parameters of various forms of ferredoxin:thioredoxin reductases from *Synechocystis* and spinach [a]

Cluster	Protein	Fe site	δ (mm/s)	ΔE_Q (mm/s)	η	$A_{xx}/g_n\beta_n$	$A_{yy}/g_n\beta_n$	$A_{zz}/g_n\beta_n$
$[4Fe\text{-}4S]^{2+}$ S = 0	Oxidized *Syn*. FTR	*a*	0.54 (2)	1.84 (3)	0.0			
		b	0.39 (2)	1.07 (3)	0.5			
		c	0.45 (2)	1.24 (3)	0.5			
	Syn. C87A	*a*	0.51 (2)	1.65 (3)				
		b	0.43 (2)	1.05 (3)				
		c	0.43 (2)	1.27 (3)				
	Reduced *Syn*. C57S FTR	*a*	0.67 (2)	2.52 (3)	0.0			
		b	0.35 (2)	1.00 (3)	0.9			
		c	0.49 (2)	1.12 (3)	0.8			
	MV-reduced spinach FTR	*a*	0.69 (2)	2.58 (3)				
		b	0.35 (2)	1.00 (3)				
		c	0.49 (2)	1.13 (3)				
$[4Fe\text{-}4S]^{3+}$ S = 1/2	Oxidized *Syn*. NEM-FTR [b]	*a*	0.32	1.2	0.3	20.5 (2.0)	20.5 (2.0)	8.0 (2.0)
		b	0.29	-0.9	0.5	22.0 (1.0)	22.0 (1.0)	19.5 (2.0)
		c	0.45	1.2	0.0	-30.0 (1.0)	-25.0 (1.0)	-25.0 (1.0)

[a] Values in parentheses indicate uncertainties in the last digits. [b] The electronic relaxation rate of NEM-FTR at high temperatures (above 200 K) is comparable to the ^{57}Fe nuclear precession rate, resulting in an extremely broad, asymmetric and poorly-defined doublet. This has prevented us from obtaining an accurate measure of the DE_Q values. In the analysis, the DE_Q values were restricted within a range (0.8-1.2 mm/s) that is not in conflict with the high-temperature data. To further reduce the number of parameters, the magnetic hyperfine *A* tensors for the three Fe sites were assumed to be axial. The uncertainties of the *A* values were estimated by varying each *A* value separately while keeping all other parameters fixed.

Figure 4.1 Crystallograhically defined active-site structure of *Synechocystis* FTR.[9]

Color code: Fe = green; S = yellow; C = gray; N = blue; O = red.

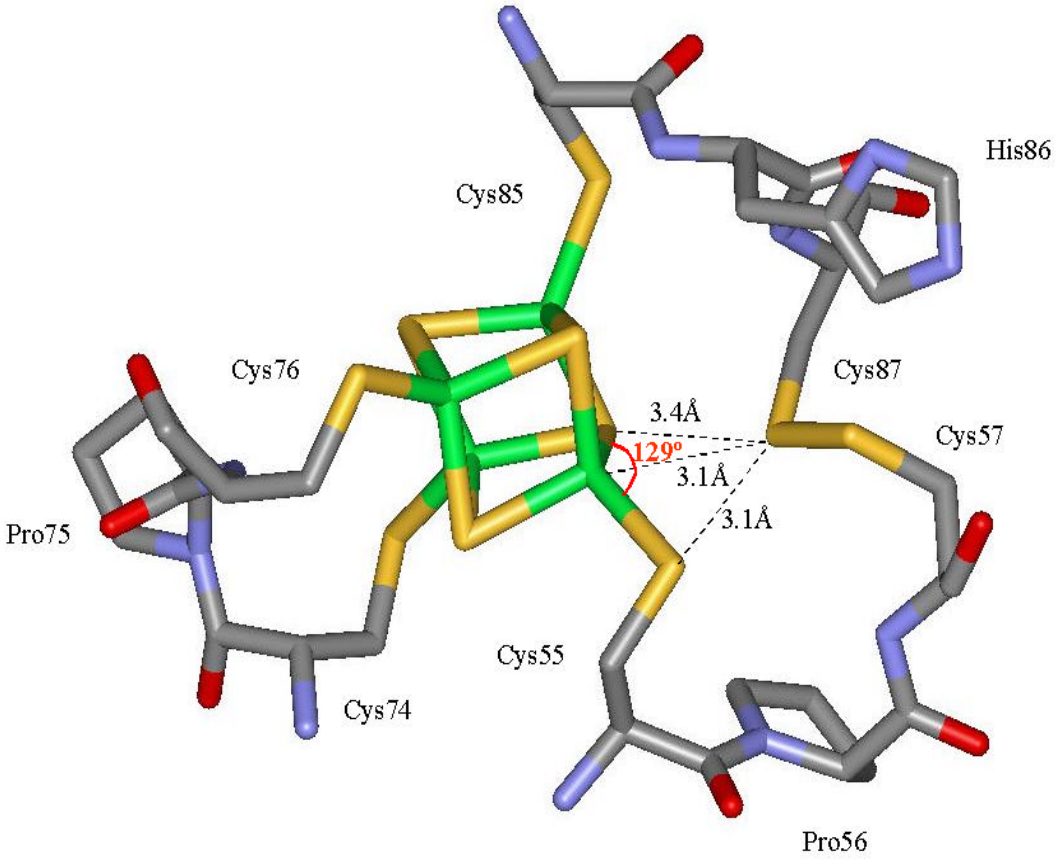
His86
Cys85
Cys76
Cys87
3.4Å
129°
Cys57
3.1Å
3.1Å
Pro75
Cys55
Cys74
Pro56

Figure 4.2 Proposed catalytic mechanism for FTR.[12] Residue numbering is for *Synechocystis* FTR. Square brackets are used to indicate transient intermediates.

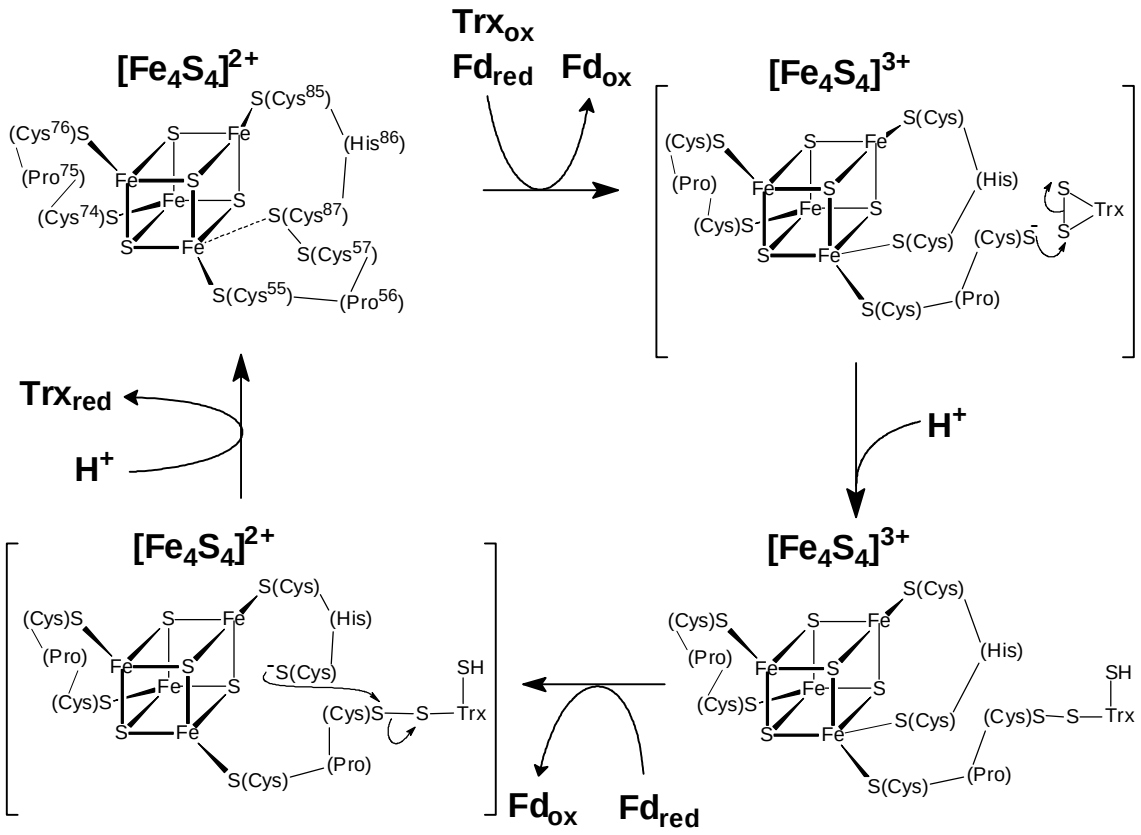
[Fe4S4]2+
Trxox
Fdred
Fdox
[Fe4S4]3+
Trxred
H+
H+
[Fe4S4]2+
[Fe4S4]3+
Fdox
Fdred

Figure 4.3 Mössbauer spectra of oxidized wild-type *Synechocystis* FTR. The data (hatched marks) were recorded at 4.2 K in a magnetic field of 50 mT (A) or 6 T (B) applied parallel to the γ-radiation. The solid lines overlaid with the experimental spectra are least-squares fits to the data using three quadrupole doublets with an intensity ratio of 1:1:2 representing three Fe sites *a*, *b* and *c* (see text and Table 4.1). The spectra representing the individual Fe sites are shown above the experimental spectra as solid lines (site *a*), dashed lines (site *b*) and dotted lines (site *c*).

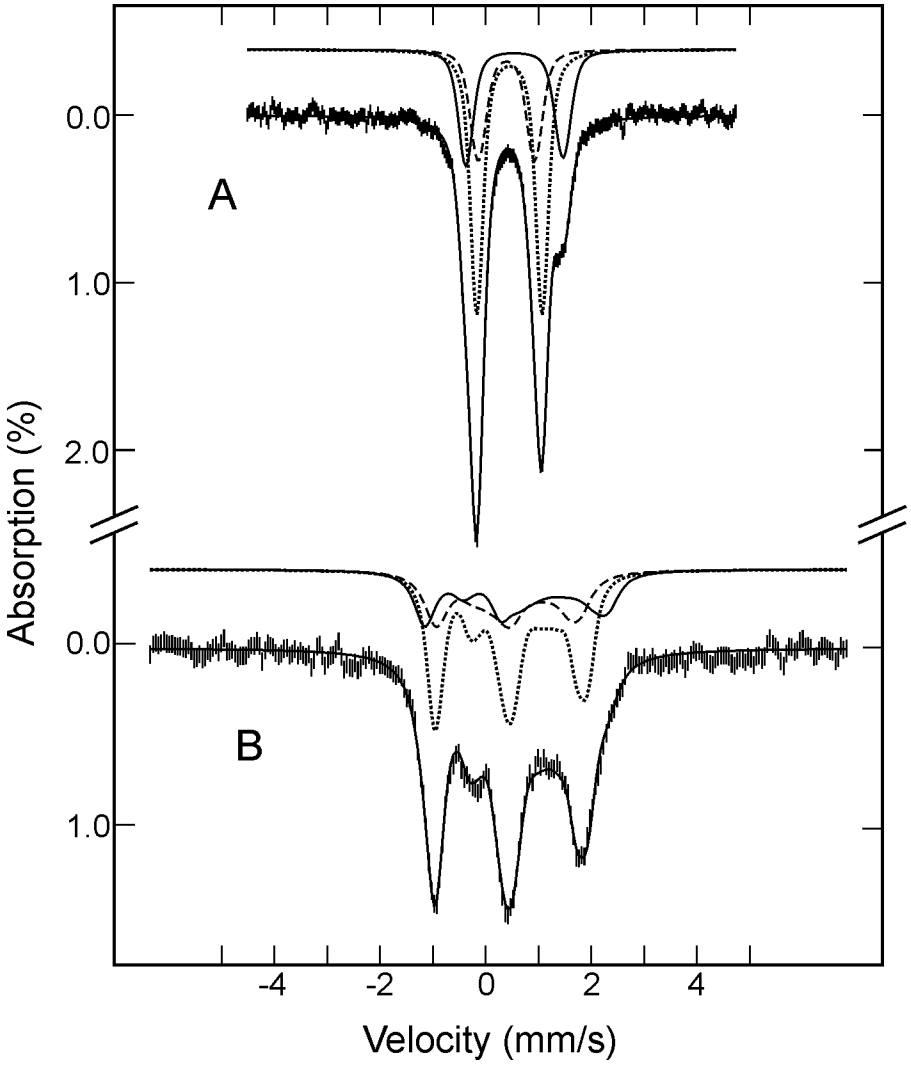
0.0
1.0
2.0
A
0.0
1.0
B
Absorption (%)
-4
-2
0
2
4
Velocity (mm/s)

Figure 4.4 Comparison of the resonance Raman spectra of $[4Fe\text{-}4S]^{2+}$ centers in wild-type, C57S and C87A *Synechocystis* FTR: (A) Oxidized wild-type FTR; (B) as purified C87A FTR; (C) dithionite-reduced C57S FTR. All samples were ~3 mM in FTR and all spectra were recorded at 17 K using 457.9-nm laser excitation with ~200 mW laser power at the sample. Each scan involved photon counting for 1 s at 1 cm^{-1} increments with 7 cm^{-1} bandwidth, and each spectrum is the sum of 80-100 scans. For all spectra, the vibrational modes originating from the frozen buffer solution have been subtracted after normalizing the intensities of the "ice-band" at 231 cm^{-1}.

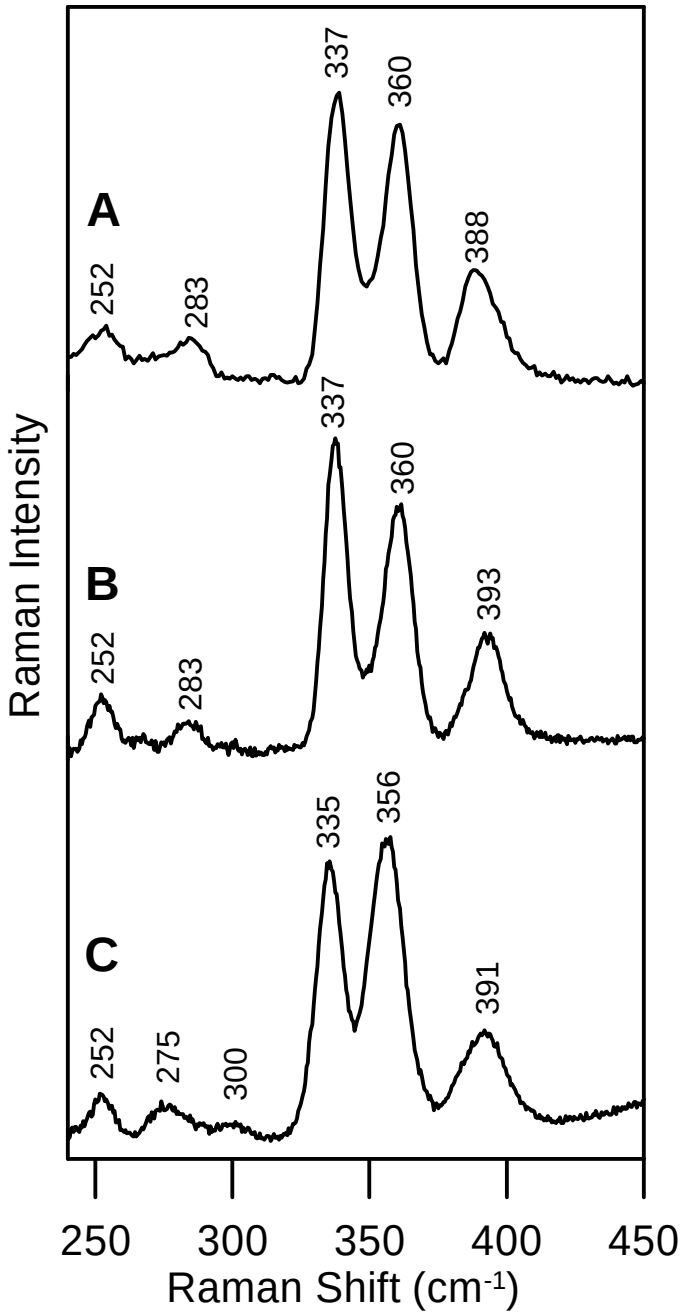
A
252
283
337
360
388
B
252
283
337
360
393
C
252
275
300
335
356
391
Raman Intensity
250
300
350
400
450
Raman Shift (cm-1)

Figure 4.5 Comparison of the X-band EPR spectra of $[4Fe\text{-}4S]^{3+}$ centers in the oxidized (as purified) forms of *Synechocystis* FTR samples: (A) NEM-FTR (185 μM); (B) wild-type FTR/C40S Trx *m* heterodisulfide complex (95 μM); (C) C57S FTR (255 μM). EPR conditions: temperature, 35 K; microwave power, 1 mW; modulation amplitude, 0.63 mT; microwave frequency, 9.60 GHz.

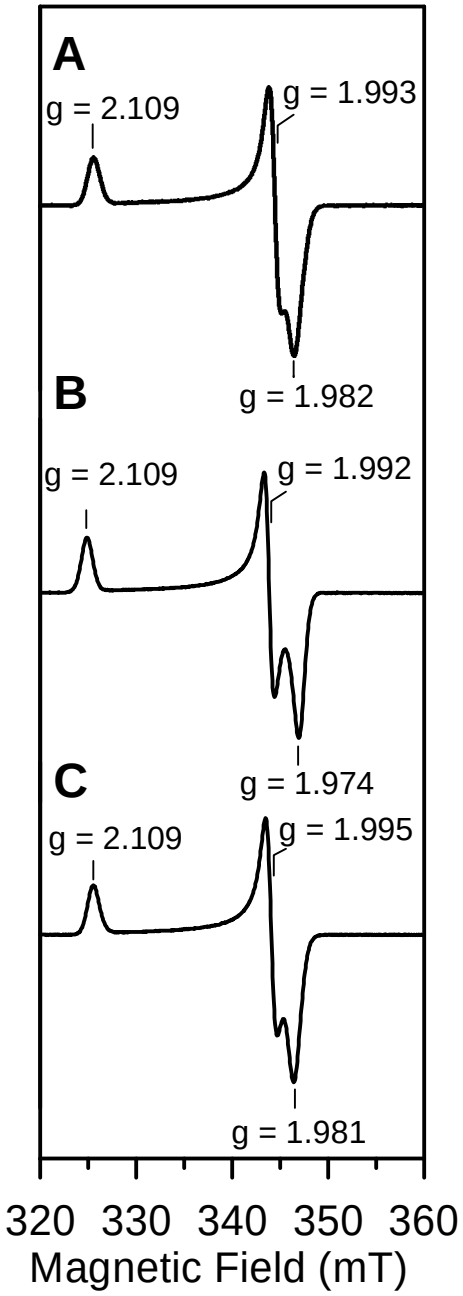
A
g = 2.109
g = 1.993
g = 1.982
B
g = 2.109
g = 1.992
g = 1.974
C
g = 2.109
g = 1.995
g = 1.981
320 330 340 350 360
Magnetic Field (mT)

Figure 4.6 Comparison of the VTMCD spectra of $[4Fe\text{-}4S]^{3+}$ centers in the oxidized (as purified) forms of *Synechocystis* FTR samples. (A) MCD spectra of NEM-FTR collected at 1.68 K, 4.22 K, and 10.4 K, with a magnetic field of 6 T. (B) MCD spectra of wild-type FTR/C40S Trx *m* heterodisulfide complex collected at 1.68 K, 4.22 K. 10.4 K, 25 K, and 50 K, with a magnetic field of 6 T. (C) MCD spectra of C57S FTR collected at 1.68 K, 4.22 K. 10.4 K, 25 K, and 50 K, with a magnetic field of 6 T. For all spectra, the intensity of all MCD bands (positive and negative) increase with decreasing temperature.

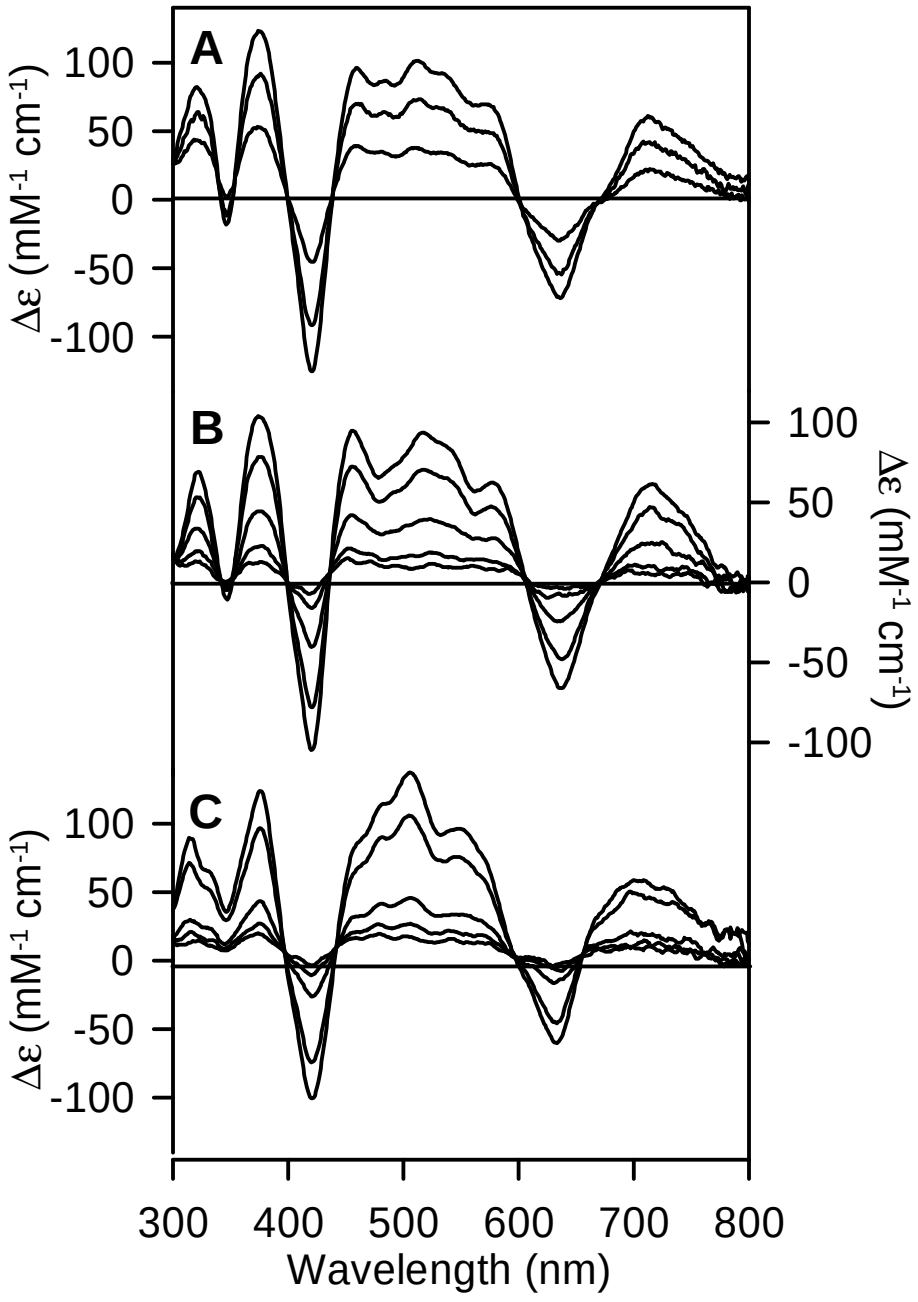
A
B
C
100
50
0
-50
-100
Δε (mM-1 cm-1)
300
400
500
600
700
800
Wavelength (nm)

Figure 4.7 Comparison of the resonance Raman spectra of $[4Fe\text{-}4S]^{3+}$ centers in the oxidized (as purified) forms of *Synechocystis* FTR samples: (A) NEM-FTR, (B) wild-type FTR/C40S Trx *m* heterodisulfide complex, and (C) C57S FTR. All samples were ~3 mM in FTR and all spectra were recorded at 17 K using 457.9-nm laser excitation with ~175 mW laser power at the sample. Each scan involved photon counting for 1 s at 1 cm^{-1} increments with 7 cm^{-1} bandwidth and each spectrum is the sum of 70-100 scans. For all spectra, the vibrational modes originating from the frozen buffer solution have been subtracted after normalizing the intensities of the "ice-band" at 231 cm^{-1}.

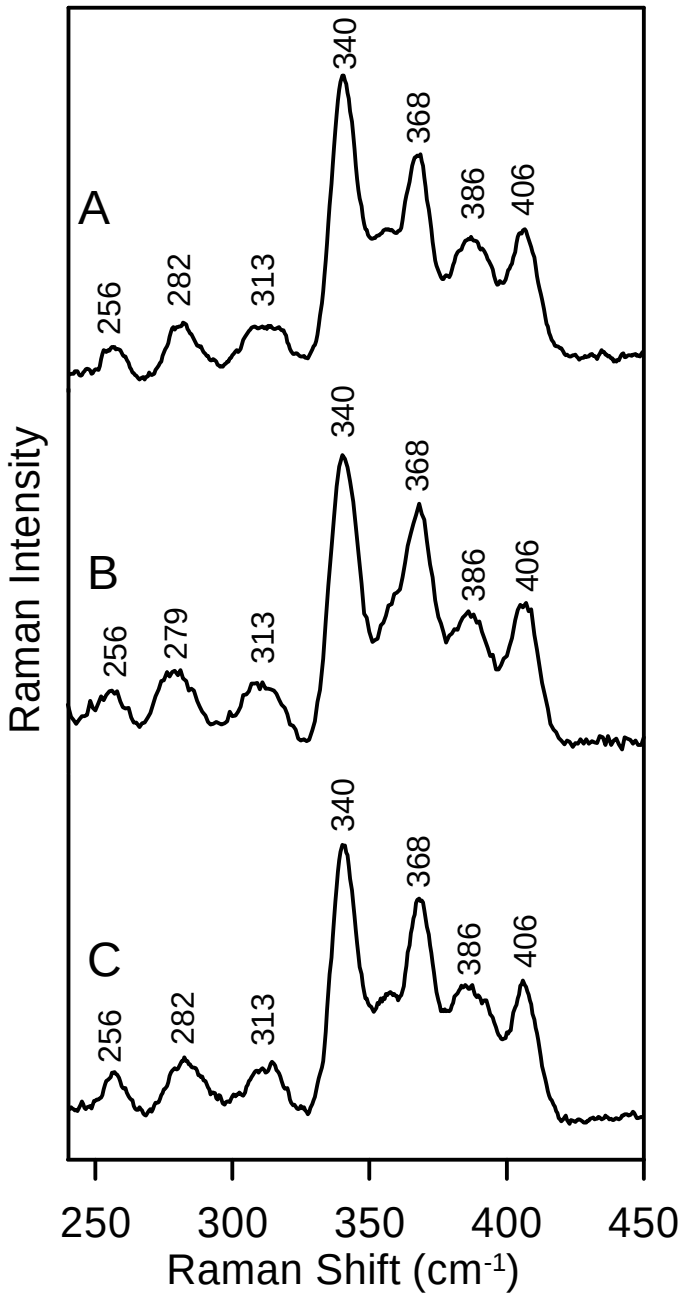
A
B
C
256
282
279
313
340
368
386
406
Raman Intensity
250
300
350
400
450
Raman Shift (cm-1)

Figure 4.8 4.2-K Mössbauer spectra of oxidized *Synechocystis* NEM-FTR recorded in a parallel field of 50 mT (A), 4 T (B) and 8 T (C). The data (hatched marks) can be decomposed into three components with an intensity ratio of 1:1:2 representing two distinct ferric sites (sites *a* and *b*) and a valence-delocalized $Fe^{2+}Fe^{3+}$ pair (site *c*). An $S = 1/2$ ground state is assumed for the analysis. The theoretical spectra corresponding to the three components are shown above the experimental spectra as solid lines (site *a*), dashed lines (site *b*) and dotted lines (site *c*). The sums of the three components are plotted as solid lines overlaid with the experimental spectra. The parameters used for the simulation are listed in Table 4.1. This NEM-reacted sample contains approximately 12% methyl viologen-reduced FTR (starting materials). For clarity, the contribution from the reduced FTR has been removed from the raw data using spectra simulated with parameters listed in Table 4.1 for the reduced FTR-C57S.

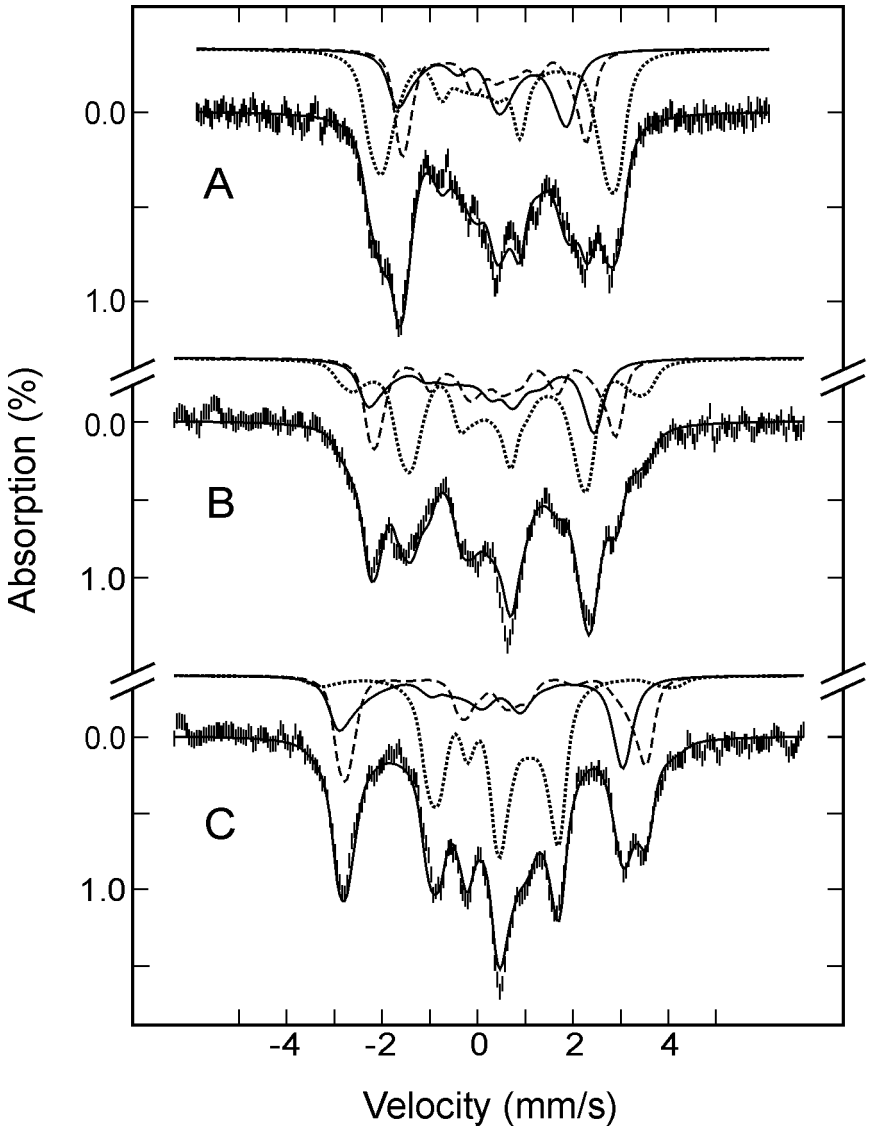
Absorption (%)
0.0
1.0
A
0.0
1.0
B
0.0
1.0
C
-4
-2
0
2
4
Velocity (mm/s)

Figure 4.9 Comparison of the Mössbauer spectra of $[4Fe\text{-}4S]^{3+}$ centers in the oxidized (as purified) forms of *Synechocystis* FTR samples: (A) NEM-FTR; (B) wild-type FTR/C40S Trx *m* heterodisulfide complex; (C) C57S FTR. The data were recorded at 4.2 K in a parallel field of 8 T.

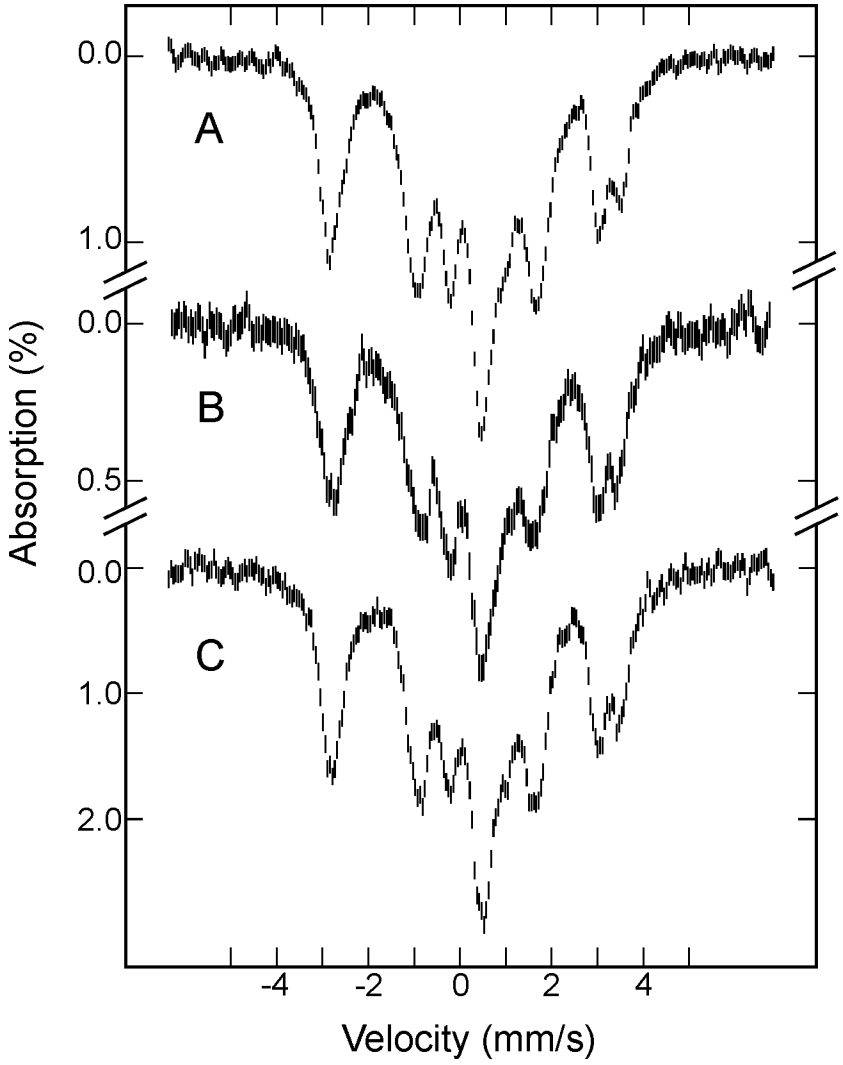
0.0
A
1.0
0.0
B
0.5
0.0
C
1.0
2.0
Absorption (%)
-4
-2
0
2
4
Velocity (mm/s)

Figure 4.10 4.2-K Mössbauer spectrum of *Synechocystis* C87A FTR recorded in a parallel field of 50 mT. The spectrum (hatched marks) is least-squares fitted to three quadrupole doublets with an intensity ratio of 1:1:2 representing three Fe sites *a*, *b* and *c*. The resulting doublets are shown above the experimental spectrum as a solid line (site *a*), a dashed line (site *b*) and a dotted line (site *c*). The sum of the three doublets is shown as a solid line overlaid with the data. The parameters are listed in Table 4.1.

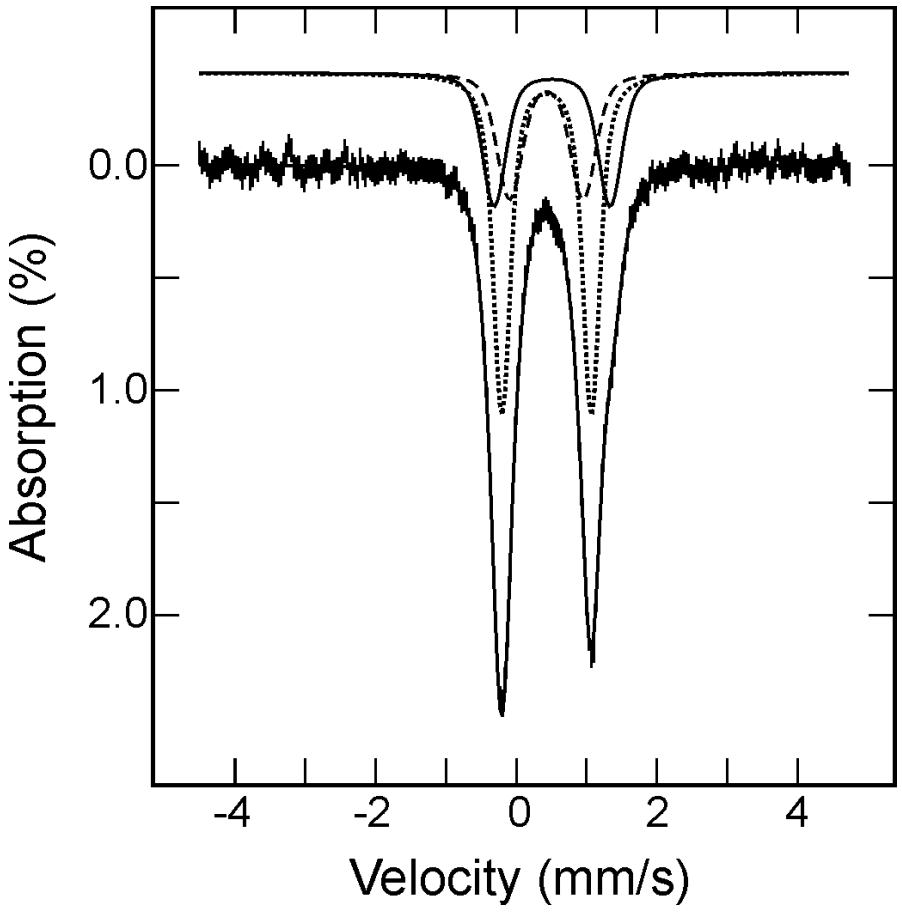
Absorption (%)
0.0
1.0
2.0
-4
-2
0
2
4
Velocity (mm/s)

Figure 4.11 Mössbauer spectra of dithionite-reduced *Synechocystis* C57S FTR. The spectra (hatched marks) were recorded at 4.2 K in a parallel field of 50 mT (A) and 8 T (B). These spectra can be decomposed into three components with an intensity ratio of 1:1:2 representing a valence-localized $Fe^{2+}Fe^{3+}$ pair (sites *a* and *b*) and a valence-delocalized $Fe^{2+}Fe^{3+}$ pair (site *c*). A diamagnetic $S = 0$ ground state is assumed in this analysis. The theoretical simulations of the individual components are shown above the experimental spectra as solid lines (site *a*), dashed lines (site *b*), and dotted lines (site *c*). The sums of the three components are shown as solid lines overlaid with the experimental spectra. The parameters are listed in Table 4.1.

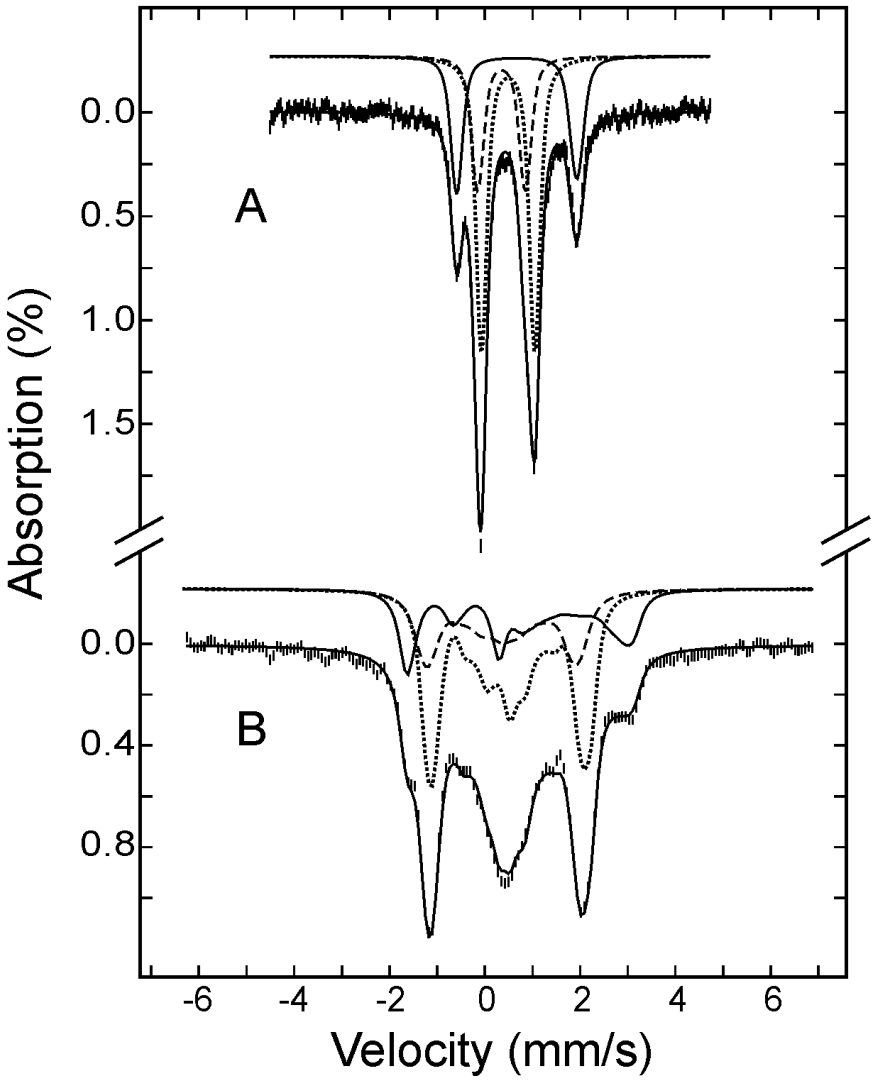
Absorption (%)
0.0
0.5
1.0
1.5
A
0.0
0.4
0.8
B
-6
-4
-2
0
2
4
6
Velocity (mm/s)

Figure 4.12 Mössbauer spectra of methyl viologen-reduced spinach FTR. Shown in (A) is the experimental spectrum (hatched marks) of a methyl viologen-reduced spinach FTR sample recorded at 4.2 K in a parallel field of 50 mT. Approximately 14% of the proteins in this sample remains in the as-purified state. The solid line in (A) is the spectrum of the as-purified FTR (Figure 1 of reference 11) normalized to 14% of the total Fe absorption of the reduced sample. Removal of the contributions of the as-purified proteins from the raw data yields the spectrum shown in (B) (hatched marks). This spectrum can be decomposed into three quadrupole doublets with an intensity ratio of 1:1:2 representing three distinct Fe sites *a*, *b* and *c*. These doublets are shown above the experimental spectrum as a solid line (site *a*), a dashed line (site *b*) and a dotted line (site *c*). The sum of the three doublets is shown as a solid line overlaid with the experimental spectrum.

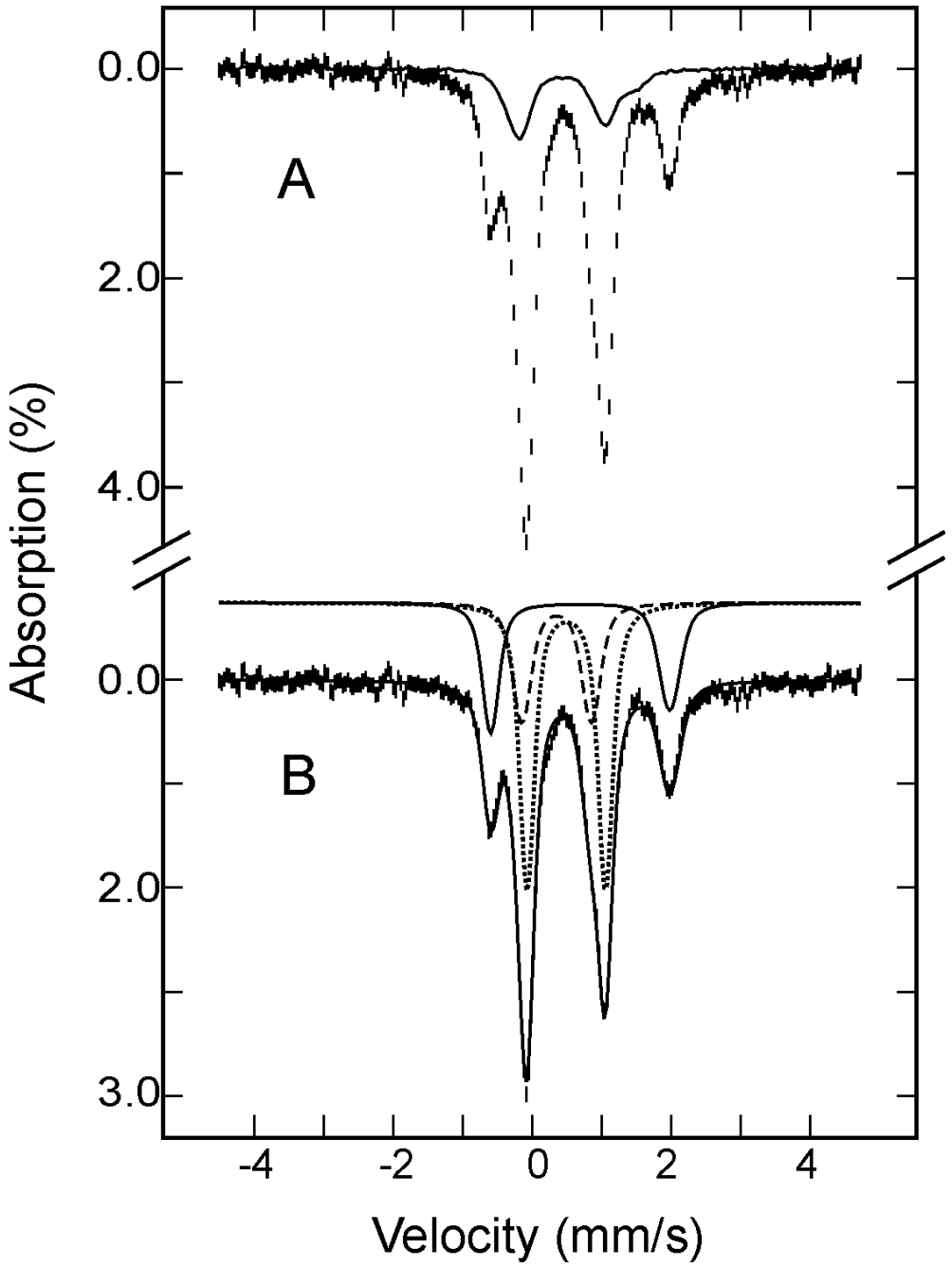
0.0
2.0
4.0
A
0.0
2.0
3.0
B
Absorption (%)
-4
-2
0
2
4
Velocity (mm/s)

Figure 4.13 EPR-monitored redox titrations of *Synechocystis* NEM-FTR (A) and wild-type *Synechocystis* FTR/C40S Trx *m* heterodisulfide complex (B). Data points correspond to the intensity of the $S = 1/2$ EPR from the $[4Fe\text{-}4S]^{3+}$ center at pH 7.0 (●) and pH 8.0 (■). The initial concentration of enzyme used in each titration was 100 μM and all data points have been normalized for dilution effects upon reductive titration with sodium dithionite. The solid lines are the best fits to one-electron Nernst equations with $E_m = -145 \pm 10$ mV (pH 7.0) and -200 ± 10 mV (pH 8.0) for NEM-FTR and $E_m = -60 \pm 10$ mV (pH 7.0) and -110 ± 10 mV (pH 8.0) for the FTR/C40S Trx *m* heterodisulfide complex.

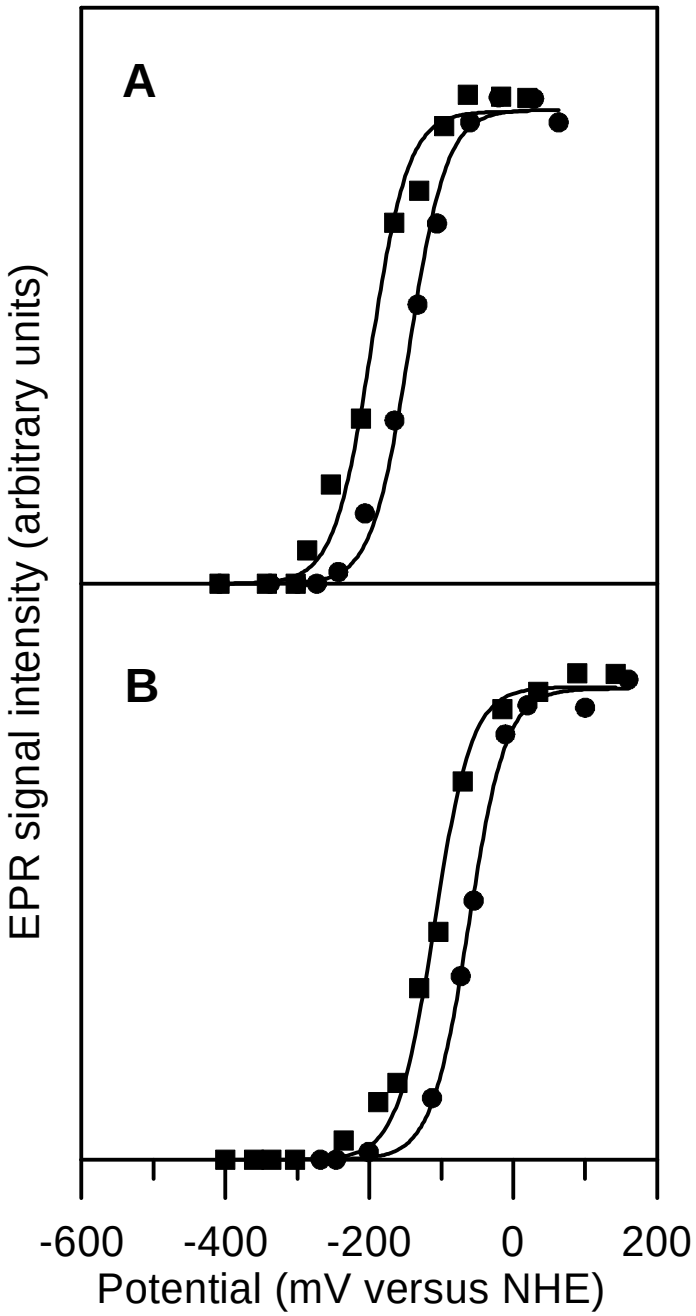
A
B
EPR signal intensity (arbitrary units)
-600
-400
-200
0
200
Potential (mV versus NHE)

Figure 4.14 Chromatographic analysis of the status of the heterodisulfide in *Synechocystis* FTR/C40S Trx *m* heterodisulfide complex poised at selected potentials (vs NHE) in an EPR redox titration: solid line, +100 mV; dashed line, –85 mV; dot-dash line, –400 mV versus NHE. FTR/Trx *m* heterodisulfide complex at pH 7.3 was incubated in redox dyes and poised at various potentials according to procedure for EPR redox titrations as described in Materials and Methods. At specified potentials, an aliquot of sample was applied to a 5-mL High-Performance Q-Sepharose column and eluted with a gradient of 0.0-0.5 M NaCl in 20 mM triethanolamine-Cl buffer, pH 7.3.

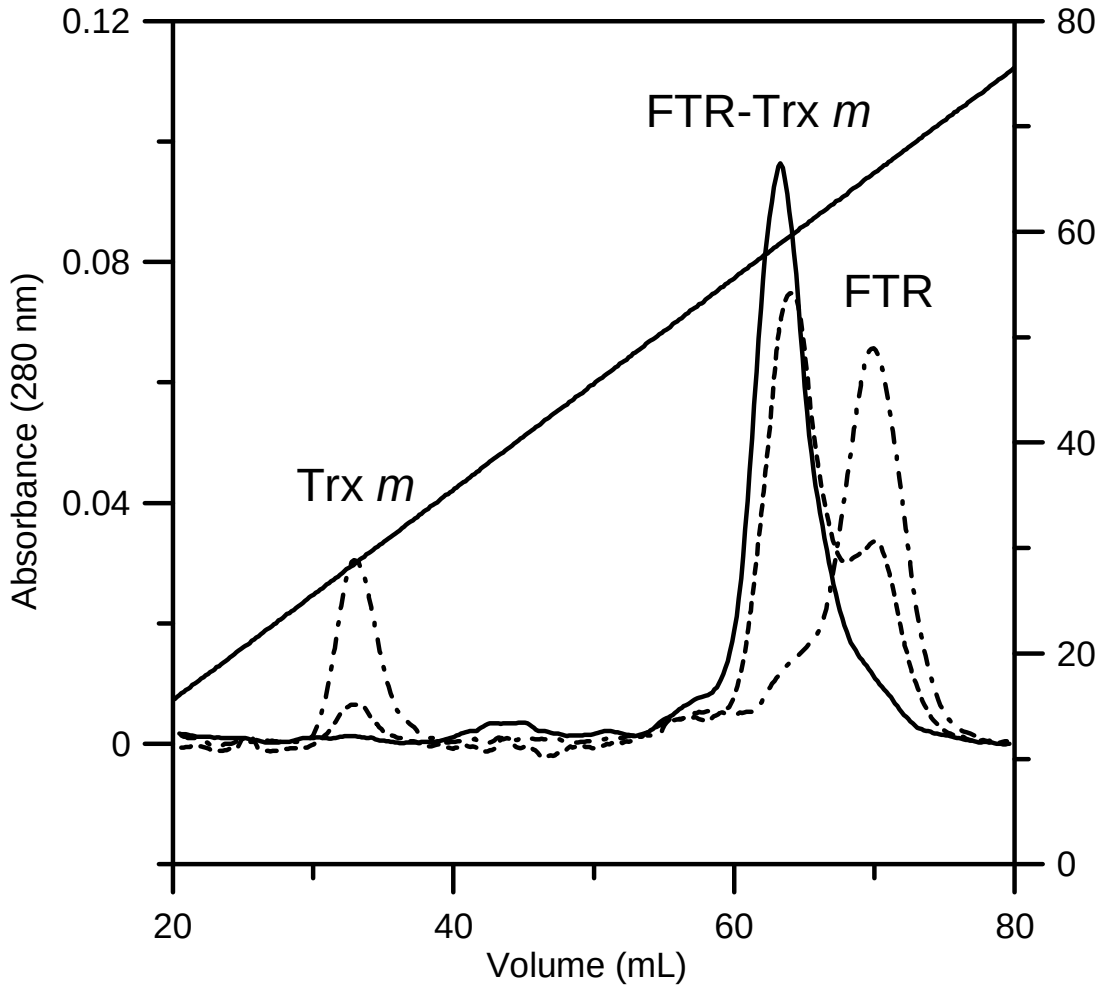
0.12
0.08
0.04
0
Absorbance (280 nm)
80
60
40
20
0
20
40
60
80
Volume (mL)
FTR-Trx *m*
FTR
Trx *m*

Figure 4.15 Alternative proposal for the catalytic mechanism of FTR. Residue numbering is for *Synechocystis* FTR. Square brackets are used to indicate transient intermediates.

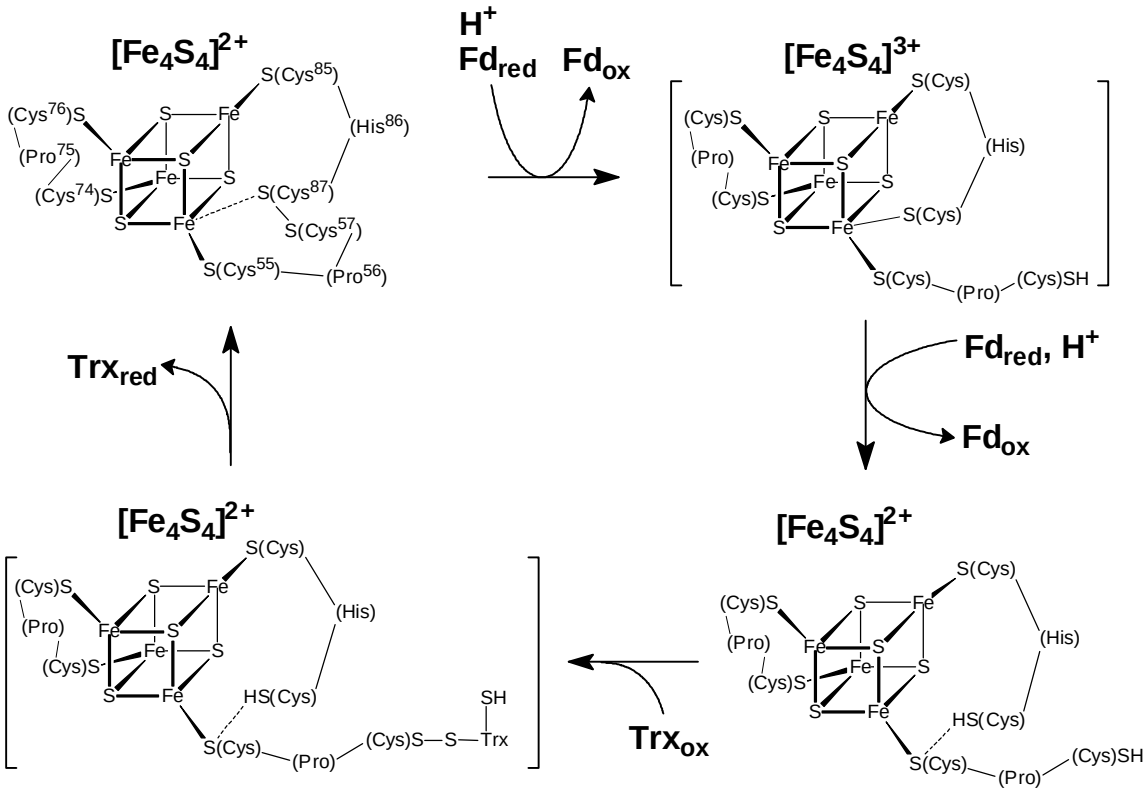
[Fe4S4]2+
H+
Fdred
Fdox
[Fe4S4]3+
Fdred, H+
Fdox
Trxred
[Fe4S4]2+
[Fe4S4]2+
Trxox

CHAPTER 5

INVESTIGATIONS INTO THE ROLE OF HISTIDINE-86 IN THE CATALYTIC MECHANISM OF FERREDOXIN:THIOREDOXIN REDUCTASE[1]

[1] Walters, E.M.[§]; Garcia-Serres, R.[†]; Glauser, D.A.[‡]; Bourquin, F.[‡]; Manieri, W.[‡]; Schürmann, P.[‡]; Johnson, M.K.[§]; Huynh, B.H.[†] *to be submitted* [§] Department of Chemistry and Center for Metalloenzyme Studies, University of Georgia, Athens, GA, 30602, [†] Department of Physics, Emory University, Atlanta, GA, 30322, and [‡] Laboratoire de Biochemie Végétale, Université de Neuchâtel, CH-2007 Neuchâtel, Switzerland.

Abstract

Ferredoxin: thioredoxin reductase (FTR) is the central enzyme of the chloroplast/FTR system, a redox regulatory system required for the control of the catalytic properties of a wide range of target enzymes involved in oxygenic photosynthesis. FTR utilizes an active-site consisting of a [4Fe-4S] cluster and an adjacent disulfide to effect the two electron reduction of regulatory disulfides using the one-electron donor reduced ferredoxin. The combination of x-ray crystallography and site-directed mutagenesis has identified histidine-86 (His86) as a potential Lewis acid/base required during catalysis based on the proximity of His86 to the active-site and the decrease in activity that occurs when histidine is mutated to tyrosine (H86Y). Here we report spectroscopic and redox characterization of the [4Fe-4S] cluster of *Synechocystis* H86Y FTR, both in the as-purified and NEM-modified forms of the enzyme, using the combination of UV-visible absorption, EPR, resonance Raman, VTMCD and Mössbauer spectroscopies. The results indicate that His86 has a role both as a proton donor/acceptor during reductive cleavage of the active-site disulfide and in anchoring the cluster interacting thiol (Cys87) to the cluster in the two-electron reduced form.

Introduction

Ferredoxin: thioredoxin reductase (FTR) is the central enzyme of the chloroplast/FTR system, a redox regulatory system required for the control of the catalytic properties of a wide range of target enzymes involved in oxygenic photosynthesis. FTR transfers a redox signal received by a $[2Fe\text{-}2S]^{2+/+}$ ferredoxin (Fd) to thioredoxins (Trxs) utilizing a unique active-site consisting of a [4Fe-4S] cluster and an adjacent disulfide. In this manner, FTR converts two one-electron light signals to one two-electron thiol signal which is then transmitted via dithiol/disulfide interchange reactions to specific enzymes which are critical to the regulation of the Calvin Cycle. FTR is one of only two members of a unique class of disulfide reductases that use a [4Fe-4S] cluster to effect disulfide reduction, however only FTR combines the [4Fe-4S] cluster with an active-site disulfide. The mechanism and the essential amino acid residues by which two-electron reduction of a disulfide is achieved using the unorthodox one-electron donor and acceptor system of Fd and FTR is of great interest.

Biological disulfide reduction is generally catalyzed by enzymes belonging to a large family of pyridine nucleotide-disulfide oxidoreductase flavoenymes, which include thioredoxin reductase, glutathione reductase, lipoamide dehydrogenase, trypanothione reductase, mercuric reductase, and NADH peroxidase. This family of enzymes has been well studied both structurally and mechanistically, and has been the subject of many thorough reviews.[1-3] Enzymes in this family reduce substrate disulfides utilizing an active-site comprised of a flavin and a nearby disulfide. An acid-base amino acid residue has been implicated in having a crucial role during catalysis in both the reductive half reaction, i.e. the reduction of the active-site disulfide, and the oxidative half reaction, i.e.

the reduction of the substrate disulfide with concomitant oxidation of the active-site disulfide. During the reductive half reaction, a two-electron reduced catalytic intermediate is generated which is stabilized via a charge transfer complex between a thiolate from the active-site disulfide and the FAD cofactor. The other cysteine residue of the active-site disulfide is stabilized as a thiol by a nearby acid-base amino acid. The specific amino acid responsible for this role is variable throughout the superfamily of enzymes, however the residue is generally a specific acid-base residue located near the active-site disulfide. In glutathione reductase, lipoamide dehydrogenase, and thioredoxin reductases from higher organisms, the acid-base catalyst is a histidine residue. However, in some members of the superfamily, the histidine residue is closely linked to a glutamate and the two amino acids work together to effect protonation and deprotonation steps.[4;5] Site-directed mutagenesis studies in which the catalytic acid-base residues are substituted for a wide range of amino acids have shown a dramatic decrease in the catalytic activity of the enzyme. Deletion of these critically important residues has a marked effect on the ability of the enzymes to stabilize thiols and to protonate thiolate anions.[5-8]

By analogy to the flavoprotein disulfide reductases, a residue with a potential role as an acid-base catalyst has been identified in FTR via analysis of the x-ray crystal structure, which has been solved for *Synechocystis* FTR at 1.6Å resolution.[9] FTR is a heterodimer in the form of a concave disk measuring only 10Å across the center where the active site is located. Six conserved cysteine residues make up the active-site; four ligate the [4Fe-4S] cluster and two comprise the active-site disulfide. The six cysteine residues are arranged in three CXC motifs, two CPC ($C^{55}PC^{57}$ and $C^{74}PC^{76}$) motifs and one CHC ($C^{85}HC^{87}$) motif (*Synechocystis* numbering scheme). The active site of FTR,

shown in detail in Figure 5.1, comprises an all-cysteinyl ligated [4Fe-4S] cluster located adjacent to an asymmetrically disposed disulfide formed between Cys57 and Cys87, with Cys87 located closer to the cluster than Cys57.[9] On the basis of the proximity of His86 to the active-site disulfide (3.9Å is the distance of closest approach), His86 has been proposed to play a critical acid/base role in the catalytic mechanism of FTR.[9]

Details of the catalytic mechanism of FTR have largely come from spectroscopic studies of native Spinach and recombinant wild-type and site-directed variants of *Synechocystis* FTR.[10-13] The resting state involves a $S = 0$ $[4Fe\text{-}4S]^{2+}$ cluster adjacent to the asymmetrically disposed disulfide and two possible mechanistic schemes have been proposed, see Figure 5.2.[13] Both involve sequential one-electron reductions via a one-electron-reduced intermediate that comprises a novel $S = 1/2$ $[4Fe\text{-}4S]^{3+}$ cluster with a fifth cysteinyl ligand (Cys87) coordinated at a unique Fe site. Three forms of FTR, i.e, *N*-ethylmaleimide (NEM)-modified FTR, a FTR/Trx *m* heterodisulfide complex, and the C57S variant, in which Cys57 has been selectively alkylated with NEM, covalently attached to one of the active-site cysteines of Trx *m*, and mutated to a serine residue, respectively, provide stable analogs of the proposed one-electron-reduced intermediate. Moreover, all three forms undergo one-electron-reduction to yield an $S = 0$ $[4Fe\text{-}4S]^{2+}$ cluster. The mechanistic proposals differ in terms of whether interaction with the substrate and formation of the heterodisulfide intermediate is formed at the one-electron-reduced level (mechanism A) or two-electron-reduced level (mechanism B). The viability of mechanism A has been demonstrated by the ability to reform the active site disulfide and dissociate Trx via one electron reduction of a FTR/Trx *m* heterodisulfide complex.[13] The viability of mechanism B stems from spectroscopic studies which indicate that the

cluster-interacting thiol, Cys87, is anchored to the cluster via a strong H-bonding interaction in the two-electron-reduced form,[13] leaving the interchange thiol free to attack the substrate disulfide.

The importance of His86 in the catalytic cycle of FTR has recently been demonstrated via mutagenesis studies. Replacing His86 with a tyrosine residue dramatically reduces the ability of FTR to activate fructose-1,6-bisphosphatase (only 10% activity versus wild-type), a physiological redox partner of reduced Trx *f*, and also slows down the rate of formation of a heterodisulfide complex with variant forms of Trxs.[14] However, the specific catalytic role of His86 has yet to be determined and the effects of the H86Y mutation on the spectroscopic and redox properties of the active-site [4Fe-4S] cluster have yet to be elucidated. Here we report spectroscopic and redox characterization of the [4Fe-4S] cluster of *Synechocystis* H86Y FTR, both in the as-purified and NEM-modified forms of the enzyme, using the combination of UV-visible absorption, EPR, resonance Raman, VTMCD and Mössbauer spectroscopies. The results indicate that His86 has a role both as a proton donor/acceptor during reductive cleavage of the active-site disulfide and in anchoring the cluster interacting thiol (Cys87) to the cluster in the two-electron reduced form.

Materials and Methods

Protein Expression and Purification

The constructions of the overexpression systems, tranformation, overexpression, and purification protocol of *Synechocystis* wild-type (WT) and H86Y FTR are described elsewhere.[14-16]

Sample Preparation and Handling

Recombinant *Synechocystis* WT and H86Y enzyme are initially purified with varying amounts of the enzyme in a form that closely resembles NEM-FTR based on EPR studies (up to 20% based on EPR spin quantitations). The EPR silent form of recombinant FTR was generally obtained only after redox cycling the enzyme by dithionite reduction followed by O_2 oxidation and is used as the starting material for all studies. NEM-modification of one of the cysteines of the active-site disulfide of FTR was carried out by reducing FTR with excess reduced methyl viologen and allowing the mixture to incubate for 30 minutes. The FTR sample was cooled on frozen cryovials filled with water. When the FTR was sufficiently cool, as determined by the color change resulting from the cooling of reduced methyl viologen, NEM was added in excess and the sample was exposed to oxygen within two minutes to quench the reaction. The sample was cleaned on a 5 mL desalting column to remove excess reagents and subsequently concentrated on a YM10 Amicon membrane. Sample concentrations were based upon ε_{410} = 17 400 M^{-1} cm^{-1} for WT and H86Y FTR, and ε_{410} = 19 500 M^{-1} cm^{-1} for WT NEM-FTR and H86Y NEM-FTR.[17] Unless otherwise stated, WT and H86Y FTR (both in the as-purified and NEM-modified forms) were in 20 mM triethanolamine hydrochloride buffer, pH 7.3; in a Vacuum Atmospheres glovebox under an Ar atmosphere (<1 ppm O_2).

EPR redox titrations were performed at ambient temperature (25-27 ºC) in a Vacuum Atmospheres glovebox under argon (<1 ppm O_2). The pH dependence of the midpoint redox potential was determined using *Synechocystis* WT or H86Y NEM-FTR in a buffer cocktail containing 200 mM each MES, MOPS, and TAPS buffers which allows

for easy variation of the pH in the desired pH range (6.0-8.5). Mediator dyes were added, each to a final concentration of 50 μM, in order to cover the desired range of redox potentials, i.e., methyl viologen, benzyl viologen, neutral red, safranin, phenosafranin, anthroquinone-1,5-disulfonate, indigodisulfonate, methylene blue, 1,2-napthoquinone, duroquinone, and 1,2-napthoquinone-4-sulfonate. Samples were first oxidized by addition of excess potassium ferricyanide followed by reductive titration with sodium dithionite. After equilibration at the desired potential, a 0.25-mL aliquot was transferred to an EPR tube and immediately frozen in liquid nitrogen. Potentials were measured with a platinum working electrode and a saturated calomel reference electrode and are reported relative to NHE.

Spectroscopic Measurements

UV/visible absorption spectra were recorded on a Shimadzu UV301PC spectrophotometer. Variable-temperature (1.5K – 300K) and variable-field (0 – 6 T) MCD measurements were recorded on samples containing 55% (v/v) poly(ethylene glycol) using an Oxford Instruments SM3 or Spectromag 4000 split-coil superconducting magnet mated to a Jasco J-500C or J715 spectropolarimeter. The experimental protocols used in variable-temperature MCD studies for accurate sample temperature and magnetic field measurement, anaerobic sample handling, and assessment of residual strain in frozen samples have been described in detail elsewhere.[18;19] The MCD intensities are expressed as $\Delta\varepsilon$ (ε_{LCP} - ε_{RCP}) where ε_{LCP} and ε_{RCP} are the molar extinction coefficients for the absorption of left and right circularly polarized light, respectively. X-band (~9.6 GHz) EPR spectra were recorded on a Bruker ESP300E spectrometer equipped with an ER-4116 dual mode cavity and an Oxford Instruments ESR-9 flow cryostat. Raman

spectra were recorded with an Instruments SA U1000 spectrometer fitted with a cooled RCA 31034 photomultiplier tube, using a 457 nm line from Coherent Innova 10-W Ar^+ laser. Scattering was collected at 90º from the surface of a frozen 15 μL droplet of protein in a specially constructed anaerobic cell mounted on the coldfinger of an Air Products Displex model CSA-202E closed cycle refrigerator.[20] The spectrum of the frozen buffer solution, normalized to the intensity of the ice-band at 230 cm^{-1} has been subtracted from all the spectra shown in this work. Mössbauer spectra were recorded using the previously described spectrometers.[21] The zero velocity refers to the centroid of the room temperature spectra of metallic iron foil. Analysis of the Mössbauer data was performed with the program WMOSS (WEB Research).

Results

The UV-visible absorption spectra of as prepared and dithionite-reduced WT and H86Y FTR and NEM-FTR are shown in Figure 5.3. Clearly the H86Y mutation has no significant effect on the absorption properties of either WT or NEM-modified samples. As prepared samples comprise a protein band at 278 nm, a shoulder at 315 nm, and a broad shoulder at 410 nm, and are characteristic of $[4Fe\text{-}4S]^{2+}$ centers.[22] The visible absorption properties are not significantly affected by dithionite, indicating that the $[4Fe\text{-}4S]^{2+}$ centers are not reduced by dithionite. In contrast, the as prepared NEM-FTR samples exhibit absorption spectra with pronounced features centered at 330 and 430 nm, in addition to the protein band at 278 nm, that are characteristic of $[4Fe\text{-}4S]^{3+}$ centers.[22] Moreover, dithionite reduction of the NEM-modified samples results in absorption spectra indistinguishable from those of as purified samples indicating one-electron reduction to the $[4Fe\text{-}4S]^{2+}$ state.[22]

Resonance Raman spectroscopy provides a more discriminating assessment of perturbations in the cluster environment via changes in the frequencies and/or relative intensities of Fe-S stretching modes in the 240-450 cm^{-1} region. Comparisons of the resonance Raman spectra using 457.9 nm excitation of WT and H86Y FTR in as prepared, oxidized NEM-modified and methyl-viologen-reduced forms are shown in Figure 5.4. The resonance Raman spectra of each of these forms of WT *Synechocystis* FTR are all distinct and each has been analyzed in detail in previous studies.[10;13] The observation that the resonance Raman spectra of as prepared and oxidized NEM-modified H86Y FTR are indistinguishable from their WT counterparts indicates that H86Y spectra can be interpreted in the same way. Hence, the spectrum of as prepared H86Y FTR is interpreted in terms of an all-cysteinyl-ligated $[4Fe\text{-}4S]^{2+}$ cluster in which one Fe site is weakly interacting with active-site disulfide and the spectrum of oxidized NEM-modified H86Y FTR is interpreted in terms of a $[4Fe\text{-}4S]^{3+}$ cluster with the unique Fe site ligated by two cysteine residues (Cys55 and Cys87).[10;12;13] In contrast, the resonance Raman spectra of the methyl-viologen reduced samples of WT and H86Y FTR are both indicative of $[4Fe\text{-}4S]^{2+}$ clusters, but are quite distinct from each other. Reduced methyl viologen is known to reduce the active-site disulfide in FTR,[17] and the anomalous resonance Raman spectrum of the methyl-viologen-reduced sample, i.e. 2-3 cm^{-1} downshifts and inversion of the relative intensities of the two dominant bands corresponding to the symmetric breathing mode of the [4Fe-4S] core (355 cm^{-1} in methyl-viologen reduced and 337 cm^{-1} in as prepared) and the asymmetric Fe-S(Cys) stretching mode (357 cm^{-1} in methyl-viologen reduced and 360 cm^{-1} in as prepared), has been rationalized in terms of changes in the core structure associated with the formation

of a valence-localized $Fe^{3+}Fe^{2+}$ pair as revealed by parallel Mössbauer studies.[13] This is unprecedented behavior for a $[4Fe\text{-}4S]^{2+}$ cluster and has been interpreted in terms of a strong H-bonding interaction between the thiol of Cys87 and the cluster-ligated cysteinate S of Cys55 in two-electron-reduced FTR.[13] The resonance Raman spectrum of methyl-viologen-reduced H86Y FTR closely resembles that of C87A variant in which there can be no interaction of the $[4Fe\text{-}4S]^{2+}$ cluster with the active site disulfide or the free Cys87 thiol.[13] Hence on the basis of the resonance Raman data, it is concluded that Cys87 is no longer H-bonded to the cluster-ligated cysteinate S of Cys55 in the two-electron-reduced form of H86Y FTR.

Preliminary Mössbauer studies of H86Y FTR add additional support to the resonance Raman results, see Figure 5.7. The spectra of both the as prepared and methyl-viologen-reduced samples, Figures 5.7A and 5.7B, respectively, are very similar and are dominated by a nearly symmetrical quadrupole doublet, δ = 0.45 mm/s and ΔE_Q = 1.28 mm/s, indicative of a predominantly valence-delocalized $[4Fe\text{-}4S]^{2+}$ cluster. More detailed studies involving additional samples will be required to assess if the spectra can be interpreted in terms of mixtures of $[4Fe\text{-}4S]^{2+}$ clusters containing different degrees of valence delocalization over one of the two $Fe^{3+}Fe^{2+}$ pairs as found in WT and C87A FTR.[13] However, it is clear that methyl-viologen-reduced H86Y FTR does not contain the anomalous type of $[4Fe\text{-}4S]^{2+}$ cluster comprising one valence-delocalized and one valence-localized $Fe^{3+}Fe^{2+}$ pair that is the hallmark of the $[4Fe\text{-}4S]^{2+}$ clusters in methyl-viologen-reduced WT FTR and dithionite-reduced C57S FTR. Taken together with the resonance Raman results discussed above, the differences in the spectroscopic properties of the $[4Fe\text{-}4S]^{2+}$ clusters in two-electron reduced forms of WT and H86Y FTR are

therefore interpreted in terms of a role for His86 in anchoring the free thiol of Cys87 close to the cluster so that it can H-bond to the cluster-ligated cysteinate S of Cys55 in order to create the valence-localized $Fe^{3+}Fe^{2+}$ pair.

The combination of EPR, VTMCD and Mössbauer spectroscopies have all been used to facilitate detailed comparison of electronic and magnetic properties of the $S = 1/2$ $[4Fe\text{-}4S]^{3+}$ centers in the oxidized NEM-modified forms of WT and H86Y FTR. As shown in Figure 5.5, the EPR spectrum is not significantly perturbed by the H86Y mutation. WT and H86Y samples show almost identical near-axial resonances (g = 2.109, 1.993, 1.982 for WT and g = 2.107, 1.994, 1.980 for H86Y), each accounting for 1.0 spins/FTR and exhibiting analogous spin-relaxation behavior as judged by temperature-dependence studies.[22] Hence the ground-state electronic properties of the $[4Fe\text{-}4S]^{3+}$ clusters in NEM-FTR are unaffected by the H86Y mutation. Likewise the excited-state electronic properties are not significantly perturbed as seen by the near coincident VTMCD spectra of the oxidized NEM-modified forms of WT and H86Y FTR,[22] see Figure 5.6. Finally the Mössbauer spectra of the paramagnetic $[4Fe\text{-}4S]^{3+}$ clusters in oxidized NEM-modified forms of WT and H86Y FTR are very similar (cf Figure 5.7C with Figure 4.8A of ref 13) and both can be fit with the same set of parameters used in fitting the WT data.[13] Hence the valence-delocalization scheme and intracluster magnetic interactions of the $[4Fe\text{-}4S]^{3+}$ cluster in oxidized NEM-FTR are also unperturbed by the H86Y mutation. Since oxidized NEM-FTR serves as a stable analog of the one-electron-reduced catalytic intermediate,[11] these spectroscopic results clearly demonstrate that His 86 is not required for formation of this intermediate.

The possibility that His86 plays a role as a general acid/base in mediating one-electron reduction of NEM-FTR, a stable analog of the one-electron-reduced intermediate, was addressed by investigating the pH dependence of the redox potential of NEM-modified H86Y FTR. Dye-mediated EPR redox titrations were performed at pH 7.0 and 8.0 for the NEM-modified forms of WT and H86Y FTR and the results are shown in Figure 5.8. In all cases the data are well fit using one-electron Nernst equations and are reported relative to the normal hydrogen electrode. At pH 7.0, the midpoint potentials for the $[4Fe\text{-}4S]^{3+/2+}$ couple in WT and H86Y NEM-FTR are the same within experimental error, −145 ±10 mV and −155 ±10 mV, respectively. However, at the physiologically relevant pH for light regulation in chloroplasts, i.e. pH 8.0, the mutation has a marked effect on the midpoint potential of NEM-FTR, −200 ±10 mV for WT and −255 ±10 mV for H86Y. The change in the midpoint potential between pH 7.0 and pH 8.0 for WT NEM-FTR (−55 mV) is consistent with reduction occurring with the addition of one proton. Cys87 is released as a cluster ligand on reduction of NEM-FTR and therefore has been proposed as the protonation site.[13] The much larger change in midpoint potential between pH 7.0 and pH 8.0 for H86Y NEM-FTR (−100 mV) indicates more complex behavior involving protonation and/or changes in cluster environment on reduction. More detailed pH dependence studies coupled with parallel structural and spectroscopic studies will clearly be required to fully understand the pH dependence of the midpoint redox potential of both WT and H86Y NEM-FTR. Nevertheless, the marked change in the redox potential of NEM-FTR at pH 8.0 that occurs when His86 is mutated to a tyrosine residue suggests a role for His86 as a proton donor/acceptor during the second one-electron step in the catalytic mechanism of FTR.

Discussion

The proximity of His86 to the active-site disulfide of FTR, Figure 5.1, led to the proposal that it plays a crucial role as a catalytic acid/base.[23] This was subsequently substantiated by biochemical characterization of the H86Y variant of FTR, which revealed greatly decreased activity in a coupled assay involving the activation of fructose-1,6-bisphosphate and decreased rate of heterodisulfide complex formation with variant forms of Trxs.[14] The results presented herein constitute the first attempt to understand the specific role for His86, via comparative spectroscopic studies of the properties and redox behavior of the active-site [4Fe-4S] cluster in oxidized, one-electron-reduced and two-electron-reduced forms of WT and H86Y FTR.

Using the combination of UV-visible absorption, resonance Raman, Mössbauer, EPR and VTMCD spectroscopies, the H86Y mutation is shown to have no significant effect on the properties of the $[4Fe\text{-}4S]^{2+}$ in the oxidized (as prepared) enzyme or the novel $[4Fe\text{-}4S]^{3+}$ cluster in NEM-FTR, which provides a stable analog of the one-electron-reduced catalytic intermediate. However, both resonance Raman and Mössbauer studies reveal distinct differences in the properties of the $[4Fe\text{-}4S]^{2+}$ clusters in the two-electron-reduced forms of WT and H86Y FTR that are prepared via reduction with reduced methyl viologen. These differences are interpreted in terms of differences in the location of Cys87 that is released on reduction of the one-electron-reduced intermediate. In WT FTR, Cys87 is anchored in close proximity to the cluster via a strong H-bond between the thiol of Cys87 and the coordinated S of the cysteinate of Cys55, giving rise to an unprecedented type of $[4Fe\text{-}4S]^{2+}$ cluster with one valence-localized and one valence-delocalized $Fe^{3+}Fe^{2+}$ pair.[13] This interaction is not present in methyl-viologen-

reduced H86Y FTR, suggesting that His86 plays a key role in anchoring Cys87 proximal to the cluster in the two-electron-reduced form of FTR.

The recent x-ray crystal structure of methyl-viologen-reduced *Synechocystis* WT FTR at 2.6 Å resolution (S. Dai, H. Eklund, P. Schürmann, unpublished results) has provided a more secure structural framework for interpreting the spectroscopic differences between the methyl-viologen-reduced forms of WT and H86Y FTR. Overlay of the active sites of oxidized and methyl-viologen-reduced forms of FTR reveals that two major structural changes accompany methyl-viologen-induced cleavage of the active-site disulfide, Figure 5.9. First, in accord with the proposed role as the interchange thiol,[13;22] Cys57 rotates by 130° away from the cluster and becomes solvent exposed. In contrast, the position of the cluster-interacting cysteine, Cys87, is essentially unchanged with the S---S distance between Cys87 and Cys55 only 3.1 Å, in accord with the proposal for a strong H-bonding interaction. Second, the imidazole ring of His86 flips 120° towards the cluster, bringing the εN of His86 within H-bonding range of the S of Cys55 and one of the cluster μ_3-S atoms (both 3.5 Å). Hence His86 is positioned to accept a proton from Cys87 in order to facilitate reformation of the active-site disulfide via nucleophilic attack of the heterodisulfide formed between the interchange cysteine on FTR and one of the active-site cysteines on Trx as part of the dithiol/disulfide interchange. Furthermore, the additional H-bonding interactions involving the εN of His86 are likely to facilitate positioning of Cys87 so that it can be anchored near the cluster via the H-bonding interaction with Cys55. This interpretation is clearly supported by the resonance Raman and Mössbauer studies of the methyl-viologen-reduced H86Y variant, which no longer show the anomalous cluster properties attributed to this strong

H-bonding interaction. Hence these crystallographic results fully support mechanism B in Figure 5.2 and are in accord with the differences and similarities in the spectroscopic properties of [4Fe-4S] centers in WT and H86Y FTR in the oxidized, one-electron-reduced and two-electron-reduced forms.

The H86Y mutation also affects the change in the midpoint potential of NEM-FTR, a stable analog of the one-electron reduced intermediate, on going from pH 7.0 to pH 8.0 (−55 mV for WT compared to −100 mV for H86Y). While this difference may also be related to the structural differences between the two-electron-reduced forms, particularly differences in H-bonding interactions or solvent exposure in the vicinity of [4Fe-4S] cluster, it does provide indirect evidence for the involvement of His86 as a proton donor/acceptor during catalytic cycling. More detailed pH dependence studies of WT and H86Y NEM-FTR monitored by redox, spectroscopic and crystallographic studies are clearly required to facilitate interpretation of the proposed role of His86 as a catalytic acid/base.

Bibliography

(1) Williams, C. H., Jr. Lipoamide Dehydrogenase, Glutathione Reductase, Thioredoxin Reductase, and Mercuric Ion Reductase-A Family of Flavoenzyme Transhydrogenases; In *Chemistry and Biochemistry of Flavoenzymes*; Müller, F., ed. CRC Press: Boca Raton, FL, 1992; pp 121-211.

(2) Williams, C. H., Jr. *FASEB J* **1995**, *9*, 1267-1276.

(3) Williams, C. H., Jr.; Arscott, L. D.; Müller, S.; Lennon, B. W.; Ludwig, M. L.; Wang, P.-F.; Veine, D. M.; Becker, K.; Schirmer, R. H. *Eur.J.Biochem.* **2000**, *267*, 6110-6117.

(4) Veine, D. M.; Arscott, L. D.; Williams, C. H., Jr. *Biochemistry* **1998**, *37*, 15575-15582.

(5) Gilberger, T.-W.; Walter, R. D.; Müller, S. *J.Biol.Chem.* **1997**, *272*, 29584-29589.

(6) Rietveld, P.; Arscott, L. D.; Berry, A.; Scrutton, N. S.; Deonarain, M. P.; Perham, R. N.; Williams, C. H., Jr. *Biochemistry* **1994**, *33*, 13888-13895.

(7) Mulrooney, S. B.; Williams, C. H., Jr. *Biochemistry* **1994**, *33*, 3148-3154.

(8) Krauth-Siegel, R. L.; Arscott, L. D.; Schönleben-Janas, A.; Schirmer, R. H.; Williams, C. H., Jr. *Biochemistry* **1998**, *37*, 13968-13977.

(9) Dai, S.; Schwendtmayer, C.; Schürmann, P.; Ramaswamy, S.; Eklund, H. *Science* **2000**, *287*, 655-658.

(10) Staples, C. R.; Ameyibor, E.; Fu, W.; Gardet-Salvi, L.; Stritt-Etter, A.-L.; Schürmann, P.; Knaff, D. B.; Johnson, M. K. *Biochemistry* **1996**, *35*, 11425-11434.

(11) Staples, C. R.; Gaymard, E.; Stritt-Etter, A.-L.; Telser, J.; Hoffman, B. M.; Schürmann, P.; Knaff, D. B.; Johnson, M. K. *Biochemistry* **1998**, *37*, 4612-4620.

(12) Jameson, G. N. L.; Walters, E. M.; Manieri, W.; Schurmann, P.; Johnson, M. K.; Huynh, B. H. *J.Am.Chem.Soc.* **2003**, *125*, 1146-1147.

(13) Walters, E. M.; Garcia-Serres, R.; Jameson, G. N. L.; Glauser, D. A.; Bourquin, F.; Manieri, W.; Schürmann, P.; Johnson, M. K. *J.Am.Chem.Soc.* **2005**, *submitted for publication*.

(14) Glauser, D. A.; Bourquin, F.; Manieri, W.; Schürmann, P. *J.Biol.Chem.* **2004**, *279*, 16662-16669.

(15) Schwendtmayer, C.; Manieri, W.; Hirasawa, M.; Knaff, D. B.; Schürmann, P. In *Photosynthesis: Mechanisms and Effects*; Garab, G., ed. Kluwer Academic Publisher: Dordrecht, The Netherlands, 1998; pp 1927-1930.

(16) Schürmann, P. *Meth.Enzymol.* **2002**, *347*, 403-411.

(17) Schürmann, P.; Gardet-Salvi, L. *Chimia* **1993**, *47*, 245-246.

(18) Johnson, M. K. In *Metal Clusters in Proteins*; Que, L., Jr., ed. American Chemical Society: Washington, D.C., 1988; pp 326-342.

(19) Thomson, A. J.; Cheeseman, M. R.; Georgie, S. J. *Meth.Enzymol.* **1993**, *226*, 199-232.

(20) Drozdzewski, P. M.; Johnson, M. K. *Appl.Spectrosc.* **1988**, *42*, 1575-1577.

(21) Ravi, N.; Bollinger, J. M.; Huynh, B. H.; Edmondson, D. E.; Stubbe, J. *J.Am.Chem.Soc.* **1994**, *116*, 8007-8014.

(22) Walters, E. M.; Johnson, M. K. *Photosyn.Res.* **2004**, *79*, 249-264.

(23) Dai, S.; Schwendtmayer, C.; Johnasson, K.; Ramaswamy, S.; Schürmann, P.; Eklund, H. *Quart. Rev. Biophys.* **2000**, *33*, 67-108.

Figure 5.1 Active-site structure of *Synechocystis* FTR.[9] Color code: Fe = green; S = yellow; C = gray; N = blue; O = red.

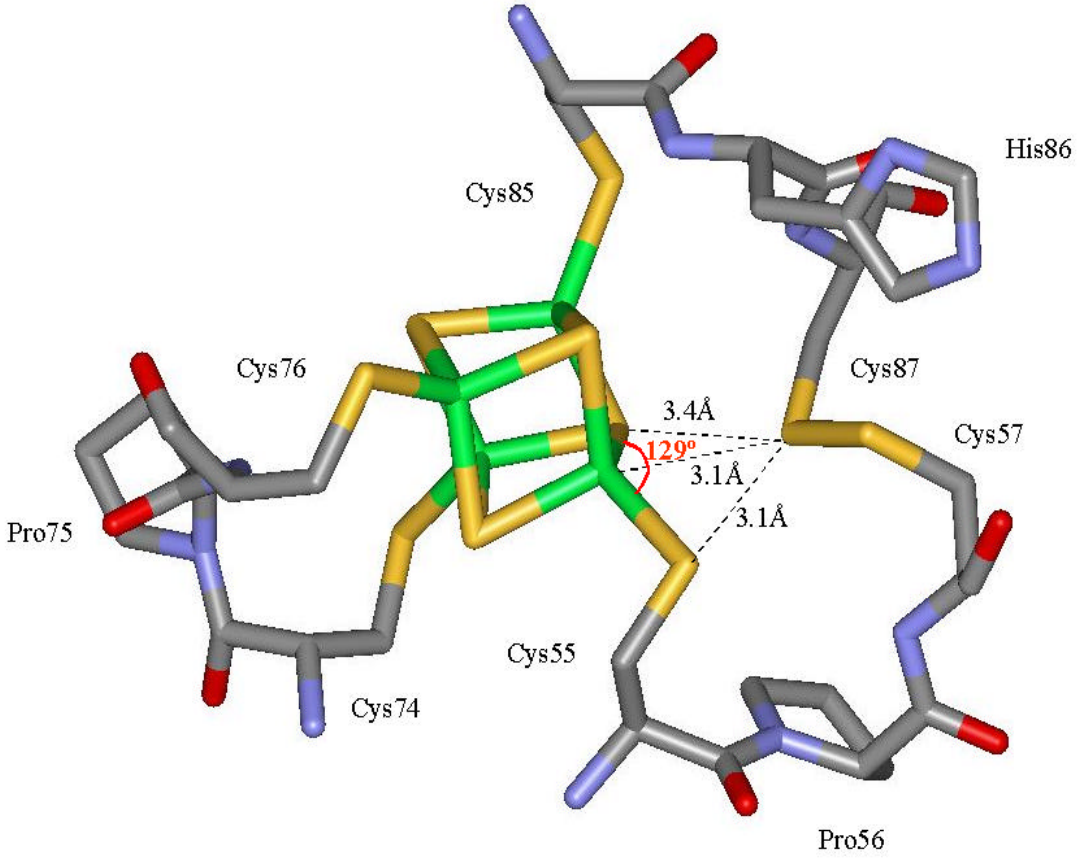
His86
Cys85
Cys76
Cys87
3.4Å
129°
Cys57
3.1Å
3.1Å
Pro75
Cys55
Cys74
Pro56

Figure 5.2 Proposed catalytic cycles for FTR in which: (A) the heterodisulfide intermediate is formed at the one-electron reduced state and (B) the heterodisulfide intermediate is formed at the two-electron reduced state. For both mechanisms, residue numbering is for *Synechocystis* FTR.

A

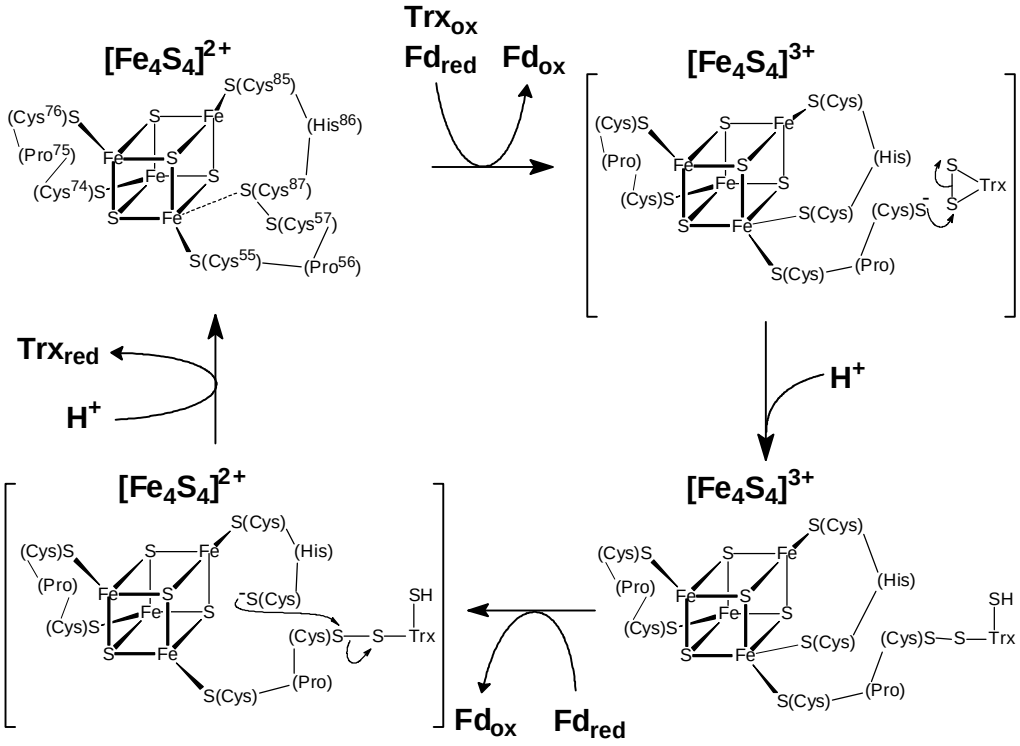
[Fe4S4]2+
Trxox
Fdred
Fdox
[Fe4S4]3+
Trxred
H+
[Fe4S4]2+
[Fe4S4]3+
Fdox
Fdred

B

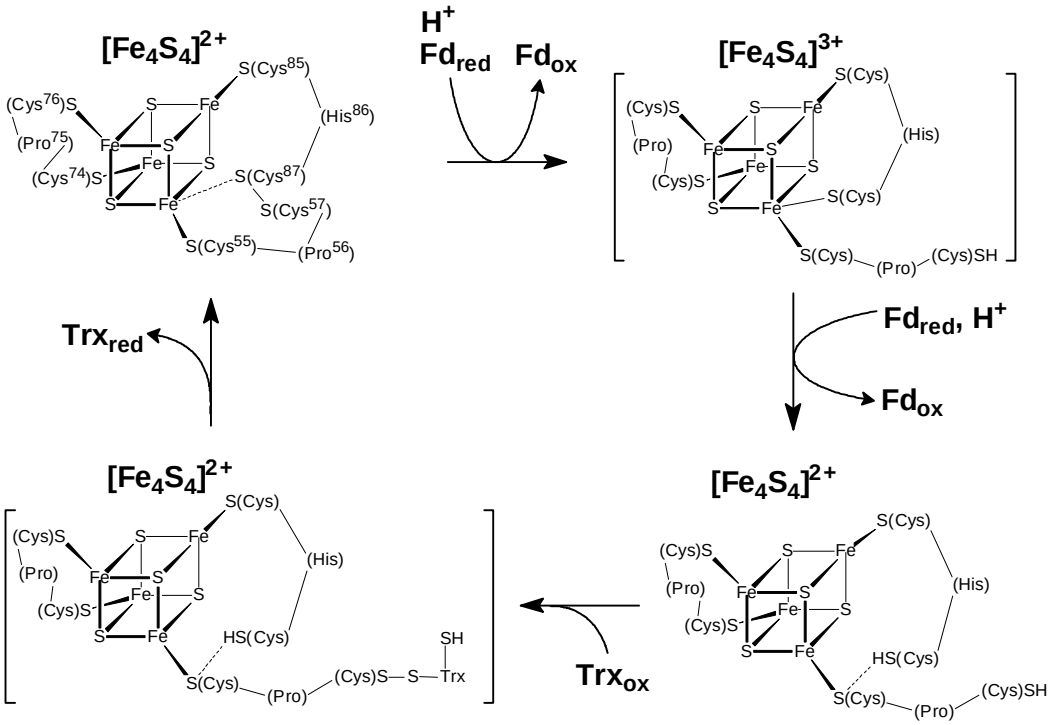
[Fe4S4]2+
H+
Fdred
Fdox
[Fe4S4]3+
Trxred
Fdred, H+
Fdox
[Fe4S4]2+
[Fe4S4]2+
Trxox

Figure 5.3 UV/visible absorption spectra of (A) WT FTR, (B) WT NEM-modified FTR, (C) H86Y FTR, and (D) H86Y NEM-modified FTR. In each case, the solid line represents the enzyme as-purified, and the dashed line represents the enzyme anaerobically reduced with excess sodium dithionite. The spectra were recorded in 1-mm cuvettes and protein concentrations were 200 μM (WT FTR), 115 μM (WT NEM-FTR), 303 μM (H86Y FTR), and 60 μM (H86Y NEM-FTR). The pronounced band at 314 nm (marked with an asterisk) in the dithionite-reduced samples originates from excess dithionite.

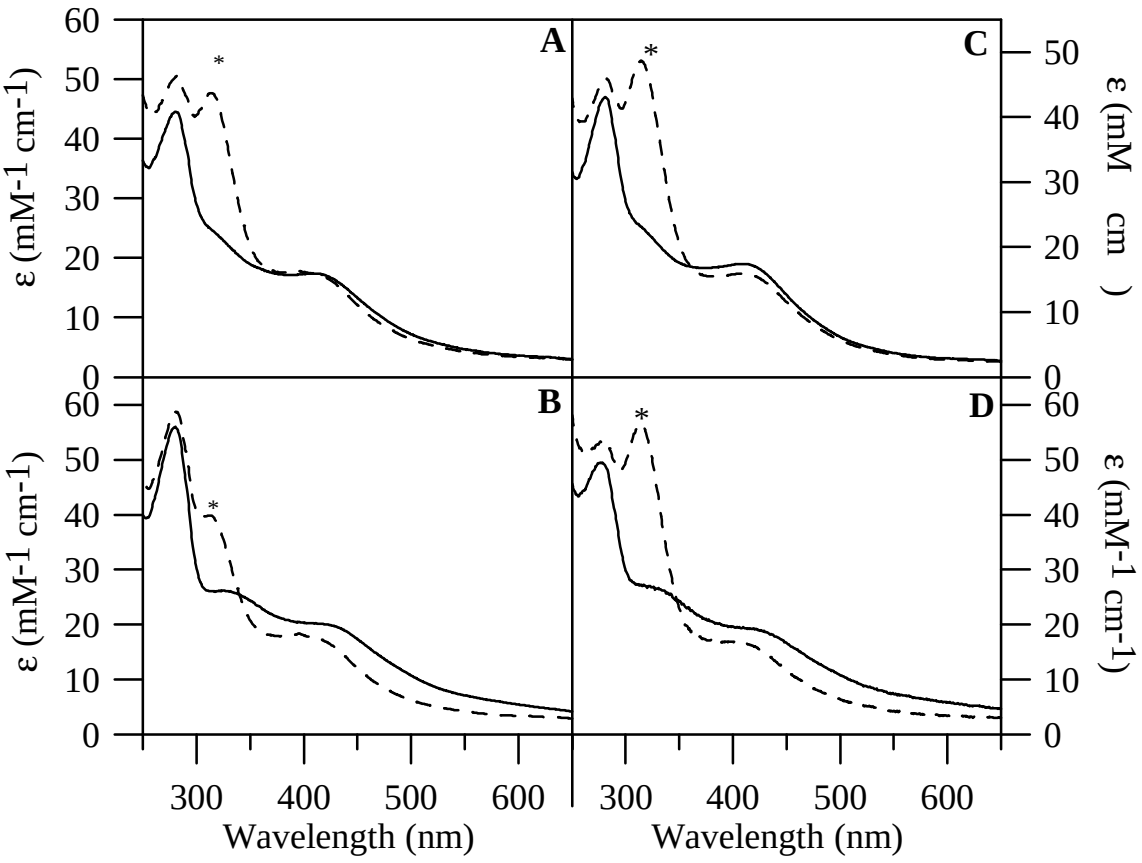
A
B
C
D
ε (mM-1 cm-1)
ε (mM cm)
ε (mM-1 cm-1)
Wavelength (nm)
Wavelength (nm)
0
10
20
30
40
50
60
300
400
500
600

Figure 5.4 Comparison of the resonance Raman spectra of WT and H86Y FTR in: (A) oxidized (as purified) enzyme, (B) oxidized NEM-modified enzyme, and (C) methyl-viologen reduced enzyme. All samples were ~3 mM in FTR (except for H86Y NEM-FTR which was ~ 1.0 mM) and all spectra were recorded at 17 K using 457.9-nm laser excitation with ~200 mW laser power at the sample. Each scan involved photon counting for 1 s at 1 cm^{-1} increments with 7 cm^{-1} bandwidth, and each spectrum is the sum of 80-100 scans (except for the spectra of H86Y NEM-FTR which is the sum of 180 scans). For all spectra, the vibrational modes originating from the frozen buffer solution have been subtracted after normalizing the intensities of the "ice-band" at 231 cm^{-1}.

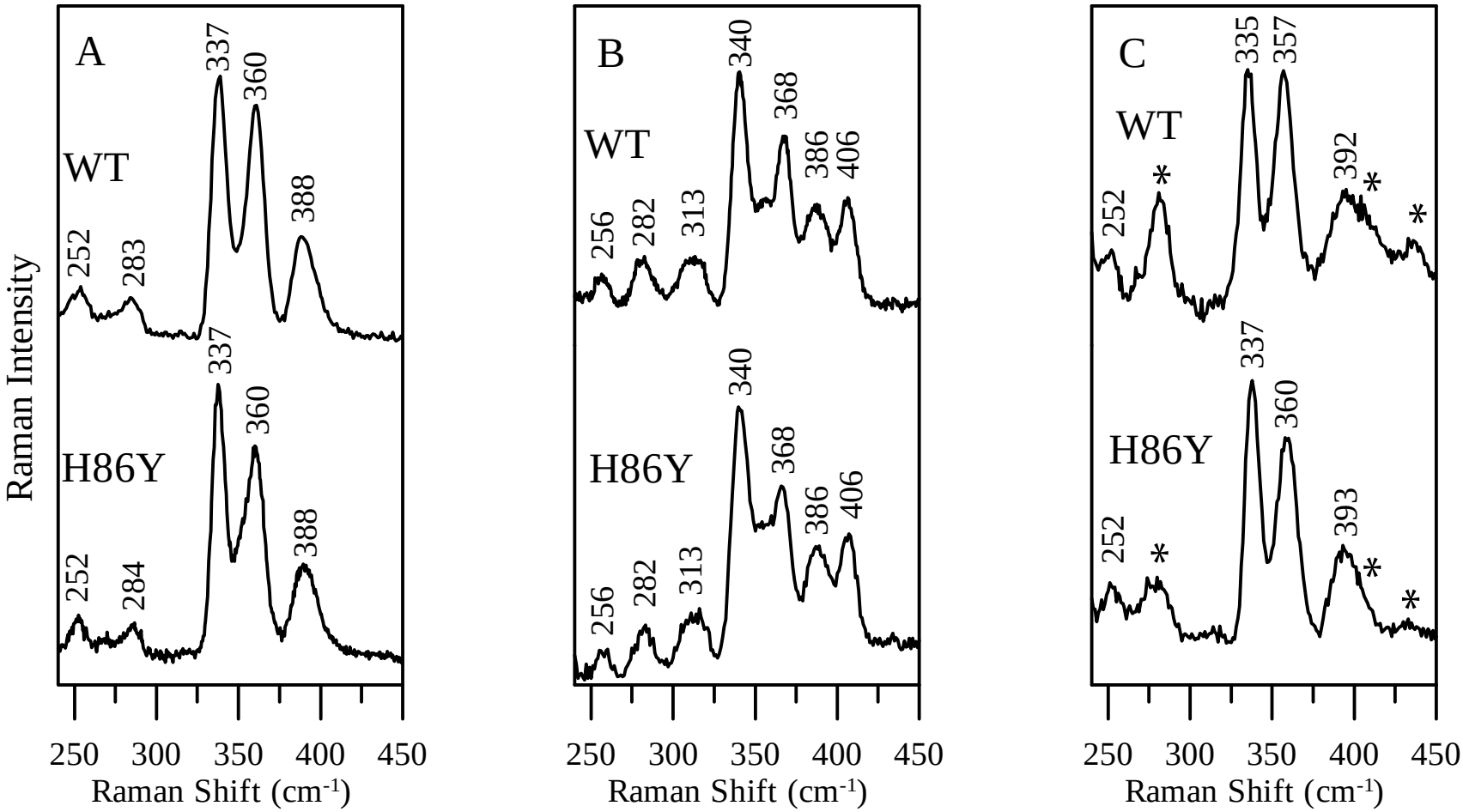
A
WT
252
283
337
360
388
H86Y
252
284
337
360
388
Raman Intensity
250 300 350 400 450
Raman Shift (cm-1)
B
WT
256
282
313
340
368
386
406
H86Y
256
282
313
340
368
386
406
250 300 350 400 450
Raman Shift (cm-1)
C
WT
252
335
357
392
*
*
*
H86Y
252
337
360
393
*
*
*
250 300 350 400 450
Raman Shift (cm-1)

Figure 5.5 Comparison of the X-band EPR spectra of $[4Fe\text{-}4S]^{3+}$ centers in the oxidized (as purified) forms of *Synechocystis* FTR samples: (A) WT NEM-FTR (185 μM) and (B) H86Y NEM-FTR (150 μM) EPR conditions: temperature, 35 K; microwave power, 1 mW; modulation amplitude, 0.63 mT; microwave frequency, 9.60 GHz.

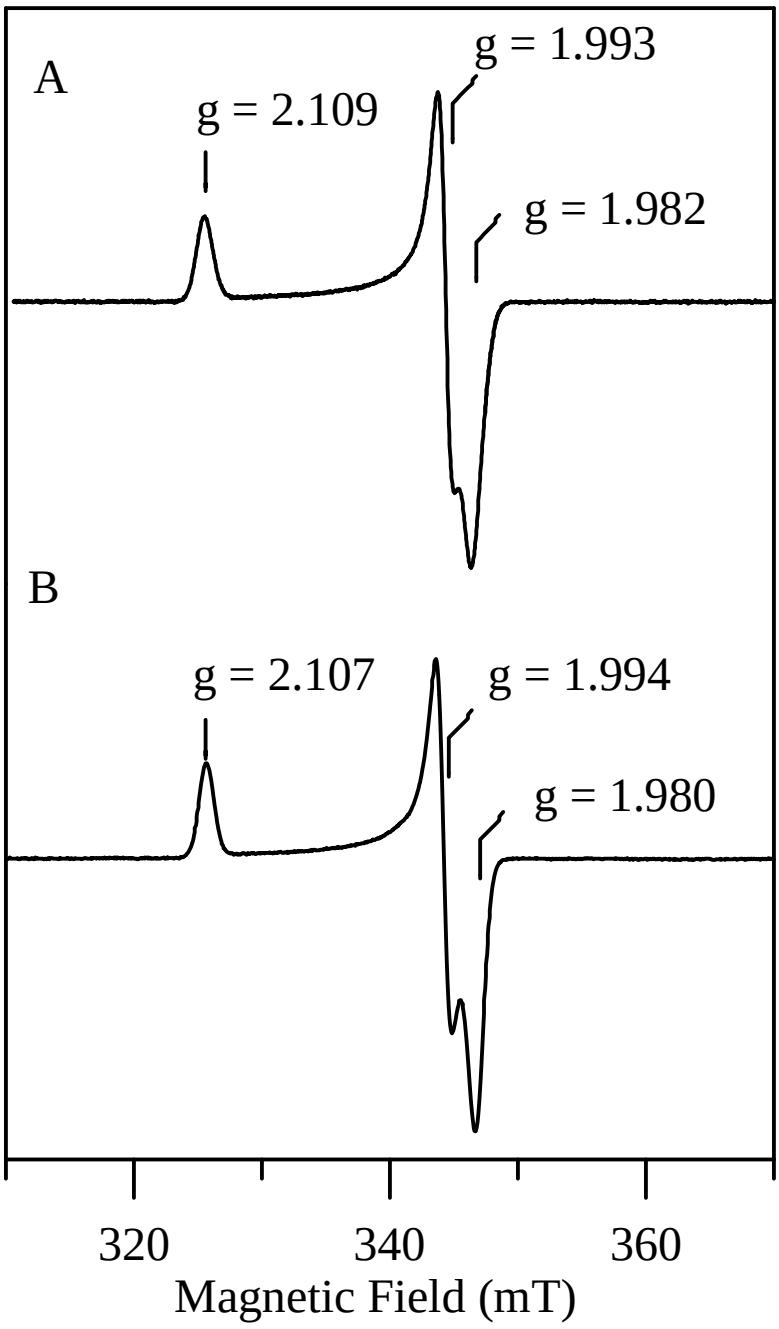
A
g = 1.993
g = 2.109
g = 1.982
B
g = 2.107
g = 1.994
g = 1.980
320
340
360
Magnetic Field (mT)

Figure 5.6 Comparison of the VTMCD spectra of $[4Fe\text{-}4S]^{3+}$ centers in the oxidized (as purified) forms of *Synechocystis* FTR samples. (A) MCD spectra of NEM-FTR collected at 1.68 K, 4.22 K, and 10.4 K, with a magnetic field of 6 T. (B) MCD spectra of H86Y NEM-FTR collected at 1.68 K, 4.22 K. 10.4 K, 25 K, and 50 K, with a magnetic field of 6 T. For all spectra, the intensity of all MCD bands (positive and negative) increase with decreasing temperature.

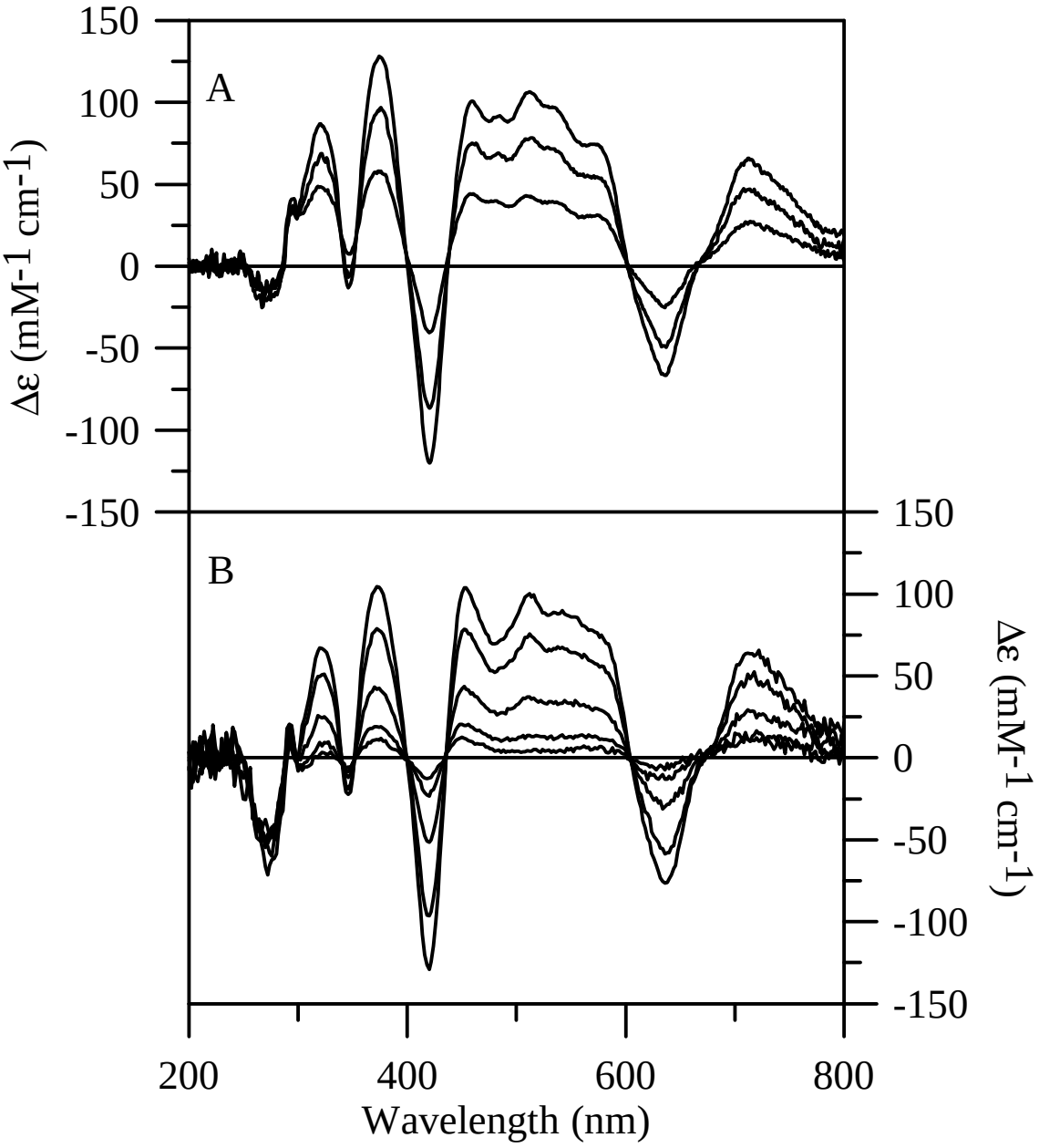
150
100
50
0
-50
-100
-150
A
B
Δε (mM-1 cm-1)
Δε (mM-1 cm-1)
200
400
600
800
Wavelength (nm)

Figure 5.7 4.2-K Mössbauer spectrum of *Synechocystis* H86Y FTR (A) oxidized, (B) NEM-modified and (C) two-electron reduced recorded in a parallel field of (A) 50 mT, (B) 8T, and (C) 50 mT.

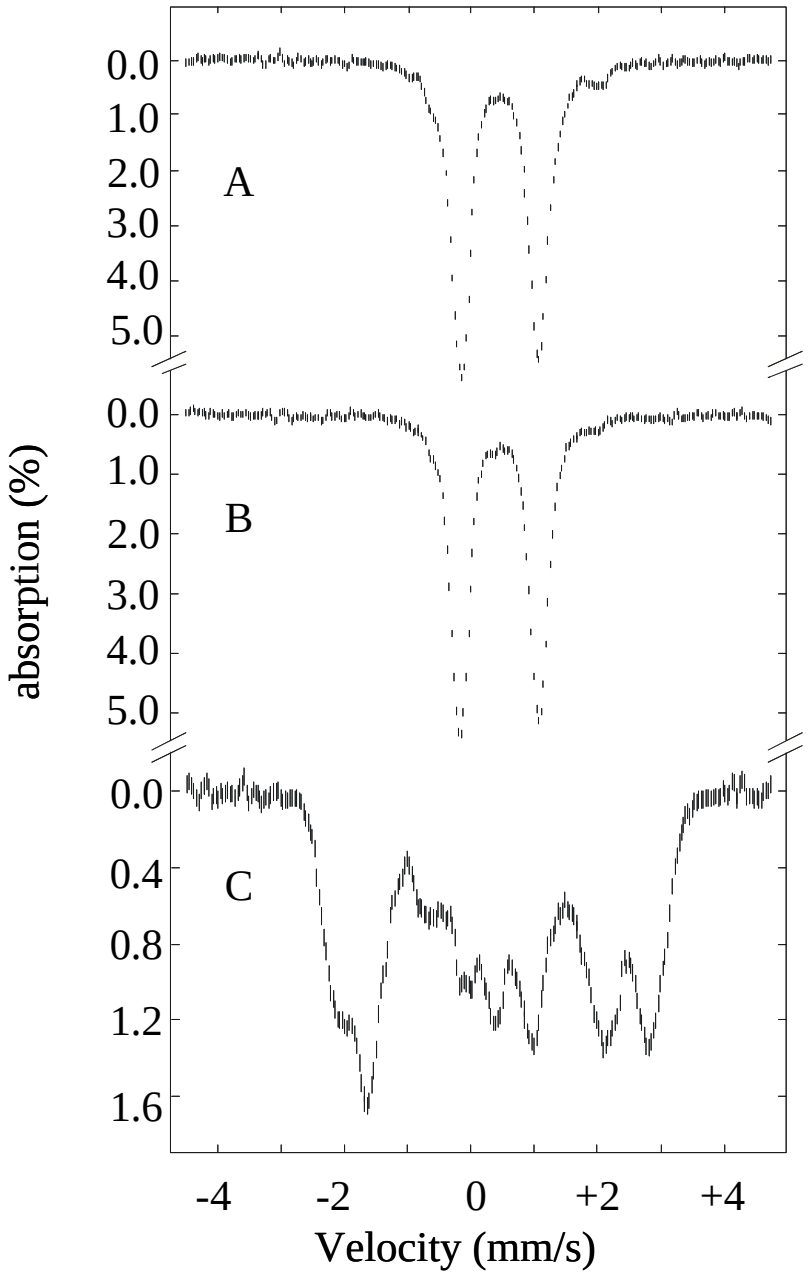
absorption (%)
0.0
1.0
2.0
3.0
4.0
5.0
A
0.0
1.0
2.0
3.0
4.0
5.0
B
0.0
0.4
0.8
1.2
1.6
C
-4
-2
0
+2
+4
Velocity (mm/s)

Figure 5.8 EPR-monitored redox titrations of *Synechocystis* WT (A) and H86Y (B) NEM-FTR. Data points correspond to the intensity of the $S = 1/2$ EPR from the $[4Fe\text{-}4S]^{3+}$ center at pH 7.0 (■) and pH 8.0 (●). The initial concentration of enzyme used in each titration is 100 μM and all data points have been normalized for dilution effects upon reductive titration with sodium dithionite. The solid lines are the best fits to one-electron Nernst equations with $E_m = -145 \pm 10$ mV (pH 7.0) and -200 ± 10 mV (pH 8.0) for WT NEM-FTR and $E_m = -155 \pm 10$ mV (pH 7.0) and -255 ± 10 mV (pH 8.0) for H86Y NEM-FTR.

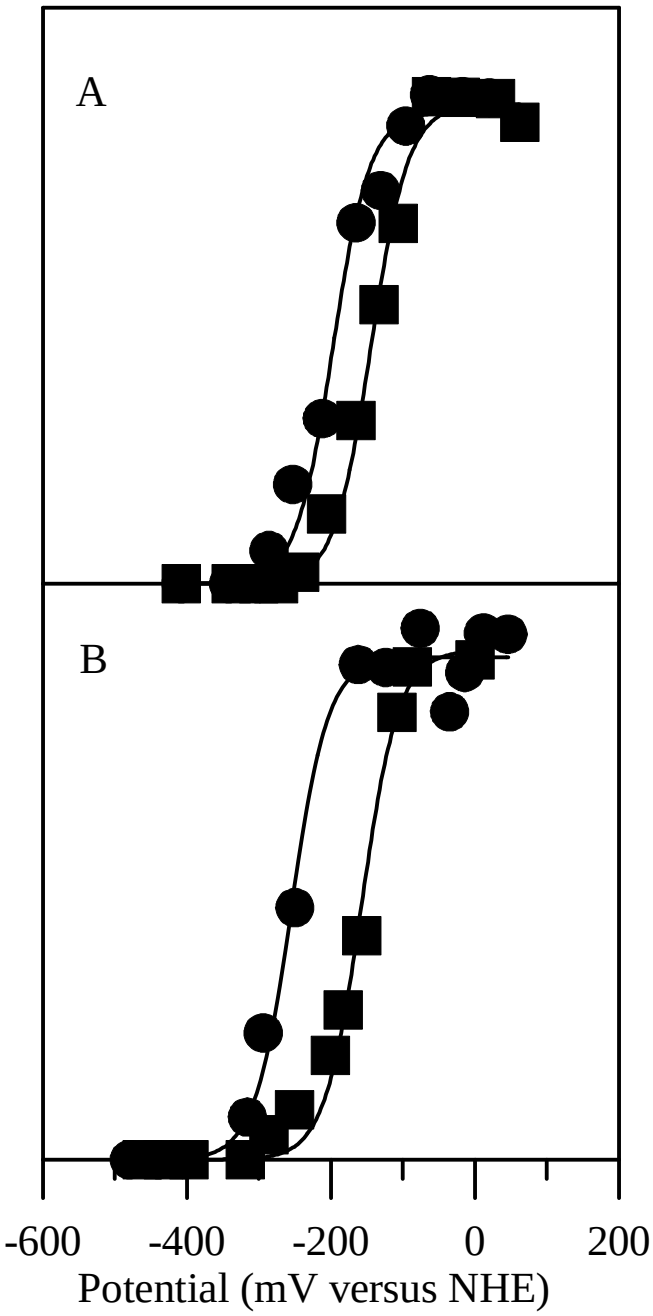
A
B
-600
-400
-200
0
200
Potential (mV versus NHE)

Figure 5.9 Overlay of the x-ray structures of the active sites of oxidized (as purified) *Synechocystis* FTR at 1.6-Å resolution (orange) and methyl-viologen-reduced *Synechocystis* FTR at 2.6-Å resolution (magenta) (S. Dai, H. Eklund, P. Schürmann, unpublished results used with permission). Selected distances between the εN of His86 and the S of Cys55 and one of the cluster μ_3-S^{2-} and between the S of Cys87 and the S of Cys55 are indicated for the methyl-viologen-reduced sample.

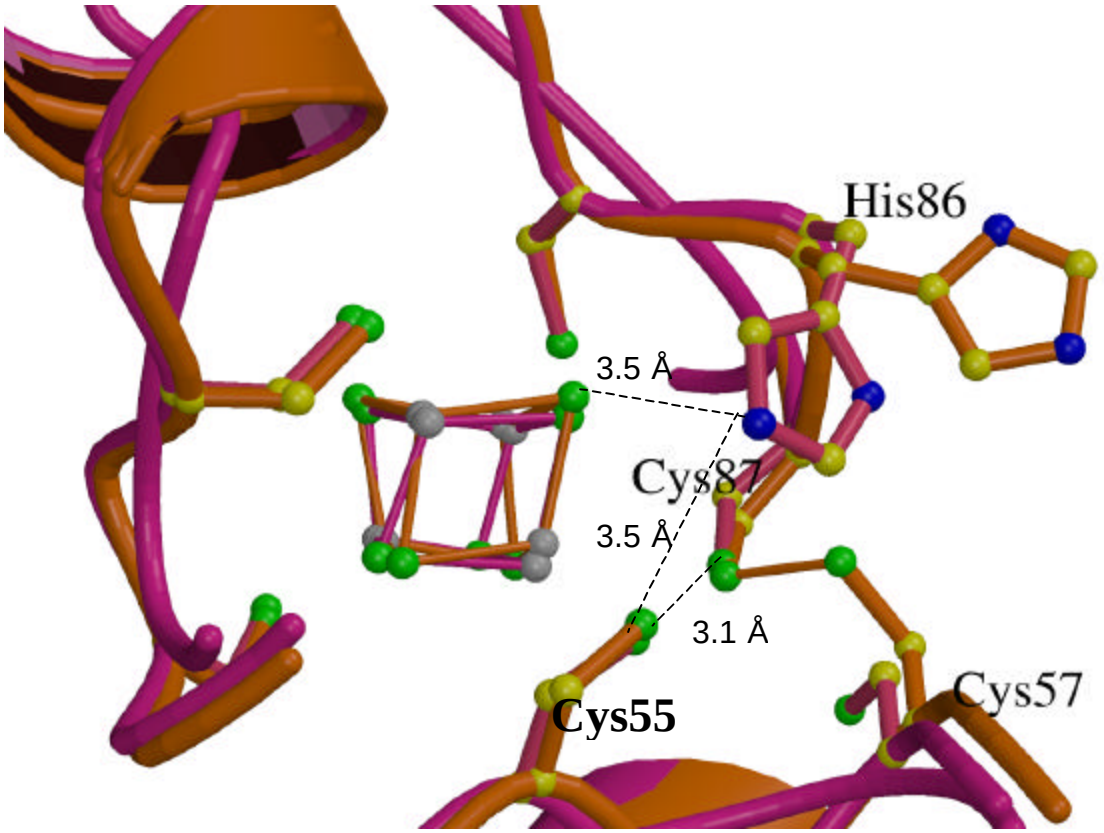
His86
3.5 Å
Cys87
3.5 Å
3.1 Å
Cys57
Cys55

CHAPTER 6

CONCLUSIONS AND FUTURE WORK

The objective of the research described in this dissertation was to investigate the catalytic mechanism of chloroplast ferredoxin:thioredoxin reductase using the combination of mutagenesis, chemical modification, spectroscopic and electrochemical approaches. Specifically, UV-visible absorption, resonance Raman, electron paramagnetic resonance, variable-temperature magnetic circular dichroism, and Mössbauer spectroscopies were used to characterize the properties of the [4Fe-4S]/disulfide active site, in each of the accessible redox states, in wild type, *N*-ethylmaleimide (NEM)-modified, C57S, C87A, and H86Y FTR, and a stable covalent complex formed between wild type FTR and a C40S variant of thioredoxin-*m* (FTR/Trx*m*). The results indicate that each cysteine residue in the active-site disulfide, Cys57 and Cys87, plays a distinct role in catalysis. Cys87 functions as the cluster interacting thiol which becomes ligated to the unique Fe site in the $S = 1/2$ $[4Fe\text{-}4S]^{3+}$ cluster found in the one-electron reduced intermediate.[1-3] Cys57 functions as the interchange thiol which attacks and forms a heterodisulfide with the substrate thioredoxin.[1-3] In addition, the results implicate an important catalytic role for His86 both in positioning Cys87 proximal to the cluster in the two-electron from of FTR and as a Lewis acid/base residue critical for catalysis.[2] Overall, the results support two possible catalytic mechanisms for FTR (Figures 6.1 and 6.2). Both employ a one-electron-reduced intermediate involving a $[4Fe\text{-}4S]^{3+}$ cluster with the cluster-interacting thiolate,

Cys87, coordinated to yield a five-coordinate Fe site, in order to facilitate disulfide reduction in two sequential one-electron steps. However, they differ in terms of whether the heterodisulfide between FTR and Trx is formed at the one- or two-electron reduced level.

Although it is not possible to distinguish between the mechanistic proposals shown in Figures 6.1 and 6.2 based on the results presented in this dissertation, the salient features of each mechanism are discussed below, along with future experiments designed to discriminate between them. The viability of the mechanism shown in Figure 6.1 has been demonstrated by the ability to cleave the heterodisulfide and reform the active-site disulfide, via one-electron reduction of the FTR/Trx*m* heterodisulfide complex.[3] This mechanism requires the formation of a triple complex to be formed between the redox partners, Fd, FTR, and Trx. Recently, a triple complex has been crystallized in which FTR is electrostatically bound to Fd and covalently bound to the C40S variant of Trx*m* (P. Schürmann, personal communication). However, at this time it is not known whether this triplex species is a stable analog of a catalytically competent intermediate. The viability of the mechanism shown in Figure 6.2 stems from the discovery that the cluster-interacting cysteine, Cys87, is interacting with the cluster in the two-electron-reduced state as well as the one-electron state, leaving the interchange thiol, Cys57, free to attack the substrate disulfide.[3] Hence, in this mechanistic scheme FTR is reduced by two electrons prior to interaction with Trx and the ensuing reaction proceeds by conventional dithiol/disulfide exchange. The resulting mechanistic scheme is similar to that utilized by the NADPH-dependent disulfide reductase class of flavoenzymes.[4-6] Moreover, it does not require all three redox partners to form a triple complex and results in a pool of

reduced FTR that is competent for thioredoxin reduction on exposing chloroplasts to light.

Future studies to discriminate between these mechanistic proposals should center on freeze-quench kinetic studies. EPR-monitored freeze-quench studies would provide useful information by enabling assessment of the rates of formation and loss of the S = 1/2 one-electron reduced intermediate. However, since similar intermediates with analogous EPR signals are present in both mechanistic schemes, this approach cannot readily discriminate between them. On the other hand, the unique Mössbauer signature of two-electron-reduced FTR which is only present in the mechanistic scheme shown in Figure 6.2, should enable discrimination between the mechanistic proposals based on freeze-quench Mössbauer studies. Parallel freeze-quench Mössbauer and EPR studies have been recently employed to great effect in understanding the mechanism of a range of oxo-bridged diiron centers.[7-18]

Excess amounts of reduced methyl or benzyl viologen are known to function as efficient electron donors for FTR with catalytic rates similar to reduced ferredoxin.[19] It has also been established that incubating FTR with reduced methyl or benzyl viologen in the absence of substrate results in two-electron reduced FTR.[3] However, the ability of two-electron reduced FTR to reduce Trx in a single turnover experiment has yet to be demonstrated. This could be tested utilizing a combination of biochemical analysis, using FTR activity assays,[20] coupled with chromatography to separate FTR and Trx and alkylation of free cysteines as assessed by biophysical spectroscopic techniques and mass spectrometry.

Aside from providing new information concerning the mechanism of FTR, the research presented in this dissertation has revealed unprecedented site-specific [4Fe-4S] cluster chemistry. Although site-specific Fe-S cluster chemistry is not a new theme in biology,[21-39] FTR utilizes a new method of functionalizing a [4Fe-4S] cluster to catalyze disulfide reduction in two sequential one-electron steps. Remarkably, FTR exhibits site-specific cluster chemistry in all three accessible redox states. In the oxidized (resting) state, mutagenesis results confirm a weak interaction between a unique Fe site and the disulfide that results in partial valance localization of one of the two valence-delocalized $Fe^{2+}Fe^{3+}$ pairs of the $[4Fe\text{-}4S]^{2+}$ cluster and primes the active site for one-electron reduction with concomitant cleavage of the active-site disulfide. Oxidized NEM-FTR and the FTR/Trx heterodisulfide complex are potential analogs of a one-electron-reduced intermediate and comprise $[4Fe\text{-}4S]^{3+}$ clusters with two cysteinate ligands at the unique Fe site. The most intriguing result is that two-electron-reduced FTR in which the disulfide is reduced to a dithiol, contains an unprecedented electron-rich $[4Fe\text{-}4S]^{2+}$ cluster comprising both valence-delocalized and valence-localized $Fe^{2+}Fe^{3+}$ pairs. This result is interpreted in terms of stabilization of a Fe^{2+} site via strong H-bonding interaction between the thiol form of Cys87 and the coordinated S atom of Cys55. As indicated in Chapter II, recent spectroscopic studies of methanogenic heterodisulfide reductases indicate that the site-specific cluster chemistry displayed by FTR is likely to be a unifying feature of all Fe-S cluster-containing disulfide reductases.[40-44]

Bibliography

(1) Jameson, G. N. L.; Walters, E. M.; Manieri, W.; Schurmann, P.; Johnson, M. K.; Huynh, B. H. *J.Am.Chem.Soc.* **2003**, *125*, 1146-1147.

(2) Walters, E. M.; Johnson, M. K. *Photosyn.Res.* **2004**, *79*, 249-264.

(3) Walters, E. M.; Garcia-Serres, R.; Glauser, D. A.; Bourquin, F.; Manieri, W.; Schürmann, P.; Johnson, M. K.; Huynh, B. H. *J.Am.Chem.Soc.* **2005**, *manuscript in preparation.*

(4) Williams, C. H., Jr. Lipoamide Dehydrogenase, Glutathione Reductase, Thioredoxin Reductase, and Mercuric Ion Reductase-A Family of Flavoenzyme Transhydrogenases; In *Chemistry and Biochemistry of Flavoenzymes*; Müller, F., ed. CRC Press: Boca Raton, FL, 1992; pp 121-211.

(5) Williams, C. H., Jr. *FASEB J* **1995**, *9*, 1267-1276.

(6) Williams, C. H., Jr.; Arscott, L. D.; Müller, S.; Lennon, B. W.; Ludwig, M. L.; Wang, P.-F.; Veine, D. M.; Becker, K.; Schirmer, R. H. *Eur.J.Biochem.* **2000**, *267*, 6110-6117.

(7) Liu, K.; Valentine, A. M.; Wang, D.; Huynh, B. H.; Edmondson, D. E.; Salifoglou, A.; Lippard, S. J. *J.Am.Chem.Soc.* **1995**, *117*, 10174-10185.

(8) Edmondson, D. E.; Huynh, B. H. *Inorg Chim Acta* **1996**, *252*, 399-404.

(9) Valentine, A. M.; Tavares, P.; Perreira, A. S.; Davydov, R.; Krebs, C.; Hoffman, B. M.; Edmondson, D. E.; Huynh, B. H.; Lippard, S. J. *J.Am.Chem.Soc.* **1998**, *120*, 2190-2191.

(10) Huynh, B. H.; Bollinger, J. M., Jr.; Edmondson, D. E. *ACS Symposium Series* **1998**, *692*, 403-422.

(11) Perreira, A. S.; Small, W.; Krebs, C.; Tavares, P.; Edmondson, D. E.; Theil, E. C.; Huynh, B. H. *Biochemistry* **1998**, *37*, 9871-9876.

(12) Krebs, C.; Huynh, B. H. *Iron Metabolism* **1999**, 253-273.

(13) Krebs, C.; Edmondson, D. E.; Huynh, B. H. *Meth.Enzymol.* **2002**, *354*, 436-454.

(14) Jameson, G. N. L.; Jin, W.; Krebs, C.; Perreira, A. S.; Tavares, P.; Liu, X.; Theil, E. C.; Huynh, B. H. *Biochemistry* **2002**, *41*, 13435-13443.

(15) Yun, D.; Krebs, C.; Gupta, G. P.; Iwig, D. F.; Huynh, B. H.; Bollinger, J. M., Jr. *Biochemistry* **2002**, *41*, 981-990.

(16) Lee, D.; Pierce, B.; Krebs, C.; Hendrich, M. P.; Huynh, B. H.; Lippard, S. J. *J.Am.Chem.Soc.* **2002**, *124*, 3993-4007.

(17) Baldwin, J.; Krebs, C.; Saleh, L.; Stelling, M.; Huynh, B. H.; Bollinger, J. M., Jr.; Riggs-Gelasco, P. *Biochemistry* **2003**, *42*, 13269-13279.

(18) Saleh, L.; Krebs, C.; Ley, B. A.; Naik, S.; Huynh, B. H.; Bollinger, J. M., Jr. *Biochemistry* **2004**, *43*, 5953-5964.

(19) Schürmann, P.; Stritt-Etter, A.-L.; Li, J. *Photosyn.Res.* **1995**, *46*, 309-312.

(20) Schürmann, P. *Meth.Enzymol.* **1995**, *252*, 274-283.

(21) Peters, J. W.; Stowell, M. H. B.; Soltis, S. M.; Finnegan, M. G.; Johnson, M. K.; Rees, D. C. *Biochemistry* **1997**, *36*, 1181-1187.

(22) Hunsicker-Wang, L. M.; Heine, A.; Chen, Y.; Luna, E. P.; Todaro, T.; Zhang, Y. M.; Williams, P. A.; McRee, D. E.; Hirst, J.; Stout, C. D.; Fee, J. A. *Biochemistry* **2003**, *42*, 7217.

(23) Lanzilotta, W. N.; Christiansen, J.; Dean, D. R.; Seefeldt, L. C. *Biochemistry* **1998**, *37*, 11376-11384.

(24) Beinert, H.; Kennedy, M. C.; Stout, C. D. *Chem.Rev.* **1996**, *96*, 2335-2373.

(25) Flint, D. H.; Allen, R. M. *Chem.Rev.* **1996**, *96*, 2315-2334.

(26) Layer.G.; Moser, J.; Heinz, D. W.; Jahn, D.; Schubert, W.-D. *EMBO J.* **2003**, *22*, 6214-6224.

(27) Jarrett, J. T. *Curr.Opin.Chem.Biol.* **2003**, *7*, 174-182.

(28) Einsle, O.; Tezcan, F. A.; Andrade, S. L. A.; Schmid, B.; Yoshida, M.; Howard, J. B.; Rees, D. C. *Science* **2002**, *297*, 1696-1700.

(29) Kim, J.; Rees, D. C. *Science* **1992**, *257*, 1677-1682.

(30) Crane, B. R.; Siegel, L. M.; Getzoff, E. D. *Science* **1995**, *270*, 59-67.

(31) Peters, J. W.; Lanzilotta, W. N.; Lemon, B. J.; Seefeldt, L. C. *Science* **1998**, *282*, 1853-1858.

(32) Nicolet, Y.; Cavazza, C.; Fontecilla-Camps, J. C. *J.Inorg.Biochem.* **2002**, *91*, 1-8.

(33) Dobbek, H.; Svetlitchnyi, V.; Gremer, L.; Huber, R.; Meyer, O. *Science* **2001**, *293*, 1281-1285.

(34) Dobbek, H.; Svetlitchnyi, V.; Liss, J.; Meyer, O. *J.Am.Chem.Soc.* **2004**, *126*, 5382-5387.

(35) Link, T. A. *Adv.Inorg.Chem.* **1999**, *47*, 83-157.

(36) Calzolai, L.; Zhou, Z.-H.; Adams, M. W. W.; La Mar, G. N. *J.Am.Chem.Soc.* **1996**, *118*, 2513-2514.

(37) Sofia.H.J.; Chen.G.; Hetzler, B. G.; Reyes-Spindola, J. F.; Miller, N. E. *Nucleic Acids Res.* **2001**, *29*, 1097-1106.

(38) Walsby, C. J.; Hong, W.; Broderick.W.E.; Cheek, J.; Ortillo, D.; Broderick.J.B.; Hoffman, B. M. *J.Am.Chem.Soc.* **2002**, *124*, 3143-3151.

(39) Cheek, J.; Broderick.J.B. *J.Biol.Inorg.Chem.* **2001**, *6*, 209-226.

(40) Madadi-Kahkesh, S.; Duin, E. C.; Heim, S.; Albracht, S. P. J.; Johnson, M. K.; Hedderich, R. *Eur.J.Biochem.* **2001**, *268*, 2566-2577.

(41) Duin, E. C.; Madadi-Kahkesh, S.; Hedderich, R.; Clay, M. D.; Johnson, M. K. *FEBS Letters* **2002**, *512*, 263-268.

(42) Duin, E. C.; Bauer, C.; Jaun, B.; Hedderich, R. *FEBS Letters* **2003**, *538*, 81-84.

(43) Bennati, M.; Weiden, N.; Dinse, K.-P.; Hedderich, R. *J.Am.Chem.Soc.* **2004**, *126*, 8378-8379.

(44) Shokes, J. E.; Duin, E. C.; Bauer, C.; Jaun, B.; Hedderich, R.; Koch, J.; Scott, R. A. *FEBS Letters* **2005**, *579*, 1741-1744.

(45) Johnson, M. K.; Smith IV, A. D. Iron-Sulfur Proteins; In *Encyclopedia of Inorganic Chemistry*; King, R. B., ed. John Wiley and Sons: Chichester, 2005; in press.

Figure 6.1: Proposed catalytic mechanism for FTR.[12;45] Residue numbering is for *Synechocystis* FTR. Square brackets are used to indicate transient intermediates.

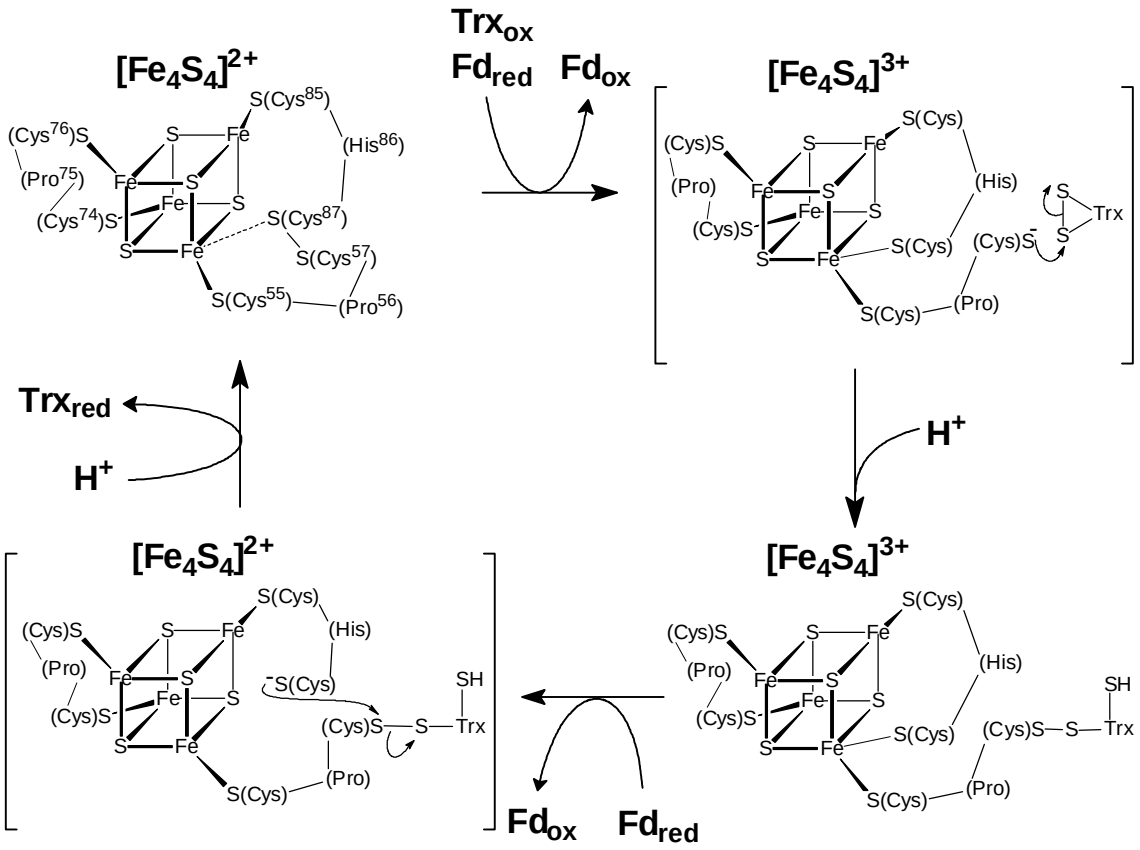
Trx$_{ox}$
Fd$_{red}$
Fd$_{ox}$
[Fe$_4$S$_4$]$^{2+}$
[Fe$_4$S$_4$]$^{3+}$
Trx$_{red}$
H$^+$
H$^+$
[Fe$_4$S$_4$]$^{2+}$
[Fe$_4$S$_4$]$^{3+}$
Fd$_{ox}$
Fd$_{red}$

Figure 6.2: Alternative proposal for the catalytic mechanism of FTR.[45] Residue numbering is for *Synechocystis* FTR. Square brackets are used to indicate transient intermediates.

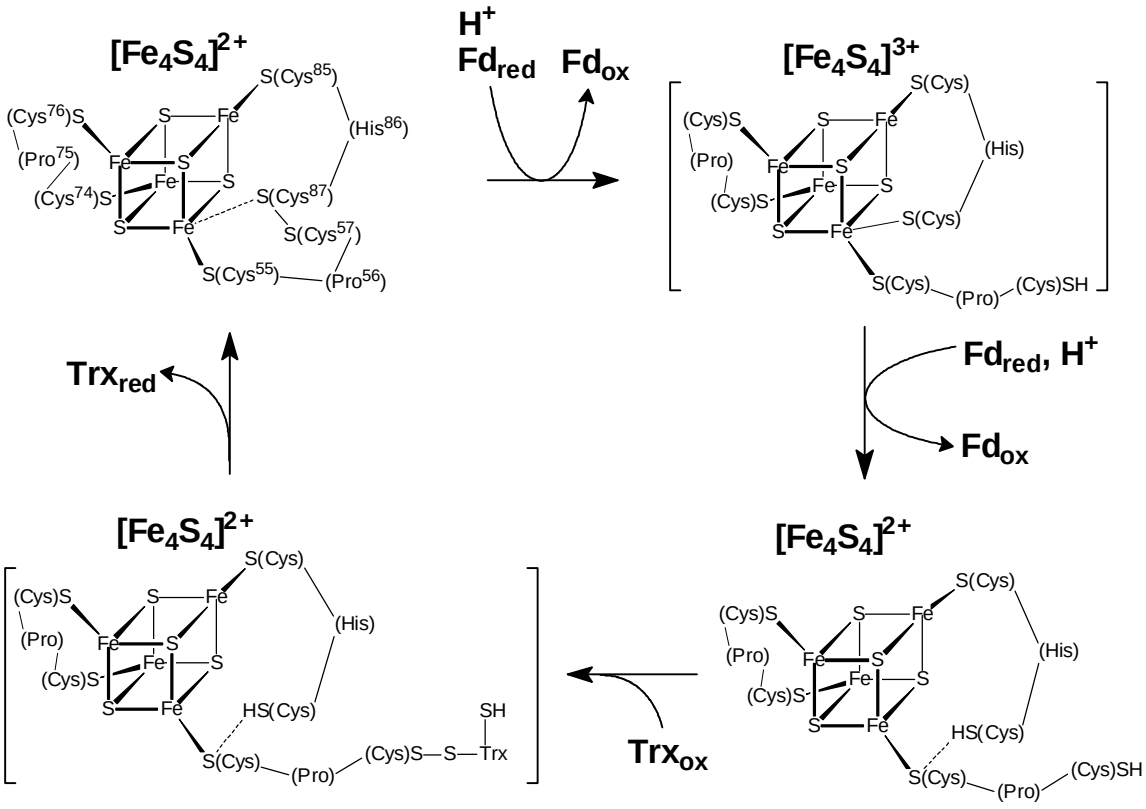
[Fe4S4]2+
H+
Fdred
Fdox
[Fe4S4]3+
Fdred, H+
Fdox
Trxred
[Fe4S4]2+
[Fe4S4]2+
Trxox